Title:

Analysis of trace elements in snow pits from Dronning Maud Land, Antarctica

Master Thesis M.Sc. Programme Marine Geoscience

Department of Geosciences
University of Bremen

Peter Sperlich

aus dem Rheinland

in Bremen, 2008

Supervisor:

1) Dr. Hubertus Fischer,
   Alfred-Wegener-Institut, Bremerhaven

2) Professor Dr. Tilo von Dobeneck,
   Universität Bremen

Table of contents

List of figures

List of tables

Abstract

The objective of this study was to analyse the spatio-temporal variability of glacio-chemical parameters in snow pits, sampled upstream the EDML deep ice core drilling site in Dronning Maud Land (DML), Antarctica. The key goal was to evaluate the systematic spatial variability of ion concentrations in the EDML catchment area that potentially superimpose the climatic records from the EDML and to suggest corrections of the EDML ion records when needed.

Therefore, 15 snow pits were sampled in high resolution of 1.5 cm (HR) and coarse resolution of 10 cm (CR) upstream the ice divide, covering a transect distance of 280 km and an altitude range of >400 m. HR and CR samples of ten snow pits were ion chromatographically (IC) analysed during this study. Presented and discussed are the concentration records of sodium, chloride, excess chloride (Clx), nitrate, and sulphate derived from HR and CR samples on a twelve year time scale (2005-1994). The interpretation of non sea-salt calcium ($nssCa^{2+}$) and methane sulfonate (MSA^{-}) records is based on CR samples, only. An age model for each snow pit was constructed by HR ion records and provided HR oxygen isotope ($\delta^{18}O$) records, which were also investigated for spatio-temporal variability.

All high resolution ion and $\delta^{18}O$ records exhibited distinct seasonal variations. In all snow pits, Na^{+} and Cl^{-} concentrations showed pronounced maxima during the austral winter half-year and minimum concentrations during the austral summer period. Furthermore, the seasonal signals of Na^{+} and Cl^{-} concentrations comprised of a distinct multi annual signal of increased winter concentrations every 4-5 years, which is most likely governed by the Antarctic Dipole. The records of $\delta^{18}O$, Clx, NO_3^{-}, and SO_4^{2-} exhibited maximum concentrations during the austral summer period and minimum values during austral winter in all snow pits. In case of $\delta^{18}O$, diffusion was addressed to smooth the signal and to eliminate distinct seasonal amplitudes.

Strong localized effects of post-depositional snow redistribution precluded the identification of coherent annual pattern snow of accumulation and chemistry. Decreasing NO_3^{-} concentrations with depth could be furthermore attributed to post-depositional outgassing. In snow pit records that reached back to 1991 and 1990, high SO_4^{2-} concentrations during 1992 and 1993 could be attributed to the volcanic eruptions of Mount Pinatubo and Cerro Hudson in 1991.

Systematic spatial variations of annual snow accumulation and chemistry could be traced back to the inclining altitude with increasing distance to the EDML drill site. Spatial depletion of $\delta^{18}O$ was found as consequence of decreased mean temperatures. The spatial decrease of accumulation with higher altitudes amplifies the rate of NO_3^- and MSA^- outgassing upstream EDML. For both Clx and SO_4^{2-}, the identified predominance of dry deposition results in increased ion concentrations with inclining altitudes due to decreased annual accumulation. Hence, the EDML ice core records of NO_3^-, MSA^-, Clx and SO_4^{2-} are suggested to be corrected for the spatial upstream effect. In contrast, no spatial effect could be identified within the concentration records of the sea-salt derived ions Na^+ and Cl^-.

1. Introduction

1.1 Fundamentals of climate and ice core studies

Earth's climate system is driven by the interplay of external forcing, such as solar radiation, and internal forcing such as volcanic outgassing of climate relevant gases and aerosols in the atmosphere. The internal climate system comprises interactions between hydrosphere, atmosphere, biosphere, lithosphere, and the astenosphere. Changes in solar radiation, tectonics and biogeochemical processes have altered the climatic settings of oceans and atmosphere on earth over billions of years. Exemplarily, the tectonic opening of the Drake Passage between Antarctica and South America some 35 million years ago led to a reorganisation of ocean circulation and gave birth to the Antarctic Circumpolar Current (ACC). The establishment of the ACC resulted in a thermal isolation of Antarctica, which resulted in the glaciation of Antarctica by 98 %. Studying Earth's history reveals that earth's climate has undergone dramatic changes during the evolution of the planet until it evolved to its recent state (HEWITT & STURGES, 1993, HARTMANN, 1994).

On a geological timescale, the recent Holocene climate epoch presents a snapshot of 10.000 years as compared to ~5 billion years which mark the total age of the earth (HARTMANN, 1994). By no means, the present global climate pattern is to be understood as a result of geological evolution only. It is widely accepted that global mean temperatures are presently rising and will do so in future, a phenomena known as global warming. It is also widely understood, that human activity contributes largely to the imminent global warming, mostly by the emission of greenhouse gases (GHG) into the atmosphere (IPCC, 2007a).
Ongoing scientific discussion about the consequences of the anticipated global warming has reached public media and public interest, as it does potentially affect large parts of the human population. Globally averaged, negative consequences of global warming will outbalance positive effects on human beings. Consequences to mention are sea level rise, more extreme heat waves and droughts, tropical storms and floods. Beside the impact on human beings, severe consequences of global warming are expected to affect marine and terrestrial flora and fauna. According to the IPCC report, 20 - 30 % of global flora and fauna will most likely die out as climate will most likely change too fast for many species to adopt (IPCC, 2007a, IPCC, 2007b).

Thus, there is a broad interest to understand how the climate system will globally and regionally adjust in response to the anthropogenic impacts. Finding robust conclusions requires a high level of understanding of why and how the previous changes took place in earth's history. In climatology, the performance of a "crucial" experiment is impossible as compared to other quantitative sciences (V. STORCH & NAVARRA, 1999).

Therefore, climatologists analyse a range of climate archives such as marine and lake sediments, tree rings and ice cores, which store information of climate history (HARTMANN, 1994). Ice cores provide qualitative and quantitative information on climatic parameters such as precipitation and isotopic temperatures on high temporal resolution. What makes ice cores an exception among other paleoclimatic records is the ability of ice to store direct information on paleoconcentrations of atmospheric gases and aerosols that are either trapped in air bubbles or recorded in continuously accumulated layers of snow (BARNOLA et al., 1987).

The diversity of climate information makes ice core studies an important tool of climate science. In order to study the paleoclimatic information stored in ice, several drilling projects were undertaken since the 1960's on both polar ice shields (Greenland and Antarctica) as well as on low latitude mountain glaciers. The time scale covered by ice cores is dependent on the drill site. While mountain glaciers cover records of mostly a few hundred to maximum 40.000 years (HARTMANN, 1994), the time scale extends from central Greenland records from one glacial cycle (NORTH GREENLAND ICE-CORE PROJECT MEMBERS, 2004) to Antarctic ice core records that cover up to eight glacial cycles (EPICA COMMUNITY MEMBERS, 2004).

The European Project for Ice Coring in Antarctica (EPICA) is one of the largest international ice core projects, carried out by research institutes from 10 European countries. The motivation of EPICA was to find answers in Antarctic ice core records on how previous climate changes affected both hemispheres (ESF, 2008). To achieve the goals, EPICA carried out two deep ice core drillings on the east Antarctic plateau, where the two different ice cores were expected to contribute on two different time scales (Figure 1). The investigations on the ice core drilled at Dome Concordia (Dome C) characterized by lower accumulation rate (recent accumulation rate 25 mm water equivalent per year (mm WE a^{-1}) (EPICA COMMUNITY MEMBERS, 2004)) aimed at retrieving an ice core record that reaches furthest back in time. The second ice core was drilled in Dronning Maud Land (called EDML). In DML, higher accumulation rates (recent accumulation rate 64 mm WE a^{-1}, (OERTER et al., 2000)) than at

Dome C allow for a higher time resolution of the ice core. Since DML is part of the Atlantic Ocean sector of Antarctica, it is climatically influenced by South Atlantic air masses. Thus, the EDML ice core represents a climatic counterpart to Greenland ice cores that could directly be compared to a north Greenland ice core (EPICA COMMUNITY MEMBERS, 2006).

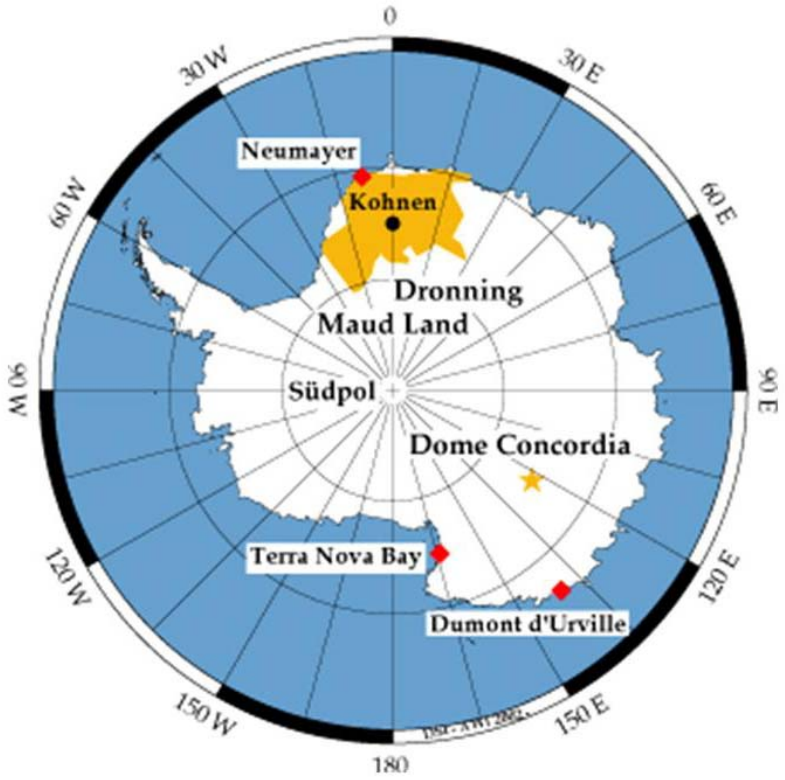

Figure 1: Map of Antarctica, the research stations Dumont d'Urville, Neumayer and Terra Nova Bay are indicates by red diamonds, further shown are the EPICA deep drilling site at Dome Concordia and the area of Dronning Maud Land including Kohnen station, where the EDML ice core was drilled.

While the Dome C core originates from a dome position, the EDML ice core was drilled on a saddle located on the ice divide at Kohnen station (Figure 3). EDML was drilled at 75°00'S, 00°04'E in an altitude of 2892 m above sea level (asl). Glacial flow is based on the surface slope and the topographic gradient of the bedrock underneath the ice. Because the EDML drilling location is on the ice divide, the ice masses of this area are moving downhill along the ice divide with an average velocity of 1 m * a^{-1} (HUYBRECHTS et al., 2007). Tracking the annual snow after its deposition, it flows in typical flow lines, (Figure 2). According to Figure 2, ice of increasing depths was formed by precipitation in higher altitudes as schematically indicated by the numbers 1-3. In case of the EDML ice core, the upper 89 % cover

approximately 170.000 years, (HUYBRECHTS et al., 2007). Referring to the average ice flow velocity of 1 m * a^{-1}, the layer of 170.000 years precipitated approximately 170 km upstream the EDML drill site, which includes an increase of ~245 m referring to the recent topography.

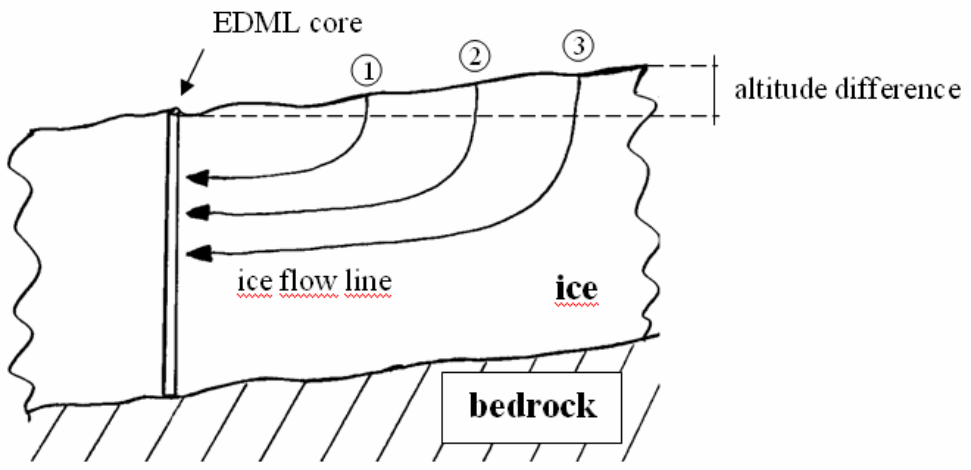

Figure 2: The ice flow scheme indicates the lines of lateral ice flow as seen from the EDML ice core drill site located on the ice divide. Vice versa, the figure displays the origin of snow and the systematic altitude variation from where it flew towards the EDML ice core.

1.2 The aim of this study

It is described that precipitation and, thus, the annual accumulation of snow varies with altitude in DML, (ROTSCHKY, 2007b). Furthermore, systematic changes in chemical and isotopic composition of snow deposits occur with increasing altitude of the respective site of deposition (GÖKTAS et al., 2002). Combining the two facts that older ice precipitated in higher altitudes and that snow accumulation/chemistry changes with increasing altitudes approaches the problem the EDML ice core records are superimposed by spatial signals, attributed to the altitude range of its catchment area (HUYBRECHTS et al., 2007). In order to study climate variability from the EDML ice core, unravelling the merged spatial and temporal variations is essential to purify the EDML ice core record.

The motivation of this study is to investigate the variability of snow accumulation and snow chemistry upstream EDML; primarily in accordance to unknown spatial variability upstream and secondly to further characterize the catchment area of EDML in terms of glaciological parameters. Therefore, the aim was to answer the following questions:

- Do spatial variations occur in snow chemistry upstream EDML?
- Can spatial signals be attributed to systematic processes?
- Can the spatial variability be quantified in order to correct for the EDML record?
- Do area-wide samples allow for reconstruction of annual deposition pattern in DML despite strong local influences of post-depositional processes?
- Does the low accumulation rate upstream EDML allow for resolution of seasonal variability of glacio-chemical parameters in snow deposits?
- What seasonal variability is typical for the investigated parameters?
- What seasonal processes drive the seasonal variability?
- Are further variations to be identified in DML records, such as pronounced single events (volcanic deposits) or regular occurring variations on multi annual time scales?
- Can additional variations in DML records be quantified and attributed to driving processes?

In order to find answers to these questions, 15 snow pits (DML 76-90) were sampled upstream EDML during the Antarctic field campaign 2005/2006, (Figure 3). The snow pits were dug in a distance of 20 km from pit to pit, covering a transect distance of 280 km in total. The upstream transect line covered an altitude range from 2890 m to 3300 m. Each snow pit was sampled to a depth of 2.10 m using a high and a coarse resolution sampling method (called UTS and UTD, respectively).

In the framework of this Master's Thesis, both UTS and UTD datasets from ten selected snow pits were analysed using ion chromatography (IC) in the Alfred Wegener Institute for polar and marine research (AWI) in Bremerhaven, where a total amount of 1610 samples was measured for anion and cation concentrations. Ions records of sodium, chloride, calcium, nitrate, sulphate and methane sulfonate will be discussed.
The UTS dataset was complemented by oxygen isotope records (OERTER, pers. com. 2007) that were used to construct an age model for each snow pit. Both UTS and UTD datasets were investigated for spatial variations of snow accumulation and chemistry. The spatial variability

of the ion concentrations and fluxes is quantified and attributed to the depositional processes that drive the variability. After all, corrections for the EDML deep ice core records are suggested if necessary.

Furthermore, annual accumulation and mean annual values of snow chemistry will be presented and discussed whether they can be considered representative for DML. Specially emphasized is the discussion of increased sulphate concentrations that were attributed to emissions of the volcanic eruptions of Mount Pinatubo and Mount Cerro Hudson in 1991.

With these objectives this study delivers essential information for a more quantitative understanding of the deposition process of glacio-chemical parameters on the Antarctic Plateau in Dronning Maud Land and, thus, for an improved interpretation of the aerosol chemistry records in the deep EDML ice core.

1.3 Study area

Dronning Maud Land is located on the east Antarctic ice sheet, extending from coastal zones (Ekströmisen) onto the high east Antarctic Plateau (Amundsenisen) with an medium ice thickness of 1678 m, (STEINHAGE, 2001). It stretches from 10° W to 10° E and from 76° S to 74° S. The boundaries of the high Antarctic plateau are built by the mountain ranges Kirvanveggen and Heimefrontfjella. Prior to the pre-site survey for the EDML deep drilling, large areas of DML were rather unexplored. Due to the intense investigation programme conducted within the framework of EPICA, glaciological and meteorological parameters could be described for the high Antarctic plateau in DML but are still spatially and temporally limited (GÖKTAS, 2002b). The annual temperature at Kohnen Station is averaged to - 44.6 °C, where the ice thickness amounts for 2892 m, (ESF, 2008).

Studies on precipitation characteristics in DML exhibited the Atlantic Ocean to be the moisture source in 40 % to 80 % of all precipitation events, where the moisture evaporates 4 days before its precipitation (TIJM-REIJMER & VAN DEN BROEKE, 2000). During 1998, the annual accumulation comprised of 4 major precipitation events that caused 80 % of the total annual accumulation (REIJMER, C. H. & M. R. VAN DEN BROEKE, 2001). Average wind speeds

in DML range from 3.7 m/s to 5.1 m/s as recorded by automatic weather stations, where the advection of moist air masses coincided with increased wind speeds of 15 m/s on average (REIJMER, C. H. & M. R. VAN DEN BROEKE, 2001).

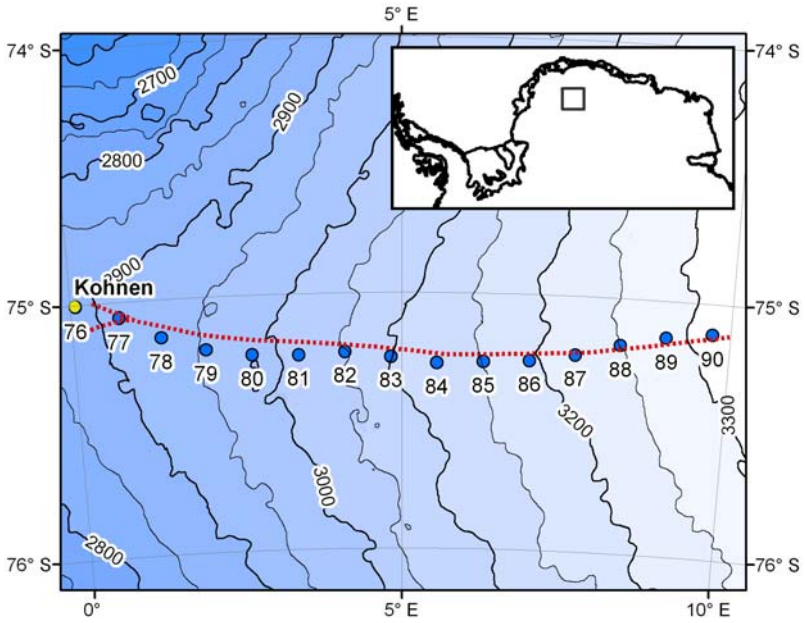

Figure 3: EDML drill site at Kohnen station (yellow circle) in Dronning Maud Land, Antarctica. The topographical map is the enlarged sector, marked by the square within the section in the top-right corner. The red dotted line marks the ice divide along which the 15 snow pits were dug with the according numbers 76-90. The contour lines indicate the altitude [m] asl. The map was provided by Christine Wesche, pers. com.

2. Depositional processes in Antarctic snow

2.1 Moisture and aerosol transport into Antarctica

The Antarctic continent is the coldest and driest continent on earth (ANSCHÜTZ, 2006), where the dry air allows any long wave radiation to escape without atmospheric warming effects. Generally spoken, extremely cold and dense air forms the anticyclonic Antarctic Polar high pressure system that generates katabatic winds flowing down the ice cap in near surface altitudes, (Figure 4). As these katabatic winds spread out at the open ocean, they form Polar easterly winds, meeting the Sub-polar low belt at about 60° S. The Westerly wind belt comprises of large cyclonic systems, circling around Antarctica in clockwise direction while exporting air masses towards Antarctica in tropospheric altitudes (GÖKTAS, 2002b, SHORT, 2008). Cyclonic systems on the one hand and Antarctic Polar high on the other hand cause meridional transportation of energy, moisture and aerosols into Antarctica (PIEL, 2004). Thus, the key source area for precipitation in DML is reported 50° - 60° S (REIJMER et al. 2002b).

However, precipitation on the Antarctic plateau in DML is not as constant as the scheme of atmospheric circulation might suggest (Figure 4). The annual precipitation in DML is rather formed by few, discrete precipitation events (REIJMER et al. 2001).

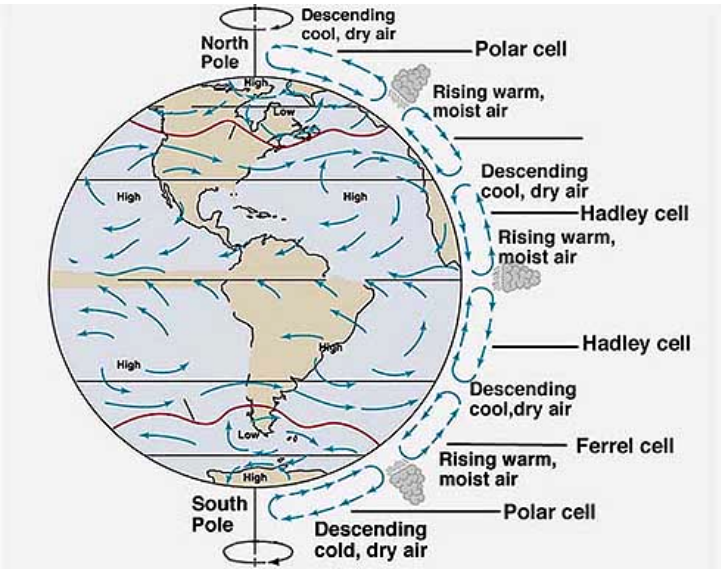

Figure 4: The atmospheric circulation scheme displays the interplay of Antarctic Polar high and Sub-polar low belt resulting in meridional transportation of energy, moisture and aerosols, (SHORT, 2008).

Aerosol of both marine and continental sources is induced into the troposphere, where it travels over far distances around the globe, fuelled by global atmospheric circulation. With advection of air masses from troposphere to the Antarctic continent, tropospheric aerosol becomes subject to depositional processes over the Antarctic ice cap (PIEL, 2004; GÖKTAS, 2002b). The deposition of aerosols can be explained by two processes, wet and dry deposition.

2.2 Dry deposition of aerosol

Dry deposition of aerosol is a process independent from any kind of precipitation. The efficiency of dry deposition strongly depends on the size-distribution of aerosol particles. While dry deposited particles with sizes of ≥ 5 µm are mostly subject to sedimentation, smaller aerosol particles are sensitive to further transport processes (FISCHER, 1997). Particles and gases descend through the atmosphere and meet the viscous sub-layer, which forms a laminar zone just above the snow surface of few millimetres thick or less. Within the viscous sub-layer, particles are subject to diffusion, interception, impaction and turbulent deposition. In contrast, gases dissolute within the viscous sub-layer and adsorb onto snow and ice crystal surfaces (GÖKTAS, 2002b).

The sum of dry depositional processes define the transport resistance parameter R_{dry}, and the velocity of dry deposition defined as $v_{dry} = 1/R_{dry}$. Typical v_{dry} values for Greenland aerosol (Summit) with particle-size distribution of 0.7 µm are 0.02 cm/s for MSA^-, SO_4^{2-}, NH_4^+; 0.07 cm/s for Na^+, K^+, Mg^{2+} and 0.11 cm/s for Ca^{2+} (FISCHER, 1997). The amount of dry deposited aerosol J_{dry} can be calculated according to FISCHER, pers. com., lecture notes:

$$J_{dry} = v_{dry}\, c_{air} \qquad (1)$$

with J_{dry} as total flux of dry deposited aerosol,
c_{air} as air concentration of the respective aerosol

2.3 Wet deposition of aerosol

In contrast to dry deposition, the process of wet deposition sums up all depositional processes that are linked to precipitation. Wet deposition comprises of two main processes, rain out and wash out.

Rain out/In-cloud-scavenging

Aerosol particles are essentially linked to precipitation formation, as they act as either condensation nuclei (CCN) or ice nuclei (IN), providing the surface on which water vapour condensates or freezes. Thus, CCN and IN successively grow in size by further water vapour condensation/freezing or agglomeration of colliding particles and form clouds. This process lasts until formed water droplets or snow crystals precipitate and remove the aerosol as CCN or IN from the atmosphere (PIEL, 2004).

Wash out/Below-cloud-scavenging

On the way to surface, precipitating rain droplets and snow crystals adsorb gases and particulate aerosol. The adsorbed material is, thus, removed out of the air column and gets deposited with the precipitation (PIEL, 2004).

Both processes rain out and wash out define the wash rate in equation 2 (FISCHER, 1997):

$$W = \frac{c_{snow}}{c_{air}} \tag{2}$$

with W as wash rate,
c_{snow} as concentration of the respective aerosol in snow,
c_{air} as concentration of the respective aerosol in air

The following equation 3 explains the total aerosol flux due to wet deposition (FISCHER, pers. com., lecture notes):

$$J_{wet} = W\, c_{air}\, A \tag{3}$$

with J_{wet} as total flux of wet deposited aerosol,
A as accumulation rate

The total flux J_{tot} comprising of wet and dry deposition according to equation 4 (FISCHER, pers. com., lecture notes):

$$J_{tot} = J_{dry} + J_{wet} \tag{4}$$

The total annual flux represents the total amount of deposited aerosol species within individual years. Therefore, the water weighted annual concentration (see chapter 3.4.3) is

multiplied by the annual accumulation in water equivalent (see chapter 3.4.1) (FISCHER, pers. com., lecture notes) according to equation 5:

$$J_{tot} = c_{ice} A \tag{5}$$

Combining equation 1 and 3, the total flux can be expressed as shown in equation 6:

$$J_{tot} = v_{dry} c_{air} + W c_{air} A \tag{6}$$

Where equation 5 and 6 can be converted into equation 7:

$$c_{ice} = v_{dry} c_{air} \frac{1}{A} + W c_{air} \tag{7}$$

Equation 7 proves the mean concentration as measured within the DML snow pits to be inversely proportional to the accumulation rate. This particular relation causes the ion concentrations from samples derived from the snow pits upstream EDML to depend on the systematic spatial changes on annual accumulation (FISCHER, pers. com., lecture notes; MINIKIN, 1994; HUYBRECHT et al., 2007). The discussion of specific ion concentration coinciding with accumulation variability will be subject of chapter (5)

2.4 Irreversible deposition of aerosol

Mineral dust, H_2SO_4 and most of the sea-salt ions are irreversibly removed from the atmosphere, once they are deposited. Therefore, dry and wet deposition processes explain the ion concentrations as measured in DML snow pit samples. However, this is not the case for all deposited aerosols and gases (FISCHER, 1997; PIEL, 2004).

2.5 Reversible deposition of aerosol and gases

In particular chloride, nitrate and methane sulfonate are subject to reversible deposition as consequence of post-depositional processes. During re-crystallisation processes of snow, HNO_3 is removed from snow crystal surfaces and enriches within the non-solid phase (FISCHER, 1997). Furthermore, particle-gas conversion can transfer deposited chloride and nitrate into gaseous HCl and HNO_3 that can be re-emitted from snow surface (WELLER, 2004; RÖTHLISBERGER, 2002a).

2.6 Glaciological background: oxygen isotopes, accumulation, aerosols

The continuous accumulation of well stratified snow on polar ice shields allows for time series analysis of snow chemistry and the reconstruction of atmospheric aerosol compositions of the past. Since the atmospheric composition of aerosols is closely linked to climatic processes, the time series analysis of snow deposited aerosols allows for climatic reconstruction on time scales from glacial to seasonal cycles (FISCHER et al. 2007a; BIGLER et al. 2006; GÖKTAS, 2002b; HARRISON et al. 2000).

Liquid and solid particles suspended in the atmosphere are described as aerosols. Aerosols can be either classified according to their size (GÖKTAS, 2002b; FORTMANN, 2004) or with respect to their genesis as primary or secondary aerosols (PIEL, 2004). While primary aerosols occur in the way they were emitted to the atmosphere, secondary aerosols are generated after precursor substances are emitted into the atmosphere (PIEL, 2004; GÖKTAS, 2002b). The suspension of terrestrial dust in the atmosphere can be considered primary aerosol, while the gas-particle conversion of gaseous nitrogen oxides into particulate nitrate makes nitrate a secondary aerosol (PIEL, 2004; HEWITT & STURGES, 1993).

Recent snow records of sodium, chloride, nitrate, sulphate, methane sulfonate and calcium will be investigated during this study. The following chapter provides an overview on the sources and the deposition of these aerosols and the mechanism driving the $\delta^{18}O$ isotope signal in snow deposits.

2.6.1 Oxygen isotope records

In a strong simplification of the complex global water cycle, water molecules evaporate into the atmosphere where they are transported to their precipitation site from where they will flow in streams and glaciers back to the ocean to eventually evaporate again. During evaporation and precipitation, the isotopic composition of the water molecule changes due to specific fractionation processes. While heavier isotopes Deuterium (D) and Oxygen-18 (^{18}O) have a lower vapour pressure than Hydrogen (H) and ^{16}O, evaporation will enrich the water vapour with lighter isotopes and depletes the residual liquid water (BOWEN, 1991). As the water vapour gets transported away from its source, condensation processes will take place. During the condensation, the heavier isotopes will concentrate in the liquid phase to form clouds and rain out. This will deplete the remaining water vapour in D and ^{18}O even further. Thus, precipitating water gets isotopically lighter and lighter, the further it is transported from its moisture source. Therefore, precipitation contains an isotopic signal that depends on the moisture source and the cooling during transport (DANSGAARD, 1964).

The greatest moisture source within the global hydrological cycle is the evaporation of ocean water. Due to its enormous size, the isotopic composition of the oceans δD and $\delta^{18}O$ is almost stable in recent time (FISCHER, pers. com., lecture notes). Therefore, the measurements of δD and $\delta^{18}O$ from water are compared to the value of the Standardized Mean Ocean Water (SMOW) and are expressed in [‰] according to equation 8:

$$\delta^{18}O\ [‰] = \left(\frac{\frac{H^{18}O^{16}O}{H_2O}}{\frac{H^{18}O^{16}O}{H_2O}_{SMOW}} - 1 \right) \times 1000 \qquad (8)$$

According to equation 8, Figure 5 displays the successive $\delta^{18}O$ depletion of precipitation and water vapour with decreasing temperature. This is the crucial point that makes the $\delta^{18}O$ records of snow and ice essential for dating. On the ice sheet, a pronounced summer and winter temperature variation can be observed. As a consequence, the temperature gradient between the water vapour source and the site of its precipitation is much steeper during winter than during summer time. Accordingly, the winter precipitation is found depleted in $\delta^{18}O$ as compared to the summer precipitation (DANSGAARD, 1964). The seasonal variation of $\delta^{18}O$ can therefore be used to detect summer and winter peaks and support defining accumulation rates.

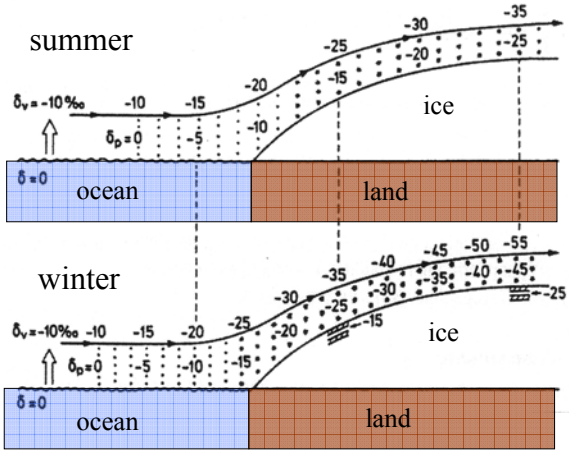

Figure 5: The isotopical depletion of precipitation with distance to its source, taken from FISCHER, pers. com., lecture notes after modification.

2.6.2 Accumulation rate

The accumulation rate is defined as the annual accumulation of snow in water equivalent [mm WE * a^{-1}] and was derived from the dating of the DML snow pits. It provides important information on meteorological characteristics of the study area and is a decisive parameter for the concentrations and fluxes of deposited ions (chapter 2.2 and 2.3). Furthermore, quantification of local accumulation rates serves as reference for mass balance calculations of ice sheets (ANSCHÜTZ, 2006). During this study, the accumulation rate is a basic measure to calculate the water weighted ion concentration for annual periods as well as for the calculation of the ions annual fluxes that will be discussed in chapter (4.2).

2.6.3 Sea-salt aerosol records

By weight, sea-salt aerosol represents the most abundant aerosol species in Earth's atmosphere and origins from oceanic sources (FISCHER et al., 2007a). Sea-salt aerosol comprises mostly of Na^+ and Cl^-, to a lesser extend sea-salt derived ions of Mg^{2+}, Ca^{2+}, K^+ and SO_4^{2-} are also abundant (PIEL, 2004). The most relevant forming process for sea-salt aerosol is the dispersion of sea water as function of wind speed and storminess, thus, the deposition of sea-salt aerosol in Antarctica is closely linked to cyclonic activity of the Southern Ocean (FISCHER et al. 2007; PIEL, 2004; HOFFMANN, 2000). Furthermore, frost flower dispersion on sea surface during sea-ice expansion was recently reported to cause export of sea-salt aerosols from the ocean. This process might also induce deposition of sea-salt aerosol on the Antarctic plateau (RANKIN et al., 2002; GÖKTAS, 2002b; KALESCHKE et al., 2004; FISCHER et al., 2007a).

The two sea-salt aerosol exporting processes are reported of different relative efficiency in exporting individual ions. Sea-salt aerosol derived from frost flowers is depleted in SO_4^{2-} and Na^+ (Na^+ to a lesser extend) due to mirabilite precipitation (FISCHER et al., 2007a). The removal of sea-salt components during mirabilite precipitation impacts on the ratio of non sea-salt versus sea-salt derived aerosols, which can be corrected (BIGLER et al., 2006).

2.6.4 Volcanic sulphate aerosol records

Among other components, considerable amounts of gaseous SO_2 are emitted by volcanic eruptions into the upper troposphere and stratosphere (GÖKTAS et al., 2002b). Gas-particle conversion transfers SO_2 into particulate H_2SO_4 that gets advected around the globe. The time of H_2SO_4 transportation depends on the geographical location of the volcano and the prevailing winds at the time of eruption. After a transportation time of 1-2 years, the volcanic H_2SO_4 signal reaches polar regions (GÖKTAS et al., 2002b), where the deposition of volcanic sulphate compounds results in snow layers of increased sulphate concentration (LEGRAND & MAYEWSKI, 1997; LEGRAND & WAGENBACH 1999; COLE-DAI & MOSLEY-THOMPSON, 1999; TRAUFETTER et al. 2004). The preserved volcanic sulphate signal can be detected by measurements on either snow electrical properties or ion chromatography (GÖKTAS, 2002b).

2.6.5 Biogenic sulphur aerosol records

A product of biogenic productivity in the ocean is the formation of Dimethylsulphide (DMS). DMS is emitted from the ocean into the atmosphere, from where DMS fractions underlie transportation towards the poles. During the transportation, a complex process oxidised DML and forms MSA^- and SO_2 in a so called "branching ratio" of 1:4 beside other sulphur-species (FISCHER, pers. com., lecture notes; PIEL, 2004; GÖKTAS, 2002b). Reaching the Antarctic ice sheet, both biogenic MSA^- and SO_2 deposit in the snow. (Note, MSA^- will be subject to discussion in chapter seasonal variability, only)

2.6.6 Nitrate aerosol records

Particulate nitrate and gaseous nitric acid deposits in Antarctic snow mostly derive from stratospheric nitrate input into Antarctica (WAGENBACH et al., 1998). On its way into Antarctica, it is built from oxidation products of nitrogen oxide (NO, NO_y) oxidation (WELLER et al., 2002; PIEL, 2004). Two main sources are described for NO and NO_y. First, biogenic processes of nitrification and denitrification occur in the ocean and soils, from where they cause NO and NO_y emissions due to outgassing from the ocean and soil exhalation (FLÜCKIGER et al., 2002; FLÜCKIGER et al., 2004). Second, the combustion of fossil fuels accounts for an anthropogenic compound of NO and NO_y emissions (HEWITT, C. N., W. T. STURGES, 1993). The conversion into nitrate in Antarctica is induced by either lightning (WELLER et al., 2002; PIEL, 2004) or descending polar stratospheric clouds from polar stratosphere (containing N_2O and NO_y). In Antarctic atmosphere, both nitrogen species NO_3^- and HNO_3 occur at the same time (FISCHER, pers. com., lecture notes).

2.6.7 Mineral dust aerosol records

Natural mineral dust aerosols are an important component of both, climate systems and biogeochemical systems, where they serve as ice or droplet nuclei to from precipitation (STAFFAN, 2007; LILJEQUIST & CEHAK, 1994), impact the global radiation budget (HARRISON et al., 2000) or fuel marine biological activity (FAN et al., 2003). Processes of rock weathering and dust raising winds enable the dispersion of fine grained continental crust material into the atmosphere (HARRISON et al., 2000). Depending on the particle size and prevailing wind systems, dust particles can be uplifted into the troposphere and transported over far distances (HARRISON et al., 2000). Thus, dust particles deposit in Antarctica where they accumulate in accumulated of snow and ice and allow for time series analysis in ice core records in order to study dust transport and source variability (FISCHER et al., 2007a; BIGLER et al., 2006; RÖTHLISBERGER et al., 2002b; FISCHER et al., 2007b; BIGLER et al., 2006; PIEL, 2004; and RÖTHLISBERGER et al., 2002b) describe Patagonia to be the key source area for mineral dust deposited in DML during glacial times, while PIEL, 2004 also discusses the recent mineral dust deposits in DML to be of Patagonian origin. In this study, non sea salt calcium ($nssCa^{2+}$) is used as proxy for spatial variability of mineral dust. Since calcium also derives from sea-salt aerosol, the $nssCa^{2+}$ fraction had to be calculated as described in chapter (3.4.6). (Note, $nssCa^{2+}$ will be subject to discussion in chapter seasonal variability, only)

3. Methods

This chapter gives an overview on the preparation of the sampling gear for the field campaign and describes the applied methods during measurements and data processing.

3.1 Methods of preparation and sampling

3.1.1 Decontamination of field equipment

To allow for accurate determination of ion concentrations in Antarctic firn with typical concentrations of 1-100 ppb, it is essential to ensure reliable decontamination of all equipment that gets in contact to the snow. To prepare for the field campaign, all respective tools and containers were subject to an extensive, standardized cleaning procedure in the clean room facilities of the AWI.

The tools were rubbed with Isopropanol and underwent 3 cycles of rinsing with de-ionized Milli-Q water (MQ water, R > 18MΩ). The sample containers were rinsed 3 times with MQ water before they were soaked in MQ water for 24 hours. Afterwards, the electrical conductivity (EC) of the MQ water was randomly measured to determine the level of residual ions. MQ-water that is in equilibrium state with atmospheric CO_2 displays an EC value of 0.55 µS/cm. If the MQ-water in which the items were soaked showed EC values of ≤ 0.55 µS/cm the items were considered clean, if the threshold of 0.55 µS/cm was violated, the item had to undergo a further cleaning cycle. The cleaned equipment was carefully wrapped in Polyethylene (PE) foil to prevent from further air contact. Just before the samples were taken during the field campaign, the tools were first rubbed with Isopropanol and second with the cleanest material available: snow.

During the decontamination process, the high resolution sampling containers (UTS) were thoroughly controlled for EC applying a random control system. In addition ion chromatographic analyses on de-ionized water filled into one UTS container showed no

contamination. Despite the containers passing these tests, all Calcium samples were found to be highly contaminated. Whether this is due to an insufficient cleaning protocol that was not detectable or by post-sampling contamination during transport of the filled containers back to Bremerhaven cannot answered at this point. A contamination during sampling can be ruled out, since the UTD samples that were filled in parallel, showed no signs of contamination.

3.1.2 Firn sampling in high resolution

For the purpose of sampling the top firn layer in the very high resolution of 1.5 cm new sampling containers, named UTS, were constructed for the AWI. Each of the UTS had a length of 30 cm and had the capacity of holding 20 samples of 55 cm^3, each 1.5 cm in length (Figure 6). By using 7 UTS at each snow pit, 140 samples were taken with a sampled firn column of 2.10 m.

Just before the samples were taken, the first centimetres of the snow pit wall were removed with a pre-cleaned spatula to prevent contamination. Then, the UTS containers were pressed into the cleaned pit wall at the distinct depth.
Tight stainless steal housings were slid over the UTS to cut the UTS off the surrounding snow and to seal it before they got further enwrapped in foil. Potentially, the stainless steel lids may have contributed to the calcium contamination.

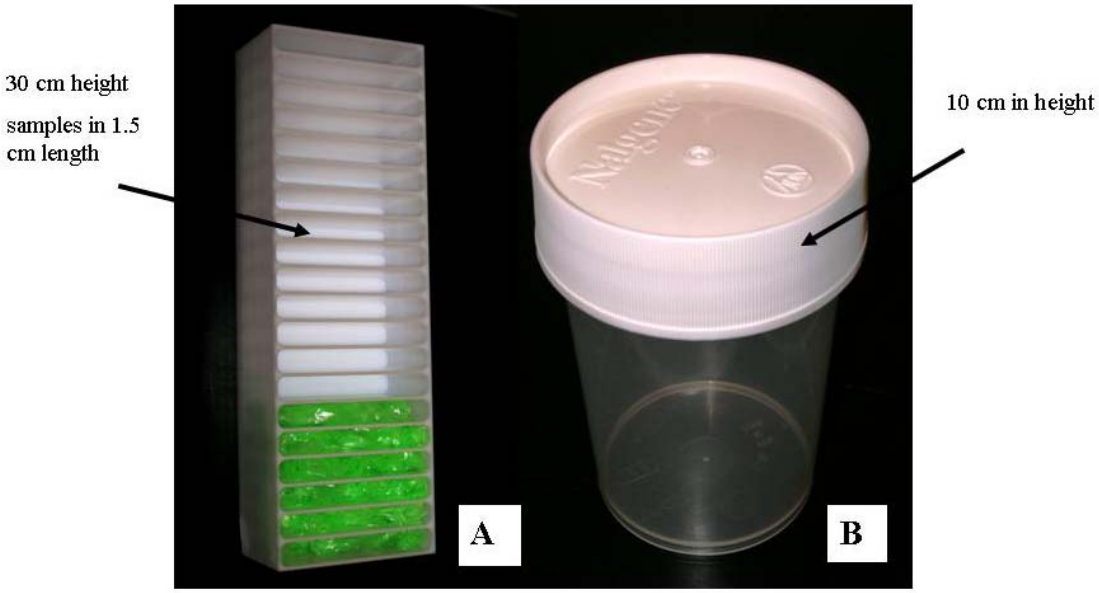

Figure 6: Picture A displays a view onto the UTS sampling container front which is pressed into the snow to aliquot the samples. The 6 lowermost compartments are stuffed with green laboratory gloves to increase the contrast in the picture. Figure B shows a Nalgene sampling container. Note that pictures A and B are assembled and do not display the real size ratio of the UTS and UTD container.

3.1.3 Firn sampling in coarse resolution

The well established coarse resolution sampling method (GÖKTAS, 2002; FISCHER, 1998), named UTD, was applied right beside the UTS samples (Figure 6). UTD measurements were used to control the high resolution UTS method and to determine the snow density of the firn column. During the UTD sampling procedure, stainless steel sheets were horizontally pressed in the pit wall at the defined 10 cm depth intervals. In the next step, the Nalgene containers were pressed top down onto the horizontal steel sheet as depth control, thus, ensuring the greatest possible sampling accuracy with respect to the density measurements. After each sample was taken, the Nalgene containers were sealed with a pre-cleaned screwcab.

3.2 Analytical laboratory methods

This study comprises of the qualitative and quantitative determination of the ion concentrations from the DML 76-90 snow pit samples in high and low resolution using Ion Chromatography (IC).

3.2.1 Measurements on the oxygen isotope ratio $\delta^{18}O$

Aliquots of 7 ml (melted snow) were measured for the oxygen isotope composition from each sample by using a Finnigan Delta S mass spectrometer and a standard CO_2 equilibration method. The precision of $\delta^{18}O$ determination is given at 0.1 ‰. The $\delta^{18}O$ data were provided by OERTER, pers. com., 2007.

3.2.2 Calculation of the snow density

The snow density data (ρ_S) were provided by OERTER, pers. com., 2007. The snow density was determined by dividing the known sample volume (V_{snow}) of the Nalgene container by the mass difference of the Nalgene container including the sample (m_{snow}) and the empty Nalgene container (m_0) according to equation 9:

$$\rho_{snow} = \frac{V_{snow}}{(m_{snow} - m_0)} \qquad (9)$$

3.2.3 Theoretical bases of the applied IC method

Chromatography is defined as a process to separate a mixture into its individual components. In the specific case of Ion Chromatography (IC), soluble inorganic ions and organic acids are separated within a flowing system. In the IC system, the flowing sample (referred to as mobile phase) is pumped through a separation column (considered stationary phase) where the analyte separation takes place as a function of the analytes affinity to the stationary phase. The higher the affinity of a certain analyte species to the stationary phase, the more time it

will take to pass through the separation column as compared to other analytes. This analyte specific amount of time is called retention time and forms the base of the ion chromatographic separation (MEYER, 2004; WESTON & BROWN, 1997).

Using this affinity-depending process for the analyte separation, IC requires two separate units, one for anions and one for cations, which mostly differ in the types of columns. The system works according to the isocratic principle, meaning it works with constant eluent concentrations. The Ion Chromatographs consist of a sequence of functional units as shown in Figure 7 and Table 1.

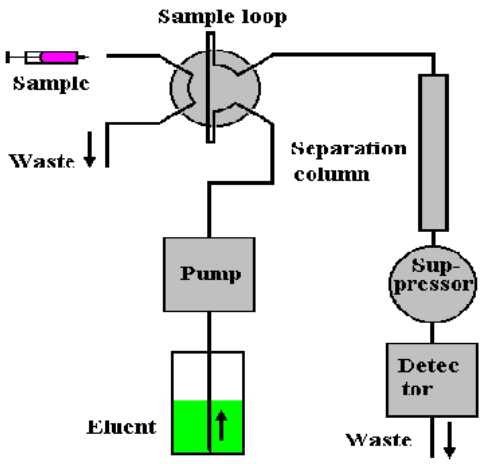

Figure 7: IC units and IC flow scheme

After separation in the separation columns (Figure 7), the eluent transports the analyte ions through a suppressing unit which replaces the eluent ions from the solution by either H^+ or OH^-, for cation and anion IC, respectively. Thus, the suppressor decreases the background conductivity and increases the signal strength of the analysed ion which is essential for the detection of ions in very low concentration (MEYER, 2004; WESTON & BROWN, 1997).

After passing the suppressor, the separated analytes pass the detector cell, which determines the analyte concentration by measuring the electrical conductivity of the eluent over time. By knowing the specific retention time, the ions can be identified in the chromatogram. Technically, the concentration of the ions was measured by comparing the peak area and peak height of the analyte ions to the peak area and peak height of applied standards of well-defined concentration (MEYER, 2004; WESTON & BROWN, 1997).

The IC unit is connected to a PC, which operates the IC unit, generates a database and compiles Ion Chromatograms for analysis. For more information about IC, see MEYER, 2004 or WESTON & BROWN, 1997.

3.2.4 Anion IC system

During the "load" phase of the anion flow scheme, the anion sample was routed through a sample loop by an automatic sampler while the eluent passed the guard column prior to the separation column. As eluent, 20 mM KOH was used at a flow rate of 0.25 ml min^{-1}. As guard and separation column, Dionex AG 18 (Ø * length = 2 mm * 50 mm) and Dionex AS 18 (Ø * length = 2 mm * 250 mm) were installed, respectively. See Table 1 for more information on the single modules installed in the anion IC unit. To reduce the memory effects from the previous sample, a fraction of each anion sample is pumped through the sample loop into the waste until the valve changes the flow scheme of the system. The eluent is pumped through the sample loop so it transports the sample onto the guard column and eventually onto the separation column and the ion separation process takes place. The anion IC of the AWI detects bromide (Br^-), chloride (Cl^-), fluoride (F^-), methane sulfonate (MSA^-), nitrate (NO_3^-) and sulphate (SO_4^{2-}).

3.2.5 Cation IC system

In contrast to the sample loop of the anion system, the cation system consists of a pre-concentration column (Dionex, TCC-LP1, Ø * length = 4 mm * 35 mm) to rise the cations concentration relative to the eluent. Subsequently, the eluent (which was MSA, 21 mM) flows through the pre-concentration column in opposite direction of which it was charged. The eluent transports the condensed cations through the guard column and eventually through the separation column, where Dionex CG 12A (Ø 4 mm * 50 mm) and Dionex CS 12A (Ø 4 mm * 250 mm) were installed, respectively. To find more information on the single units the IC consisted of, please see Table 1. Potentially, calcium (Ca^{2+}), potassium (K^+), magnesium (Mg^{2+}), sodium (Na^+) and ammonium (NH_4^+) can be detected by the cation IC at the AWI.

Table 1: Identification of all components within the anion and cation units

Unit	anion IC	cation IC
IC	Dionex, IC 20	Dionex, IC 20
separation column	Dionex, AS 18, Ø2*250 mm	Dionex, CS 12A, Ø4*250 mm
guard column	Dionex AG 18, Ø2*50 mm	Dionex, CG 12A, Ø4*50 mm
pre-concentration column	----	Dionex, TCC-LP1, Ø4*35 mm
sample loop	300 µl	----
suppressor	Dionex, ASRS ultra2, Ø2 mm	Dionex, CRS ultra2, Ø4 mm
eluent generator	Dionex, EG 40	Dionex, EG 40
eluent	KOH, 20 mM	MSA, 21 mM
eluent flow rate	0.25 ml*min^{-1}	1 ml*min^{-1}
IC enclosure	Dionex, LC 20	Dionex, LC 20
Auto sampler	Dionex, AS 40	Dionex, AS 40
run time	17 minutes	20 minutes

3.2.6 Procedure of IC measurements in the laboratory

All laboratory items that came in contact to the samples underwent a standardized protocol of decontamination. The items were rinsed three times and soaked for 24 hours in MQ water before they were checked for contamination by measuring EC prior to their use. If an EC threshold value between 0.55 µS/cm and 0.8 µS/cm was violated, the respective item was not considered clean and had to undergo a further sequence of decontamination. Sample volumes of 1.5 ml and 2.5 ml were applied for anion and cation analysis, respectively.

The IC measurements were conducted by the IC instruments executing a programmed sampling schedule. Each schedule consisted of 80 to 90 samples (depending on UTS or UTD measurements), 42 measurements of reference standards S1-S7 for the IC calibration, 4 Dionex standards DS 2-DS 5 to determine accuracy and reproducibility, as well as 25 MQ water samples. The latter were either used as blanks or to prevent the system from memory effects, after high concentrated standards were applied.

During this study, 140 high resolution samples per snow pit as well as 21 coarse resolution samples per snow pit were measured from 10 snow pits for anion and cation IC, thus accounting for a total number of 1610 samples and 3220 measurements.

3.3 Quality of measurements

3.3.1 Calibration of IC measurements

The IC system determines the composition of ions from a sample as a function of retention time and peak height/area. Therefore, the IC compares the unknown signal of the sample to the well defined signals of the calibration standards S1-S7 to quantify the sample concentration. In every schedule, 4 calibration standards of increasing concentration level are used to generate the calibration curve by regression analysis. Linear regression analysis was applied to all ions (apart from NH_4^+) and showed regression coefficients of about $r^2 = 1$. In case of NH_4^+, exponential analysis indicated $r^2 = 1$, (Figure 8).

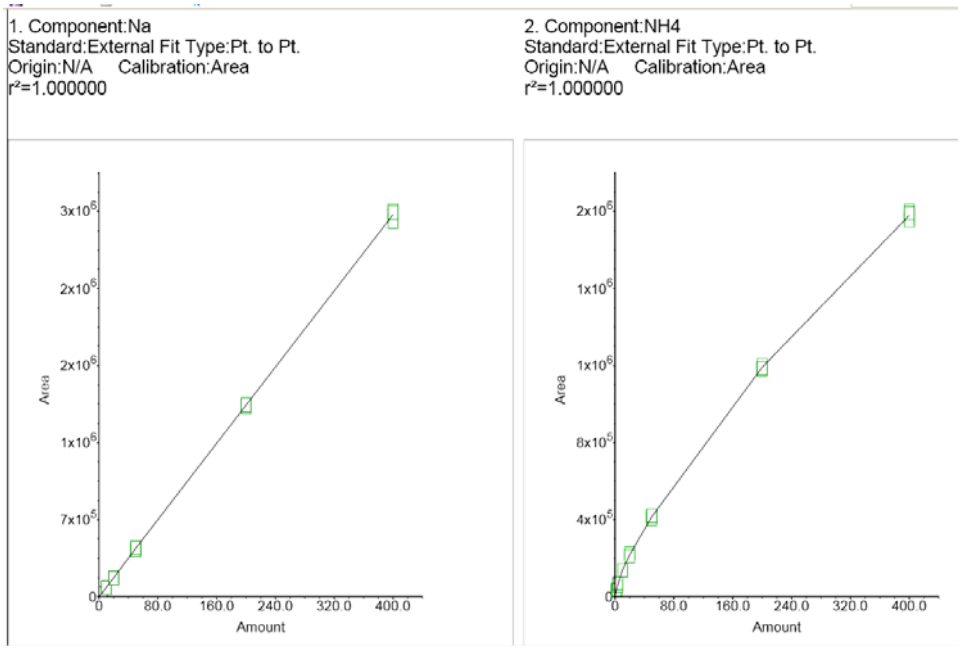

Figure 8: Regression analysis of calibration curves results of cation IC calibration using linear regression analysis for Na^+ and exponential regression analysis for NH_4^+. The coefficient is determined to be $r^2 = 1.0$ for all cations.

3.3.2 Accuracy of IC measurements

The accuracy of measurements shows the closeness of received measurement results to the theoretical value and is calculated according to equation 10:

$$\text{Accuracy [ppb]} = \text{actual concentration [ppb]} - \text{DS [ppb]} \qquad (10)$$

Unfortunately, the performance of cation measurements from all UTS and three UTD samples (DML 76, 77 and 90) is biased by a systematic error that lead to an underestimation of cation concentrations. This particularly affected the measurements of NH_4^+, K^+, Mg^{2+}, and Ca^{2+}, as these ions appear in very low concentrations (0.1 and 3.8 ppb). The error was unambiguously attributed to aging effects of the pre-concentration column and, thus, solved. The accuracy was calculated separately for the cation measurements using the old and the new pre-concentration column. Both calculations revealed an accuracy of 0.0 for Na^+ (Table 2). Therefore, all measurement runs of anions and Na^+ were considered accurate. As most of the UTD samples were measured using the new pre-concentration column, accurate cation concentration data are available in coarse resolution for all snow pits but DML 76, 77, and 90. Table 2 shows the accuracy as calculated for all anion and cation measurements using the old and the new pre-concentration column and indicates the improvement of accuracy after the renewing. The displayed DS levels are closest to the measured concentrations of the samples.

Table 2: The accuracy of IC measurements as calculated for anions and cations. Note the cation data were split for accuracy calculation according to measurements using the old and the new pre-concentration column.

		Na^+ [ppb]	**NH_4^+ [ppb]**	**K^+ [ppb]**	**Mg^{2+} [ppb]**	**Ca^{2+} [ppb]**	**F^- [ppb]**	**Cl^- [ppb]**	**SO_4^{2-} [ppb]**	**NO_3^- [ppb]**
	DS aim	**25**	**12.5**	**25**	**12.5**	**25**	**2**	**25**	**50**	**50**
old	DS actual	25.0±0.6	4.7±1.9	21.4±2.3	9.1±0.5	17.0±1.5	2.0±0.4	25.4±0.8	52.7±2.9	54.3±6.2
column	**Accuracy**	**0**	**-7.8**	**-3.6**	**-3.4**	**-8**	**0**	**0.4**	**2.7**	**4.3**
new	DS actual	25.0±0.3	4.6±2.6	23.2±0.9	11.1±0.4	23.0±1.0				
column	**Accuracy**	**0**	**-7.9**	**-1.8**	**-1.4**	**-2**				

Figure 9 displays, how the accuracy evolved for the cations during the measurements of 17 measurements using the old pre-concentration column and the three last runs using the new pre-concentration column. The ideal value of 0 ppb is marked with a bold line. Particularly in case of Mg^{2+} and Ca^{2+} measurements, the accuracy improved significantly due to the renewed pre-concentration column and ranges around 2 ppb ± 1 ppb. Only NH_4^+ remained significantly below the expected value, which is related to contamination in NH_4^+ by NH_3 within the laboratory air (FISCHER, 1997).

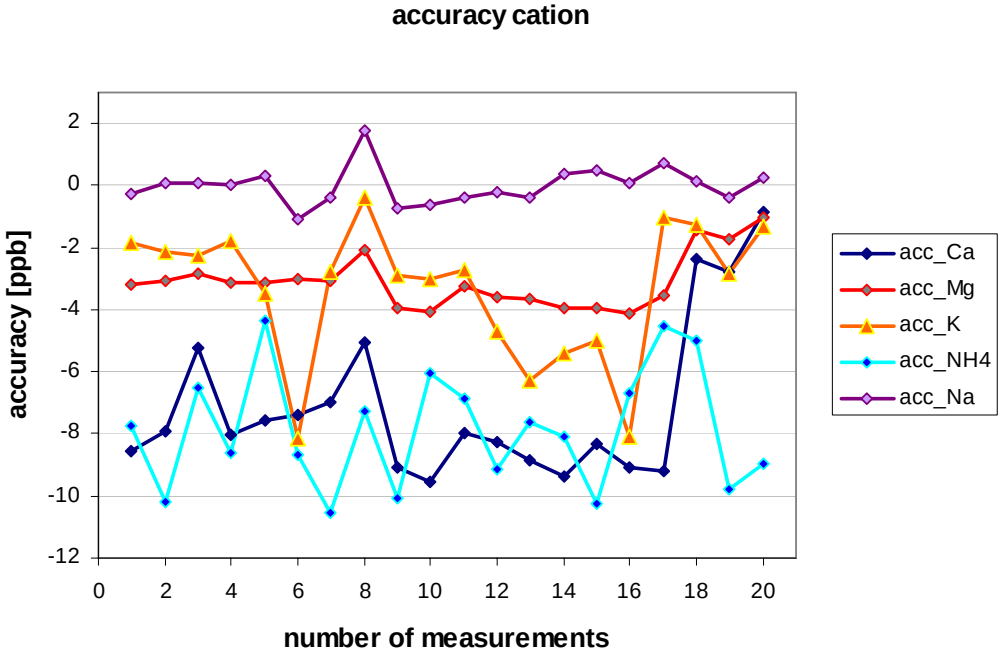

Figure 9: Development of accuracy during all 20 cation measurement runs displayed for all detected cations: Ca^{2+}, K^+ Na^+, NH_4^+ and Mg^{2+}. Note the improvement of accuracy for Ca^{2+}, K^+ and Mg^{2+} during the last runs and the general inaccuracy of NH_4^+ due to air contaminations.

During the analysis of the of DS (DS 3 – DS 5), outlying concentration values which deviated more than 20 % from the theoretical concentration were considered wrong and were, thus, deleted. (The low concentrated DS 2 was expected to vary strongly and was not tested for outliers.)

Concerning the anions, 14 DS values out of all 400 DS were found to be more than 20% off the theoretical DS concentration. Out of these outlying 14 DS values, 8 were clustered (NO_3^- and Br^-) suggesting a contamination during the processing of the affected DS. This could be

proven by comparing the DS error to the MQ blank measurements of the same schedules. The respective MQ blank measurements revealed a mean variation of only 2 ppb indicating no contamination. Thus, the MQ blank values verify the measurements and justify the deletion of the mismeasured DS. The other 6 outliers of anion Dionex standards were randomly allocated within the whole dataset.

Out of all DS cations measurements, 4 DS samples were found to deviate more than 20 %. These deflections were demonstrable based on a wrong standard composition of DS 5, since all cation measurements of the same standard DS 5 were affected by the same ratio (schedule UTD 008-UTD 011) (measurement # 20, Appendix, Figure 52).

Summary

- The accuracy test proved the data of Na^+, Cl^-, SO_4^{2-}, and NO_3^- to be accurate in all UTS and UTD measurement runs.
- Due to the renewed pre-concentration column, all following cation measurements of UTD samples from the snow pits DML 78-89 were considered accurate, apart from NH_4^+.

3.3.3 Precision of IC measurements

The precision of measurements represents the degree of scattering to which repeated measurements of the same samples under prescribed conditions generate reproducible results. The precision is a measure of how changing conditions, such as different analysts, temperature variations etc. can affect the measurements (MEYER, 2004; BLIESNER, 2004). In addition, the reproducibility strongly depends on the absolute concentration, since low concentrated samples and standards are particularly vulnerable to be affected by blank contamination. The reproducibility is expressed as relative error and calculated according to equation 11:

$$\text{Reproducibility [\%]} = \frac{2*\sigma}{\mu} * 100 \qquad (11)$$

μ represents the mean value of the tested DS of the same concentration level

σ represents the standard deviation of the tested DS of the same concentration level

As expected, higher relative errors can be observed in lower DS concentrations according to Figure 10. The high variations of relative errors within the standards of lowest concentration also appeared in FISCHER (1997) and MINIKIN (1994) and were therefore justified and accepted for this study. For the determination of reproducibility, outlying data of DS 3-DS 5 measurements were identified according to the description in chapter (3.3.2) and were not considered for the determination of reproducibility. Table 3 provides an overview on all theoretical and means of measured ion concentrations from DS.

Table 3: Direct comparison of scheduled and the mean of actual concentration of each ion in all DS levels.

DS of anion measurements

	F^-		Cl^-		Br^-		SO_4^{2-}		NO_3^-	
DS level	**DS [ppb]**	**sample [ppb]**	**DS [ppb]**	**sample [ppb]**	**DS [ppb]**	**sample [ppb]**	**DS [ppb]**	**sample [ppb]**	**DS [ppb]**	**sample [ppb]**
DS2	2	2.0±0.4	10.00	10.5±1.0	10.00	10.4±0.8	10.00	10.3±0.5	10.0	10.9±1.7
DS3	5	5.0±0.4	25.00	25.4±0.8	25.00	25.7±1.9	25.00	25.7±3.2	25.0	25.6±3.0
DS4	10	10.1±0.4	50.00	51.3±1.8	50.00	51.5±5.0	50.00	52.6±2.9	50.0	52.5±6.2
DS5	25	25.3±1.9	125.00	127.9±2.3	125.00	127.6±6.9	125.00	133.3±7.1	125.0	127.6±14.2

DS of cation measurements using old pre-concentration column

	Na^+		NH_4^+		K^+		Mg^{2+}		Ca^{2+}	
DS level	**DS [ppb]**	**sample [ppb]**	**DS [ppb]**	**sample [ppb]**	**DS [ppb]**	**sample [ppb]**	**DS [ppb]**	**sample [ppb]**	**DS [ppb]**	**sample [ppb]**
DS2	10	9.9±0.6	12.50	4.7±1.9	25.00	21.4±2.3	12.50	9.1±0.5	25.0	17.0±1.3
DS3	25	25.0±0.7	31.25	11.6±2.5	62.50	58.3±4.3	31.25	27.3±0.7	62.5	56.0±1.8
DS4	50	50.1±1.8	62.50	24.5±3.42	125.00	116.8±8.3	62.50	56.4±1.4	125.0	118.3±3.5
DS5	125	126.9±5.2	156.25	69.3±5.0	312.50	297.3±16.8	156.25	144.5±2.1	312.5	304.8±3.7

DS of cation measurements using new pre-concentration column

	Na^+		NH_4^+		K^+		Mg^{2+}		Ca^{2+}	
DS level	**DS [ppb]**	**sample [ppb]**	**DS [ppb]**	**sample [ppb]**	**DS [ppb]**	**sample [ppb]**	**DS [ppb]**	**sample [ppb]**	**DS [ppb]**	**sample [ppb]**
DS2	10	9.4±0.2	12.50	4.6±2.6	25.00	23.2±0.9	12.50	11.1±0.4	25.0	23.0±1.0
DS3	25	25.0±0.3	31.25	11.0±3.1	62.50	59.0±0.3	31.25	29.7±0.2	62.5	62.0±0.5
DS4	50	49.4±2.4	62.50	24.5±2.1	125.00	115.7±2.9	62.50	58.2±1.9	125.0	122.0±3.8
DS5	125	124.8±1.0	156.25	72.1±2.6	312.50	289.1±1.5	156.25	147.2±1.1	312.5	308.2±2.5

Relative error calculations of DS measurements revealed an adequate reproducibility except for K^+ and NH_4^+. FISCHER (1997) and MIEDING (2004) describe high relative errors in NH_4^+ as consequence of unavoidable NH_3 contamination by the laboratory atmosphere. The measurements of K^+ and NH_4^+ also failed in their accuracy as shown in chapter (3.3.2) and will no longer be part of any further discussion. Reproducibility determinations for all anions and cations are displayed in Figure 10.

Table 4: Relative errors of all detected ions in dependence of the according DS concentration

level	F^- [%]	Cl^- [%]	Br^- [%]	SO_4^{2-} [%]	NO_3^- [%]	Na^+ [%]	NH_4^+ [%]	K^+ [%]	Mg^{2+} [%]	Ca^{2+} [%]
DS2	37	19	15	10	31	12	83	21	19	28
DS3	14	6	10	9	13	5	43	14	8	10
DS4	7	7	9	11	10	7	26	13	6	6
DS5	5	4	4	11	7	8	14	11	3	2
mean	16	9	10	10	15	8	42	15	9	12

Summary

- The precision of measurements was found at a satisfactory level of < 15 % for F^-, Cl^-, Br^-, SO_4^{2-}, NO_3^-, Na^+, K^+, Mg^{2+}, and Ca^{2+} with improving precision with increasing concentration, where the blank variability becomes less important.
- The precision of 41.5 % is considered very poor for NH_4^+.

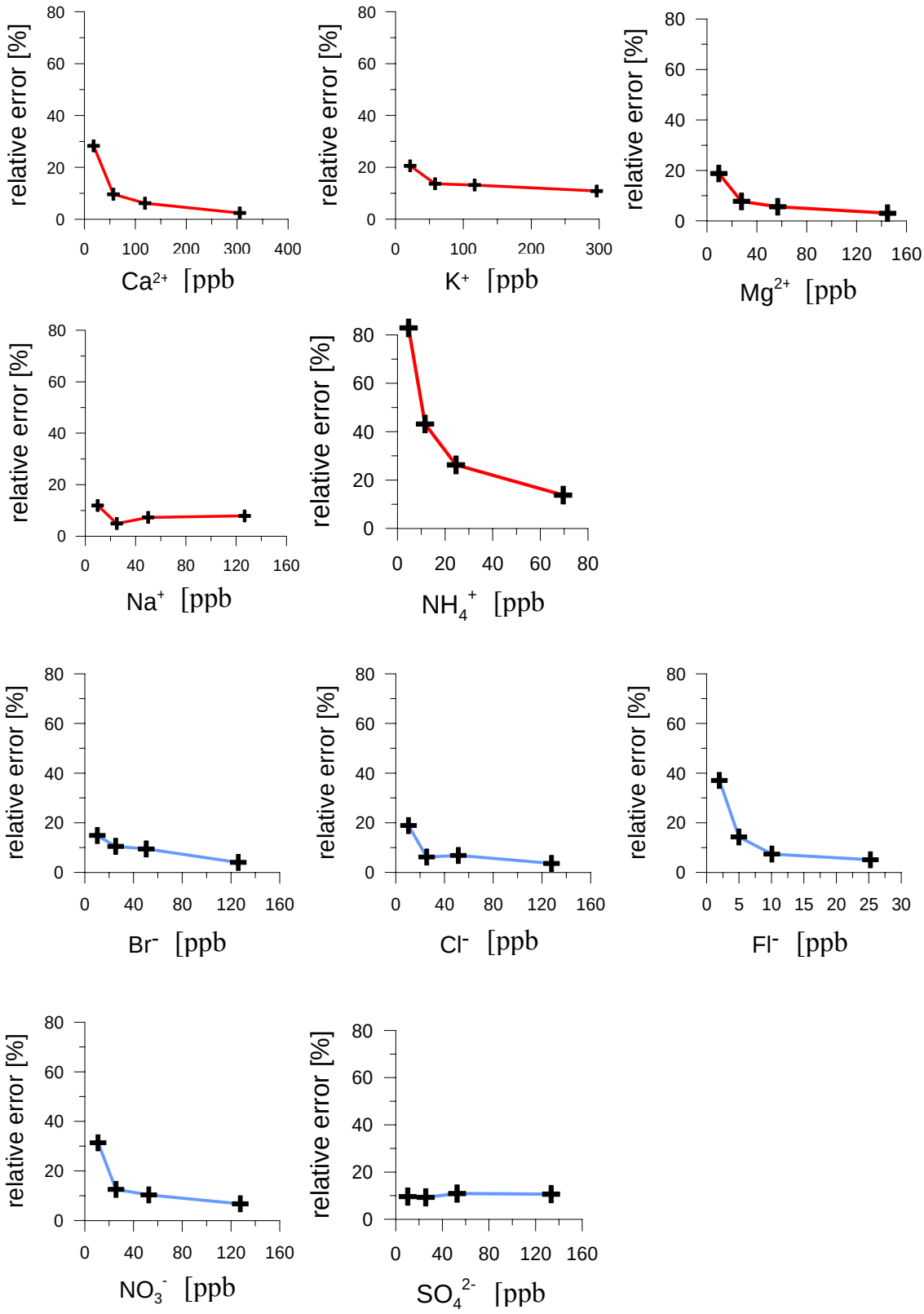

Figure 10: Displays the relative errors of IC measurements over mean concentrations of individual ions, for all concentration levels of DS. Generally, decreasing errors with increasing DS level were observed.

3.3.4 Test for contamination, validation of UTS by UTD samples

The UTS sampling method was introduced as a new technique. To test if the new technique allows for reliable ion measurements, the UTS results were compared to results of the established sampling method using UTD containers, Figure 6. For the contamination test, the mean ion concentration of the entire UTS and UTD samples per snow pit was compared. Comparing the mean of UTS and UTD over the whole sampling length levelled out potential errors resulting from stratigraphic differences between the two records.

The mean water weighted ion concentrations (3.4.3) of all ions were calculated from UTS and UTD samples. The results of Ca^{2+}, Na^{+}, Cl^{-}, NO_3^{-}, and SO_4^{2-} from all snow pits are displayed in the Tables 5-9. Column 1 names the snow pit location, column 2 and 3 display the water weighted concentration values [ppb] of UTS and UTD, respectively. Column 4 and 5 display the deviation of UTS to the reference UTD values in absolute concentration [ppb] and relative values [%], respectively.

The Ca^{2+} concentrations of UTS samples were constantly overestimated compared to the UTD samples by more than one order of magnitude which could only be explained by contamination of UTS as shown in Table 5.

Table 5: Comparison of the Ca^{2+} measurement results derived from UTS and UTD sampling method. The test reveals the UTS samples to be highly contaminated in Ca^{2+}.

snow pit	Ca^{2+}, UTS [ppb]	Ca^{2+}, UTD [ppb]	abs. error [ppb]	relative error [%]
DML 76	64	3	61	1840
DML 77	105	3	103	3517
DML 79	92	2	90	4183
DML 81	112	2	110	5499
DML 83	101	2	99	5119
DML 85	110	2	109	6229
DML 87	105	2	103	4251
DML 88	103	2	101	5496
DML 89	103	2	101	4185
DML 90	83	3	80	3143

According to table 6, the UTS Na^+ records exhibit a slight overestimation of 1.5 ppb or ~10 % for DML 77, 79, 81, and 89. The overestimation increases for DML 83, 85, 88, and 90, respectively and reaches up to 10 ppb or 81 % at DML 83. Accordingly, Na^+ contamination may have occurred in those UTS samples. Only in DML 76, UTS show an underestimation of Na^+ as compared to UTD.

Table 6: Comparison of Na^+ measurement results derived from UTS and UTD sampling method. The test reveals higher concentrations in the UTS samples of DML 83 and 85 than in the respective UTD samples. However, the mean Na^+ concentration of DML 83 and 85 ranges in an order of magnitude that is comparable to other snow pit records and to other publications from DML (GÖKTAS, 2002).

snow pit	Na^+, UTS [ppb]	Na^+, UTD [ppb]	abs. error [ppb]	relative error [%]
DML 76	22	23	-1	-5
DML 77	16	15	2	11
DML 79	15	13	2	12
DML 81	15	14	2	11
DML 83	23	13	10	81
DML 85	16	11	5	43
DML 87	16	14	2	15
DML 88	15	12	3	24
DML 89	15	14	2	11
DML 90	18	14	4	26

Figure 11 shows a graphical comparison between UTS and UTD records of Na^+ and Cl^- samples from DML 83 and DML 77. In DML 83, the UTD concentrations range at the base level of UTS samples in both, Na^+ and Cl^- records. In contrast, UTD records for Na^+ and Cl^- follow the amplitude observed in UTS samples at DML 77. Even though DML exhibits comparably high values for Na^+ and Cl^- (Table 6 and 7) which suggests contamination of UTS samples, the maximum concentration of DML 83 varies in comparable ranges. Thus, the divergence between UTS and UTD in DML 83 could also be due to high local variability of Na^+ and Cl^- deposition.

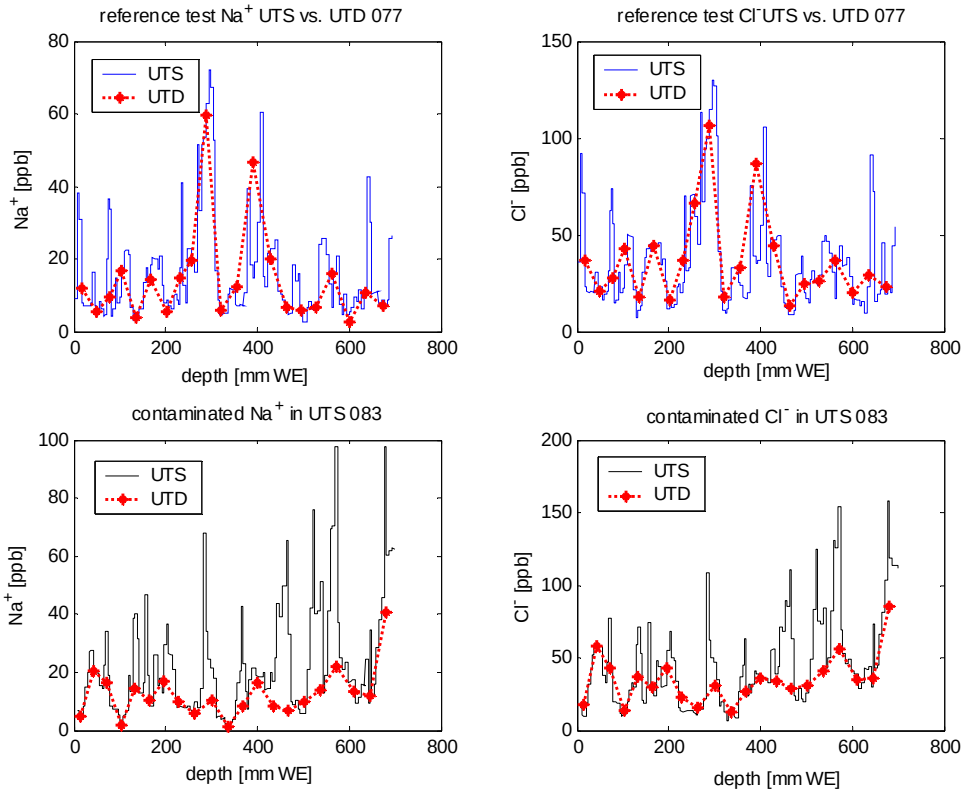

Figure 11: Comparison of UTS and UTD measurements for Na^+ and Cl^- of uncontaminated (DML 77) and of contaminated snow pits (DML 83).

UTS and UTD measurements for Cl^- correlate throughout most of the DML snow pits on a deviation of < 2 ppb or < 5 % as displayed in Table 7. The DML snow pits 83 and 85 were overestimated by 11 ppb and 6 ppb (31 % and 20 %, respectively). In comparison to UTD, the UTS samples of 83 and 85 show higher values of Na^+ and Cl^- in almost the same ratio for both of the snow pits.

Table 7: Comparison of the Cl^- measurement results derived from UTS and UTD sampling method. The test revealed the high resolution samples of DML 83 and 85 to show higher concentrations than the respective coarse resolution samples. However, the mean Cl^- concentration of DML 83 and 85 still ranges in an order of magnitude that is comparable to other snow pit.

snow pit	Cl^-, UTS [ppb]	Cl^-, UTD [ppb]	abs. error [ppb]	relative error [%]
DML 76	49	50	-1	-3
DML 77	37	37	0	0
DML 79	35	34	1	2
DML 81	40	38	1	4
DML 83	46	35	11	31
DML 85	37	31	6	20
DML 87	41	40	0	1
DML 88	39	37	1	4
DML 89	40	39	0	0
DML 90	42	40	2	5

As shown in Table 8, the DML snow pit measurements for NO_3^- are almost on the same level for all the UTS and UTD measurements. Comparable to Na^+ and Cl^-, the values for snow pits DML 83 and 85 display an insignificant overestimation for NO_3^- of 3 ppb and 4 ppb or 6 % and 8 %, respectively.

Table 8: Comparison of the NO_3^- measurement results derived from UTS and UTD sampling method.

snow pit	NO_3^-, UTS [ppb]	NO_3^-, UTD [ppb]	abs. error [ppb]	relative error [%]
DML 76	51	53	-1	-2
DML 77	61	64	-3	-5
DML 79	57	59	-1	-2
DML 81	56	53	2	4
DML 83	49	47	3	6
DML 85	49	46	4	8
DML 87	43	52	-8	-16
DML 88	39	41	-1	-4
DML 89	39	41	-2	-5
DML 90	33	33	0	1

According to Table 9, the SO_4^{2-} concentrations of UTS and UTD samples of DML 76-83 range from 66 ppb to 90 ppb where they agree within 12 % to 18 %. In contrast, the snow pits with mean water weighted SO_4^{2-} concentrations > 100 ppb do agree on a level that is better that 10 %.

Table 9: Comparison of the SO_4^{2-} measurement results derived from UTS and UTD sampling method.

snow pit	SO_4^{2-}, UTS [ppb]	SO_4^{2-}, UTD [ppb]	abs. error [ppb]	relative error [%]
DML_076	66	58	8	14
DML_077	80	68	12	18
DML_079	78	68	10	15
DML_081	93	82	11	14
DML_083	90	81	9	12
DML_085	101	94	7	7
DML_087	104	101	3	3
DML_088	91	85	6	7
DML_089	113	103	10	9
DML_090	106	101	4	4

3.3.5 Results of tests for contamination and quality of measurements

As discussed in chapter (3.3.2 and 3.3.3), the data of Na^+, Cl^-, NO_3^-, and SO_4^{2-} allowed for reliable data quality. In contrast, Ca^{2+} and Mg^{2+} of UTS samples suffered from either unreliable measurements or contamination. In the following only UTS and UTD samples are considered, which show no sign of significant contamination. That rules out K^+ and NH_4^+ ions, as they are always subject to elevated blank levels due to the laboratory protocol and are, therefore, not discussed in this study. Br^- and F^- were not detected in sufficient amount of samples and are not representative.

Therefore, the following study exclusively deals with Na^+, Cl^-, NO_3^-, and SO_4^{2-} IC data, when high resolution data are investigated for seasonal and annual variability. For the discussion of spatial variability, mean snow pit concentration values are used. Therefore, UTD data are applicable and allow for interpretation of Ca^{2+} and MSA^- records.

3.4 Data processing using Matlab

3.4.1 Correction of the depth scale into water equivalent [mm WE]

Antarctic snow density underlies strong spatial variations on a three dimensional scale: It varies with geographical position and depth, (KOJIMA, 1964). Therefore, discrete snow samples contain snow of mostly higher densities with increasing depth. Thus, the ion concentration of denser samples is representative for higher amounts of absolute precipitation with depth. Therefore, the primary depth scale [cm snow] is corrected for the snow density into the new depth scale measured in water equivalent [mm WE] according to equations 12-15:

$$d_{WE\ top\ 1} = d_{snow\ top\ 1} * \rho_{snow\ 1} \quad (12)$$

$$d_{WE\ bot\ 1} = (d_{snow\ bot\ 1} - d_{snow\ top\ 1}) * \rho_{snow\ 1} \quad (13)$$

$$d_{WE\ bot\ 1+n} = d_{WE\ bot\ (n-1)} + (d_{snow\ bot\ n} - d_{snow\ top\ n}) * \rho_{snow\ n} \quad (14)$$

$$d_{WE\ top\ 1+n} = d_{snow\ bot\ (n-1)} \quad (15)$$

$d_{snow\ top}$ marks the top depth of the sample interval as measured in snow
$d_{snow\ bot}$ marks the bottom depth of the sample interval as measured in snow
$d_{WE\ top}$ marks the top depth of the interval as calculated in water equivalent
$d_{WE\ bot}$ marks the bottom depth of the interval as calculated in water equivalent

When the intervals of the density data didn't match the borders of the UTS sample, the neighbouring density data were taken into account according to their relative contribution to the particular sample interval.

3.4.2 Resampling to equidistant samples intervals

For further calculations with the DML snow pit dataset, all records of ions and $\delta^{18}O$ were transferred to an equidistant depth scale in water equivalent [WE mm]. To avoid generating higher data densities than the original dataset provided, the new depth intervals were calculated to the greatest interval sizes which occurred in the original data of each snow pit (Table 10). The resampled ion concentrations on the water equivalent depth scale were used for all further calculations and plotting. On average the resolution was about 6 mm WE, which allowed for a temporal resolution of 6-10 samples per year in this very low accumulation area.

Table 10: Presented are the equidistant intervals in which the respective snow pit records were resampled. The displayed depth interval was derived from the largest depth interval found within the records of each pit, thus, oversampling was prevented.

DML	76	77	79	81	83	85	87	88	89	90
depth interval [mm WE]	6.00	5.83	5.98	6.21	6.13	7.24	5.66	5.52	6.37	7.83

3.4.3 Calculation of water weighted ion concentration

The water weighted ion concentration reflects the averaged ion concentrations in accordance to the respective depth interval in water equivalent [mm WE a^{-1}]. This is of particular importance, when mean concentrations were calculated for entire snow pits or annual layers, where stacked samples contribute in different amounts to the mean value.

The water weighted ion concentration $\overline{C}$ is determined after equation 16:

$$\overline{C} = \frac{\sum_i C_i * {}_\Delta X_i}{\sum_i {}_\Delta X_i} \qquad (16)$$

where C_i is the ion concentration as measured from IC [ppb]

and ${}_\Delta X_i$ the length of the depth interval according to C_i [mm WE a^{-1}]

3.4.4 Chloride excess (Clx)

Sea salt deposition in Antarctic snow mostly consists of Na^+ and Cl^-. To some extent, Mg^{2+} and Ca^{2+} as well as SO_4^{2-} are recorded as sea-salt deposits. Due to the constant mixing ratio of both Na^+ and Cl^- in sea water, sea-salt aerosol contributes to Na^+ and Cl^- deposits in snow in a constant ratio. With the beginning of the polar daytime, increasing amounts of sunlight increase the biological productivity of the phytoplankton within the ocean. As a consequence, increasing amounts of biogenic Sulphate are emitted by the oceans as Dimethylsulphide, (DMS). DMS can be transferred into H_2SO_4 that reacts with sea-salt Cl^- ions according to equation 17:

$$2\mathrm{NaCl} + \mathrm{H}_2SO_4 = 2HCl + Na_2SO_4 \qquad (17)$$

The produced HCl exhibits a longer atmospheric life time than does Cl^-. Thus, Cl^- gets faster removed from the air column than does HCl. As consequence, the atmospheric transport distance for HCl is longer than for Cl^-, resulting in relative enrichment of HCl with further distance to the source as compared to Cl^-. With the onset of the biological activity of phytoplankton, HCl adds to the amount of Cl^- in central Antarctica and therefore increases the concentration of Cl^- in relation to Na^+, which is expressed as Chloride excess (Clx), (LEGRAND & MAYEWSKI, 1997). Since the IC analysis does not distinguish between sea-salt and non sea-salt derived ions, the quantity of Na_2SO_4 and HCl contributions to the total deposits need to be calculated by subtracting the amount of Cl^- that is derived from sea-salt from the total amount of Cl^- referring to the amount of deposited Na^+ after equation 18:

$$Clx = Cl^- - 1.80 * Na^+ \qquad (18)$$

Even though some UTS samples might be subject to slight contamination in sea-salt aerosol, the calculation of Clx was considered reliable since the Na^+ and Cl^- records exhibited the same anomalies in comparison to UTD (see chapter 3.3.4 and 3.3.5). According to equation 18, the Clx is calculated after the Cl^-/ Na^+ mixing ratio in ocean water (factor 1.80). BIGLER et al. (2006) describe a factor of 2.0 for the Clx calculation, in case a larger fraction of sea-salt aerosol is derived from frost-flowers than sea spray. During this study, the Clx was calculated after the presented equation.

3.4.5 Non-sea-salt sulphate ($nssSO_4^{2-}$)

Apart from sulphate of volcanic origin, most of the sulphate that is deposited in DML is of biogenic origin. The measured SO_4^{2-} record contains a certain portion of sea-salt derived sulphate which is subtracted in most studies according to the mixing ratio of SO_4^{2-} and Na^+ in sea water according to the equation 19:

$$\mathrm{nssSO_4^{2-}}[ppb] = SO_4^{2-}[ppb] - 0.252\,Na^+[ppb] \qquad (19)$$

Due to the irregularly occurring contaminations of Na^+ (see chapter 3.3.4 and 3.3.5), the $nssSO_4^{2-}$ could not be reliably determined in the UTS samples. To prevent the dataset from any kind of error propagation, the $nssSO_4^{2-}$ record was not considered during this study. On average, the $nssSO_4^{2-}$ concentration from UTD samples accounted for 95 ± 2 % of the total SO_4^{2-} concentration in all snow pit records. Vice versa, marine SO_4^{2-} accounted for 5 ± 2 % of the total sulphate deposition in the DML snow pits.

3.4.6 Non-sea-salt calcium ($nssCa^{2+}$)

Sodium, chloride and calcium ions deposited in Antarctic snow originate from both marine and continental sources (LEGRAND & MAYEWSKI, 1997). Time series of these ions are interpreted in order to reconstruct past climate processes, however, this requires disentangling the deposited marine and continental ion fractions (BIGLER et al., 2006). Even though continental ion sources contain a range of cations (Na^+, Mg^{2+}, K^+, and Ca^{2+} (LEGRAND & MAYEWSKI, 1997)) calcium records are commonly referred to as proxy of continental deposit (BIGLER et al., 2006).

The following equations are presented by BIGLER et al., (2006), to uncover the continental fraction of $nssCa^{2+}$ from sea-salt calcium ($ssCa^{2+}$):

$$\left[nssCa^{2+}\right] = \left[Ca^{2+}\right] - \left[ssNa^{+}\right] * \left(Na^{+}/\ Ca^{2+}\right)_{ss}^{-1} \qquad (20)$$

Calculating the sea-salt fraction of sodium ($ssNa^+$) requires furthermore:

$$\left[ssNa^+\right] = c \left[\left[Na^+\right] - \left[Ca^{2+}\right] * \left(Na^+ / Ca^{2+}\right)_{ss} \right] \quad (21)$$

$$\text{with} \qquad c = \left[1 - \left(Na^+ / Ca^{2+}\right)_{nss} * \left(Na^+ / Ca^{2+}\right)_{ss}^{-1} \right]^{-1} \quad (22)$$

The calculations can be adjusted according to the predominant sea-salt aerosol source which is either of bulk seawater or brine. For the calculations performed in this study, the sodium/calcium ratio of sea-salt aerosol ($[Na^+/Ca^{2+}]_{ss}$) was selected for bulk sea water which was 26 (and is consistent with the setup for Clx calculation that was also adjusted for predominance of bulk seawater as key source). The applied ratio of non sea-salt sodium/calcium ($[Na^+/Ca^{2+}]_{nss}$) was determined 0.94 (BIGLER et al., 2006).

Note, due to contamination of UTS samples in calcium, the UTS calcium records could not be interpreted. The non sea-salt calcium records will be discussed in chapter (5.5), only.

3.4.7 Dating of the UTS snow pits using $\delta^{18}O$ and ion chemistry

As described in chapter ($\delta^{18}O$ in Antarctic snow), the seasonal variation of $\delta^{18}O$ indicates summer maxima and winter minima within snow stratigraphy that allows to distinguish between snow deposits of individual years. The mean annual accumulation rates on the Antarctic Plateau in Dronning Maud Land has been determined < 97 mm WE according to OERTER et al., (2000); 62 mm WE according to ROTSCHKY et al., (2007a) and 44 mm WE - 63 mm WE as suggested by SOMMER et al. (2000a). As a consequence of the fairly low accumulation rate, the distinctiveness of the $\delta^{18}O$ signal suffers from post-depositional diffusion of water vapour that occurs within the pore space of the snow matrix (JOHNSON, 1977; LEGRAND & MAYEWSKI, 1997; SCHLOSSER & OERTER, 2002). Hence, the amplitude of the $\delta^{18}O$ signal can lose up to two thirds of its original value during the first year of its deposit (SCHLOSSER & OERTER, 2002).

Furthermore it needs to be considered, that snow including its $\delta^{18}O$ information can be redistributed by wind drift that also biases the $\delta^{18}O$ signal. As consequence of both processes, the dating of the snow pits by identification of seasonal $\delta^{18}O$ peaks becomes more complicated. Particularly the DML snow pits 85, 87, 88, 89, and 90 were affected by attenuation of the $\delta^{18}O$ signal and showed strong smoothing of seasonal $\delta^{18}O$ cycles. The weakness could be compensated by taking ion signals of Na^+, Cl^-, NO_3^-, and SO_4^{2-} into account towards a multi parameter dating method. Particularly the SO_4^{2-} record was of great importance, as all snow pit records apart from DML 76, 77 and 81 contained a peak of high SO_4^{2-} that was attributed to deposits of the volcanic eruption of Mount Pinatubo and Cerro Hudson in 1991 (5.9), thus forming a clear base of absolute age. Vice versa, due to the lack of the Pinatubo signal, DML 76, 77, 81, were clearly deposited past the Pinatubo eruption.

To reconstruct the amplitude of the $\delta^{18}O$ signal, a back-diffusion model was applied to the $\delta^{18}O$ records in this study that had been previously developed by FISCHER, pers. com. The back-diffusion model is based on $\delta^{18}O$ diffusion studies of JOHNSEN (1977) and assumes the $\delta^{18}O$ signal to vary on constant frequencies, equal to constant accumulation rates. Thus, the back-diffusion model can also create pseudo-peaks as annual cycle and was applied with careful consideration of the ion chemical data.

The result of the dating is exemplary displayed for the snow pit DML 76 in Figure 12. According to Figure 12, DML 76 contains 13 annual cycles of $\delta^{18}O$ and ions. During the dating of all DML snow pits, the top layer from snow surface to the first peak in $\delta^{18}O$ was considered one full calendar year, as the sampling campaign took place in austral summer (January 2006).

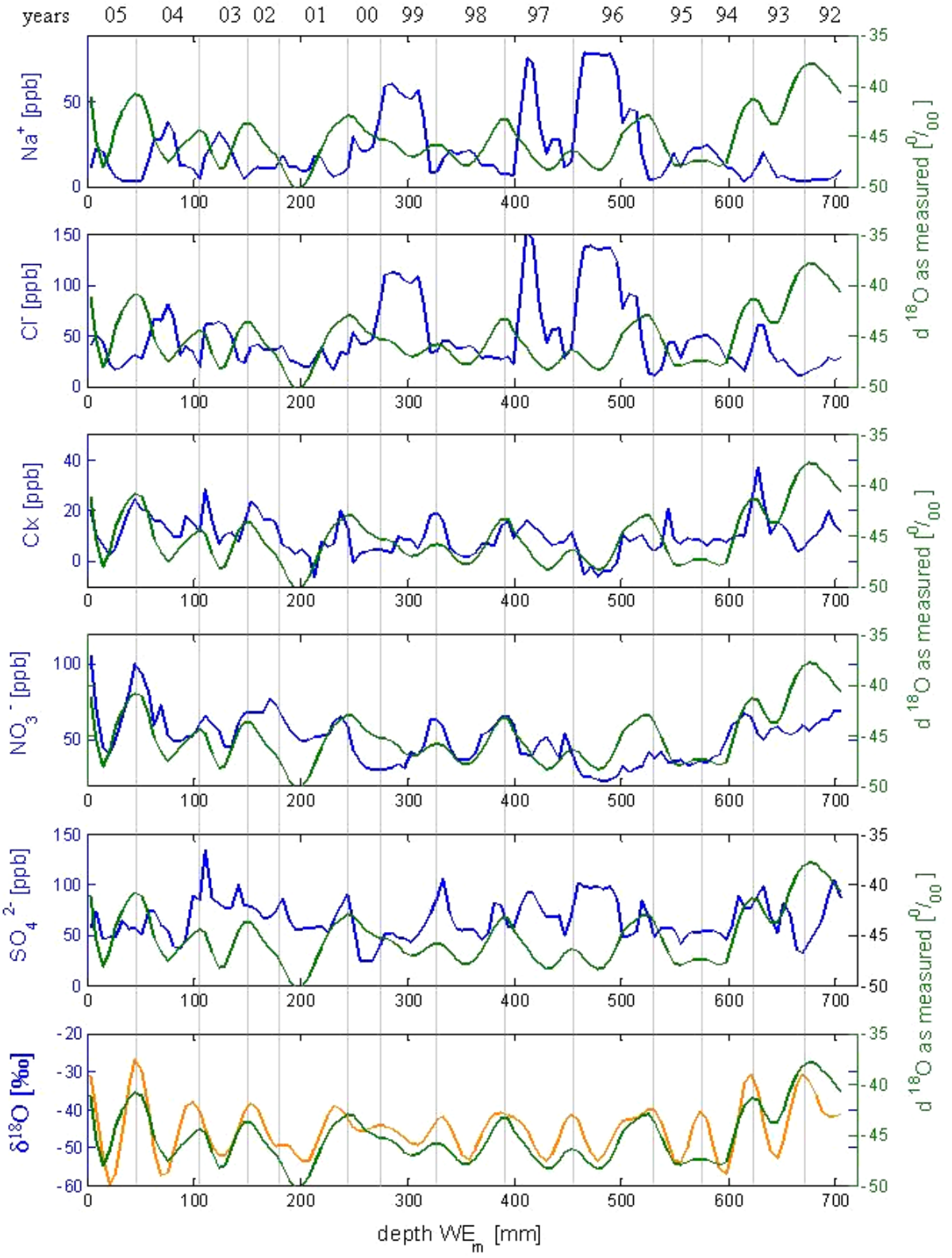

Figure 12: Dating of DML 76 using records of Na^+, Cl^-, Clx, NO_3^-, SO_4^{2-}, and $\delta^{18}O$.The ions are displayed with blue lines, the green $\delta^{18}O$ line is plotted on top of the ion figures for better comparison. The lowermost plot shows in orange the $\delta^{18}O$ signal which was suggested by the back-diffusion model.

4. Temporal variability of glacio-chemical parameters in snow

A key goal of this study is to analyse the temporal variability in glacio-chemical records (ion concentrations, $\delta^{18}O$ signal and accumulation rate) from the DML snow pits which represent the degree of variability at individual DML sites in recent climate and atmospheric composition.

The temporal variability of several glacio-chemical parameters was investigated on two time scales: interannual and seasonal. The basis for the interpretation is the snow layer deposited from 2005-1994 that occurred in all snow pits along the transect. The annual boundaries defined during the dating procedure (3.4.7) were used as markers of the depth intervals to divide the snow pack that accumulated during the 12 years for 12 individual annual time slices.

The following chapter (4.1) discusses the seasonal variability of the chemical records as they were preserved in the snow. In the subsequent chapter (4.2), the annual variability of glacio-chemical records will be discussed. Throughout the discussion, all relative variations of the parameters will be presented as calculated by:

$$\text{variability [\%]} = \frac{\sigma}{\mu} * 100 \qquad (23)$$

with σ as standard deviation,
μ as mean value

4. 1 Seasonal variability of glacio-chemical parameters in Antarctic snow

Distinct seasonal variations were found within in the glacio-chemical records of the EDML snow pit samples as presented in Figure 13. The interpretation of the temporal pattern of ion deposition in DML is based on the seasonality of the $\delta^{18}O$ signal, which serves as a reference in time, because it is driven by the annual temperature variations throughout the seasons (see chapter 4.1.1). Thus, high $\delta^{18}O$ values indicate austral summer periods, in contrast, the minimum values of $\delta^{18}O$ account for the time of coldest temperatures during austral winter (GÖKTAS, 2002).

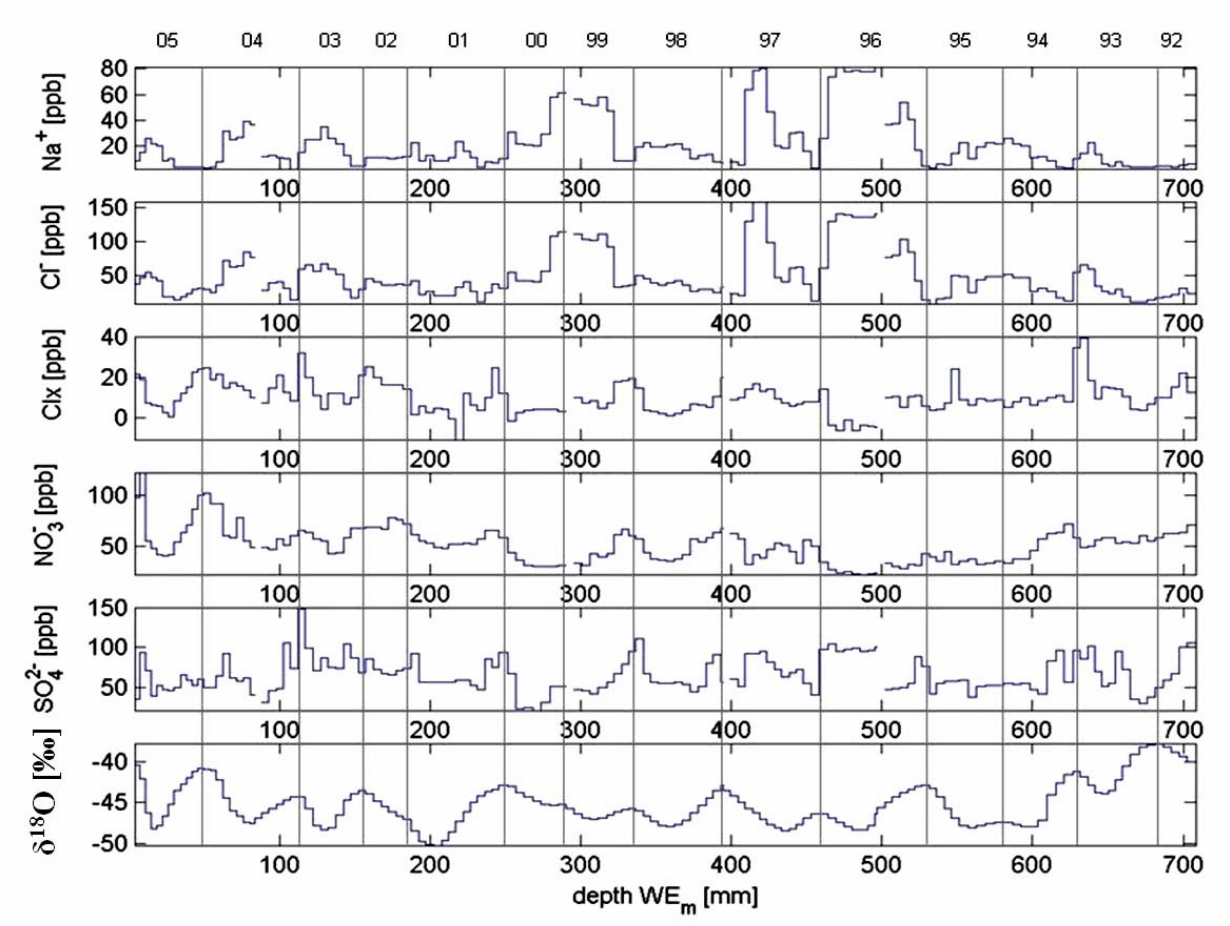

Figure 13: Ion records of Na^+, Cl^-, Clx, NO_3^-, SO_4^{2-}, and $\delta^{18}O$ from snow pit DML 76 exhibits a distinct seasonal cyclicity of the signals. The annual boundaries are marked by grey lines across all records.

To visualize the seasonal variability of glacio-chemical parameters between 1994 until 2005, three dimensional plots were created. These 3-D plots visualize the seasonal variability during the course of each year (1994-2005) as mean of all snow pits. The calculations, that formed the basis of the 3-D plots required accurate definition of annual boundaries within the snow column, according to chapter 3.4.7. Next, the annual layer depth of each year was divided into 6 subintervals of equidistant length to which the according values of the records were assigned. The start of season 1 represents the beginning of each annual cycle which was chosen to be the summer maximum of the $\delta^{18}O$ signal. Consequently, season 6 ends at the consecutive maximum of the $\delta^{18}O$ signal. GÖKTAS (2002) and references therein described the highest temperatures in DML to occur during December-January. To use a more intuitive time scale, each of the 6 seasons that form an annual cycle are attributed to 2 months of the calendar year. Hence, January-February substitute season 1 while the consecutive seasons 2-6 are represented by pairs of the respective months. Assigning the seasonal intervals to calendar months assumes the annual accumulation to be evenly distributed throughout the year and ignores the uneven distribution of precipitation that actually takes place according to REIJMER et al. (2002). Thus, a relative timing error has to be kept in mind.

The investigation for seasonality of each individual glacio-chemical parameter exhibited a consistent seasonal cyclicity throughout the study area. To display the variability in an even more representative way, the seasonal signal is presented in the following plots as mean for all snow pits. Note, the absolute concentrations represent the mean of all snow pits and can thus mask potential geographical variations of the respective parameter. Hence, the regional differences in concentration levels among the individual pits were eliminated by this procedure.

4.1.1 Seasonal variability of $\delta^{18}O$

The $\delta^{18}O$ records of the DML snow pits display a distinct pattern of seasonal variation in the $\delta^{18}O$ ratio as shown in Figure 14 and Table 11. According to Figure 14, the seasonal $\delta^{18}O$ signal in all snow pits reaches its peak values during Jan-Feb and Nov-Dec, which is the case for most of the years. On average, the $\delta^{18}O$ signal exhibits slightly higher values for Nov-Dec than for Jan-Feb. The minimum $\delta^{18}O$ values appear during May-June and Jul-Aug, indicating,

as expected, lowest temperature during mid austral winter, which is a general feature of central Antarctica and was also described by GÖKTAS (2002) and references therein. The seasonal variability of the $\delta^{18}O$ signal as averaged over all snow pits is most pronounced during the last years of deposit (2005 and 2004), after which the seasonal amplitude successively decreases with depth and time. The observed loss of $\delta^{18}O$ amplitude is essentially due to post-depositional diffusion processes of water vapour within the snow column that will continue to degrade the $\delta^{18}O$ information with increasing depth. Below a depth of ~7 m, the seasonal $\delta^{18}O$ amplitude is expected to be completely lost in DML (JOHNSON pers. com., 2008).

During 1999, the mean $\delta^{18}O$ signal in Figure 14 strongly increases already from Jul-Aug onwards and reaches its extraordinary high maximum in Nov-Dec in 1999. During 2000, the $\delta^{18}O$ signal continuously decreases throughout the whole year, during the austral spring and summer period of late Sept-Oct and Nov-Dec and even further during the following year 2001. A comparable pattern is visible two years afterwards, when the $\delta^{18}O$ signal continuously builds up again during 2002 and rapidly decreases in 2004. Summing this last finding up, the mean $\delta^{18}O$ signal exhibits clear interannual variability in the mean annual temperature in two $\delta^{18}O$ cycles that seem to stretch out over more than one year. However, to find out whether the two $\delta^{18}O$ anomalies represent a systematic cyclicity in $\delta^{18}O$ that refers to a specific periodic meteorological situation from DML or not, longer $\delta^{18}O$ records that reach further back in time are need to be investigated in order to gain statistically more robust results.

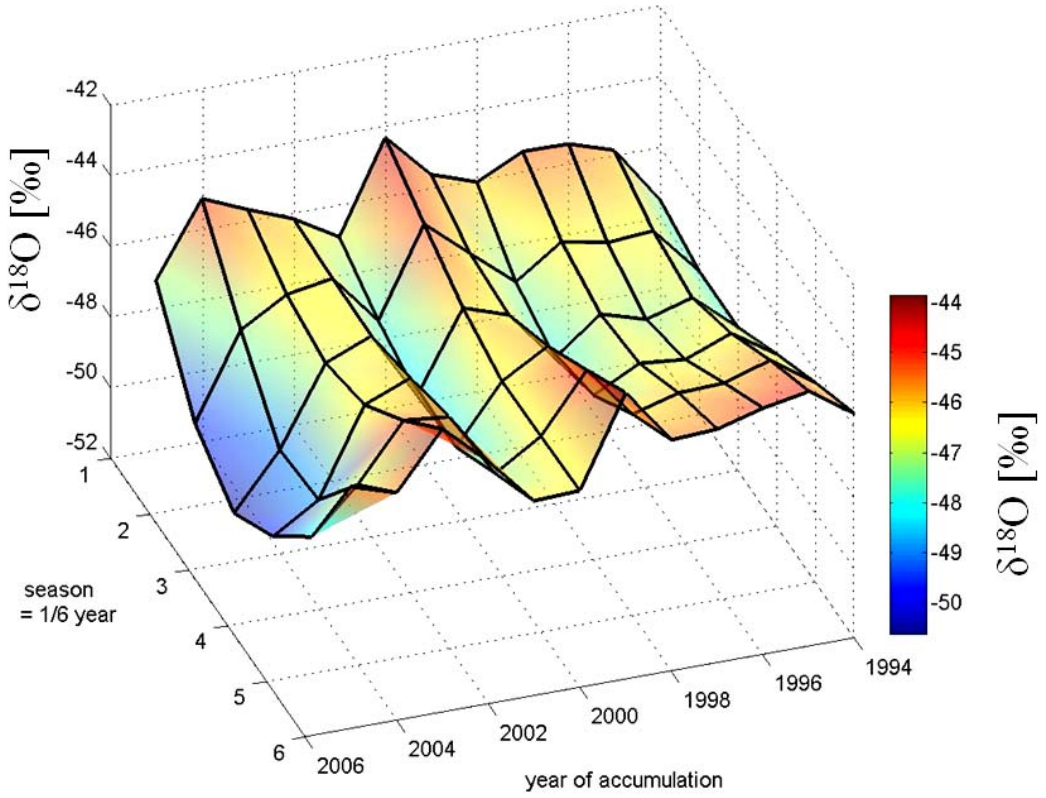

Figure 14: Seasonal signal of $\delta^{18}O$ as mean over the data from all snow pits for each year. Season 1 represents the summer peak of the year, equal to season January-February. Consequently, season 3 and 4 represent the austral winter period Mai-June and July-August, respectively, when season 6 represents the early austral summer months November-December.

Table 11: Presented is the seasonal signal of $\delta^{18}O$. Presented are the mean $\delta^{18}O$ values for the respective season from all snow pits and the standard deviation. In addition, the table displays the minimum and maximum values of the respective seasonal signal and the amount of interseasonal variation of $\delta^{18}O$ in comparison of the previous season in absolute and relative values.

	$\delta^{18}O$					
season	1. Jan-Feb	2. Mar-April	3. May-June	4. Jul-Aug	5. Sept-Oct	6. Nov-Dec
mean [‰]	-46.0±3.0	-47.0±2.8	-47.6±2.8	-47.2±2.9	-46.2±3.1	-45.3±3.2
min [‰]	-54.9	-54.8	-55.7	-54.4	-54.3	-54.5
max [‰]	-37.5	-38.3	-39.8	-39.7	-39.3	-37.1
diff. abs [‰]	-0.7	-1.0	-0.6	0.4	0.9	1.0
diff. rel [%]	1.6	2.3	1.2	0.8	2.0	2.1

4.1.2 Seasonal variability of Sodium and Chloride

Between 1994 and 2005, both sodium and chloride exhibit the same pronounced seasonality of concentrations in DML snow samples (Figure 15, 16), as they are mostly derived from the same source as sea-salt aerosols (see chapter 2.6.3). Therefore, their seasonality will be discussed together. According to Figure 15 and 16, the Na^+ and Cl^- maxima were found during the austral winter seasons Jul-Aug. The timing is in line with findings of Na^+ concentration in DML ice cores and atmospheric samples by SOMMER et al., (2000b), GÖKTAS, (2002b) and WELLER & WAGENBACH, (2007). The winter maxima of both the Na^+ and the Cl^- concentration suggest an increased sea-salt deposition during winter times. GÖKTAS et al. (2002a) discuss higher storminess during the winter season to cause faster air-mass transport leading to the higher concentration of sea-salt ions observed in DML snow. RANKIN et al. (2002) found the increasing appearance of frost flowers that built during sea-ice formation on the ocean surface to amplify its aerosol source strength, and thus, enhance the export of sea-salt aerosol. Consequently, this accounts for both the Na^+ and the Cl^- export.

After the Na^+ and Cl^- concentration have reached their maximum value during Jul-Aug, the concentration of Na^+ decreases by 9 %, significantly faster than the concentration of Cl^- does with 2 %. According to Table 12 and 13, it is a general finding that Cl^- concentration slower decrease than the Na^+ concentrations do throughout the year. When Na^+ displays its minimum during Nov-Dec (Table 12), the Cl^- concentrations further decrease until they reach their minimum during Jan-Feb (Table 13). This slightly decoupled development of Na^+ and Cl^- can be explained by the onset of Cl^- aerosol import via HCl, which was transferred from sea-salt NaCl by H_2SO_4 produced by oxidation of organic sulphur components (DMS) and is expressed by the Chloride excess (Clx).

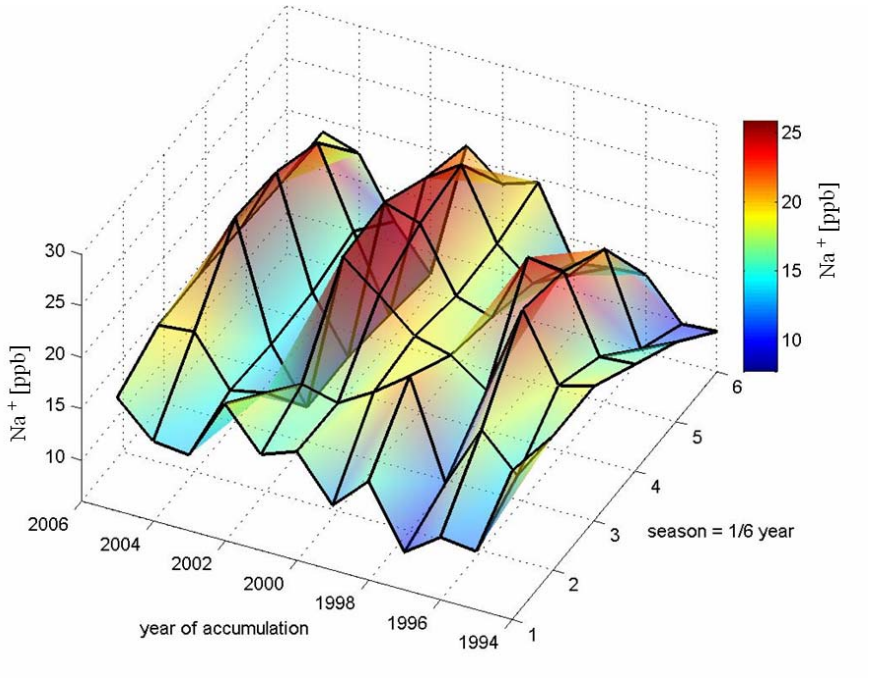

Figure 15: Seasonal signal of Na^+ as mean over the data from all snow pits for each year. Season 1 represents season January-February. Consequently, season 3 and 4 represent the austral winter period Mai-June and July-August, respectively, when season 6 represents the early austral summer months November-December.

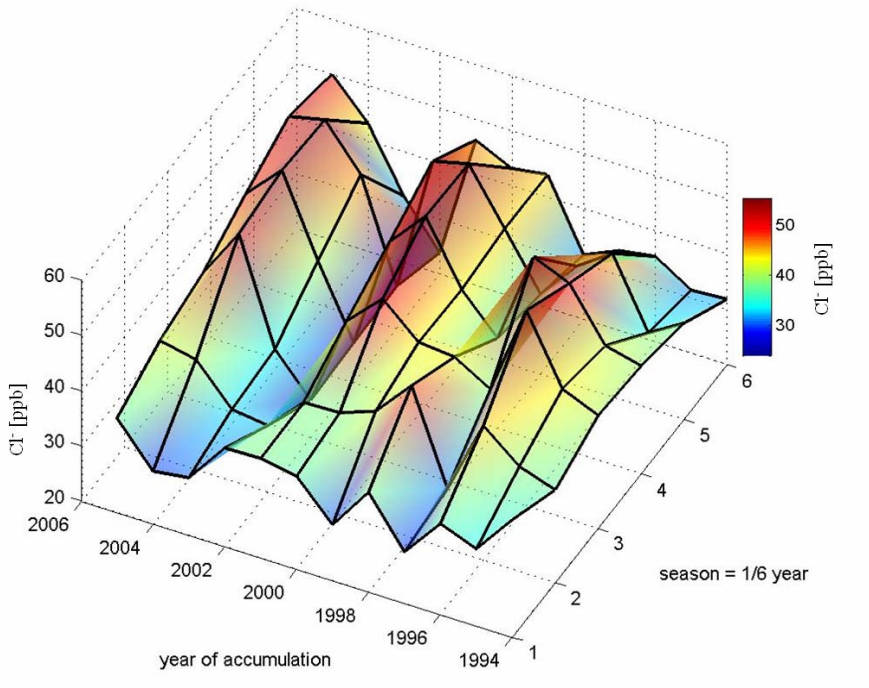

Figure 16: Seasonal signal of Cl^- as mean over the data from all snow pits for each year. Season 1 represents season January-February. Consequently, season 3 and 4 represent the austral winter period Mai-June and July-August, respectively, when season 6 represents the early austral summer months November-December.

Table 12: Presented are the mean Na^+ values for the respective season from all snow pits and the standard deviation. In addition, the table displays the minima and maxima of the respective seasonal signal. Furthermore, the amount of interseasonal variation of Na^+ is shown in comparison to the previous season in absolute and relative values.

Sodium						
season	1. Jan-Feb	2. Mar-April	3. May-June	4. Jul-Aug	5. Sept-Oct	6. Nov-Dec
mean [ppb]	15±11	17±11	19±14	19±14	18±13	14±11
min [ppb]	2	2	2	1	1	2
max [ppb]	53	49	74	78	79	60
diff. abs [ppb]	0	2	2	0	-2	-3
diff. rel [%]	2	15	13	1	9	19

Table 13: The table presents seasonal signal of Cl^-. The further structure of the table 13 is in accordance to the description of Table 12 seasonal signal of Na^+.

Chloride						
season	1. Jan-Feb	2. Mar-April	3. May-June	4. Jul-Aug	5. Sept-Oct	6. Nov-Dec
mean [ppb]	35±17	39±18	43±24	45±25	44±24	37±20
min [ppb]	10	10	10	12	11	9
max [ppb]	88	95	130	139	138	111
diff. abs [ppb]	-2	4	4	2	-1	-7
diff. rel [%]	5	10	11	4	2	15

In comparison to firn and ice core studies, records of snow pits are limited to short time records. Due to the generally high variability of glacio-chemical parameters, relatively short snow pit records are less likely to exhibit multi annual cycles in a statistically robust way (ROTSCHKY et al., 2007b). However, Figure 15 and 16 of seasonal resolved mean Na^+ and Cl^- concentrations exhibits 3 cycles of significantly increased Na^+ concentrations. The anomalies of high concentration appeared in a cyclicity of approximately 4 years during 1996, 2000, and 2004 and particularly affected the austral winter months May-June, Jul-Aug, and Sept-Oct, while the mean austral summer concentrations of Na^+ and Cl^- were found in the typical range Figure 15 and 16. Thus, the anomalies superimpose the winter maximum of both Sodium and Chloride and form years of increased seasonal variability in contrast to the intermediate years. This perennial periodicity of Na^+ concentrations was found in DML within four ice core records before (DML03, DML05, DML07 and DML17) by FUNDEL et al. (2005). FUNDEL et al. (2005) discussed the Antarctic Dipole (ADP) to result in an increased import of sea-salt aerosol into DML. As an extraordinary result of this study, the imprint of this feature could be visualized out of the DML snow pit data, showing that the sea salt cycles are mainly a winter phenomenon.

4.1.3 Seasonal variability of sulphate

The sulphate record from the snow pit samples of Dronning Maud Land features a distinct seasonal variability. Figure 17 exhibits low seasonal SO_4^{2-} concentrations during May-June and Jul-Aug throughout the austral winter period for all years but 1996. The highest SO_4^{2-} concentrations were either found at Jan-Feb, at Sept-Oct or at even both. According to Figure 17, the pattern of seasonal SO_4^{2-} concentrations can include one or two peaks of high concentration in one year, occurring during any time between austral spring and autumn.

According to Figure 17, the seasonal pattern accounts for all years of the period 1994-2005, except for one anomaly during 1996. The seasonal SO_4^{2-} signal for 1996 was completely out of phase, which could unambiguously be attributed to exceptionally high SO_4^{2-} concentrations and a very low accumulation in snow pit DML 89 throughout 1996.

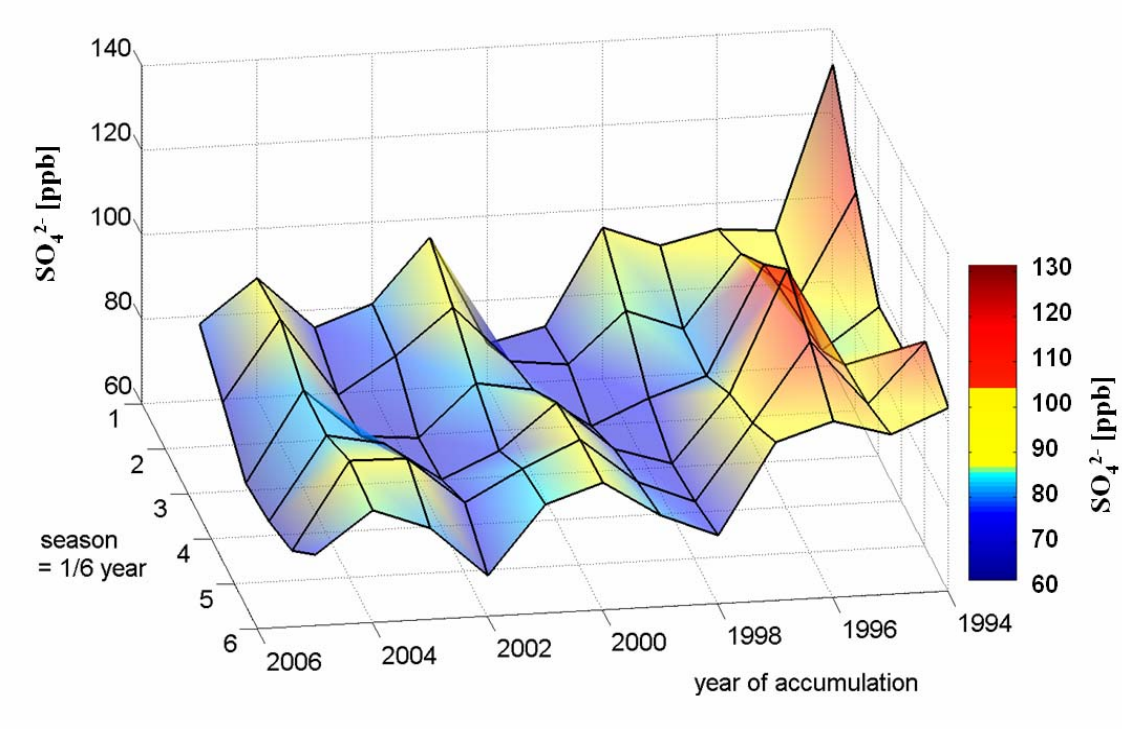

Figure 17: Seasonal signal of SO_4^{2-} as mean over the data from all snow pits for each year. Season 1 represents season January-February. Consequently, season 3 and 4 represent the austral winter period Mai-June and July-August, respectively, when season 6 represents the early austral summer months November-December.

4.1.4 Seasonal variability of nitrate

The seasonal variability of nitrate in the DML snow pit records exhibits maximum concentrations during the austral summer seasons of January-February and November-December Figure 18. However, the seasonality of NO_3^- concentrations is most pronounced during the last years of deposition (2005 and 2004). The seasonal amplitude of the NO_3^- signal successively decreases with the total NO_3^- concentration in the records, which is due to post-depositional NO_3^- loss that is described in detail within the chapter 4.2.

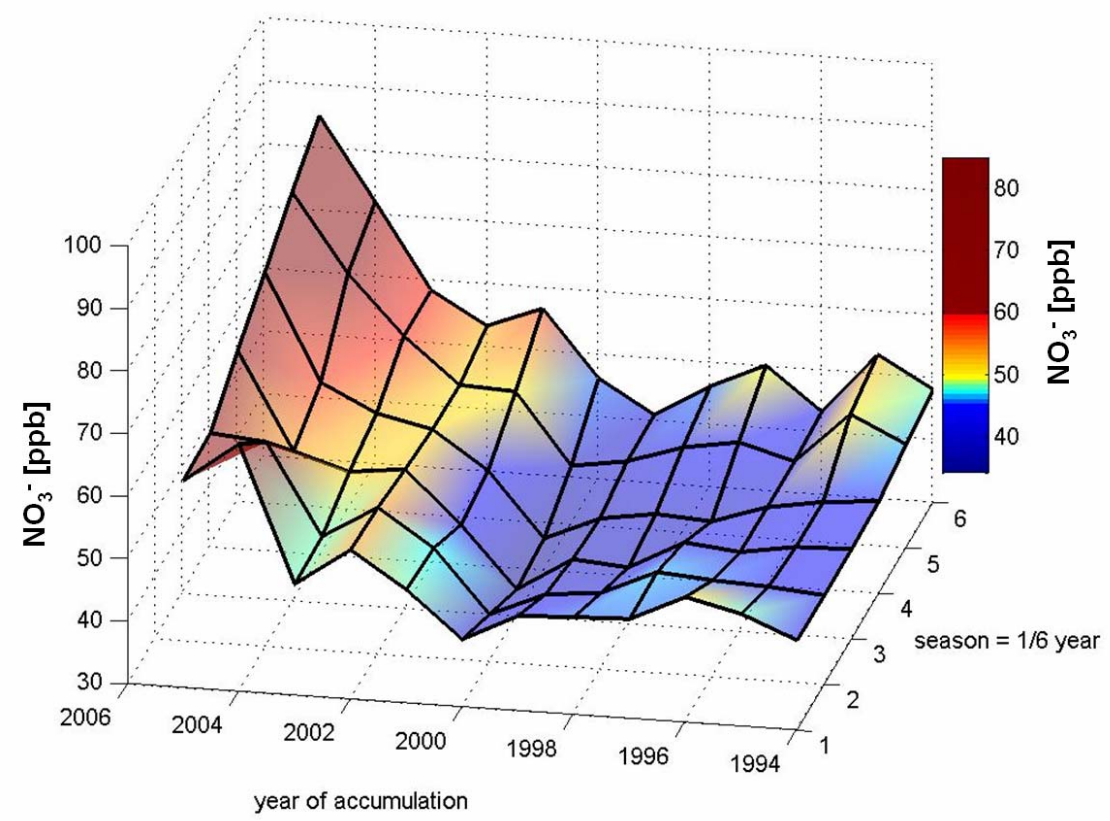

Figure 18: Seasonal signal of NO_3^- as mean over the data from all snow pits for each year. Season 1 represents season January-February. Consequently, season 3 and 4 represent the austral winter period Mai-June and July-August, respectively, when season 6 represents the early austral summer months November-December.

The post-depositional loss of NO_3^- explains the wide range of a factor of 10 between minimum and maximum NO_3^- concentrations found within the records of individual seasons according to Table 15.

Table 14: Shown is the seasonal signal of nitrate. The further structure of the table 14 is in accordance to the description of Table 12 seasonal signal of Na^+.

Nitrate						
season	1. Jan-Feb	2. Mar-April	3. May-June	4. Jul-Aug	5. Sept-Oct	6. Nov-Dec
mean [ppb]	50±17	48±16	46±18	47±18	51±20	53±21
min [ppb]	9	21	17	19	15	18
max [ppb]	138	137	145	159	132	167
diff. abs [ppb]	-3	-2	-2	1	4	2
diff. rel [%]	6	4	3	2	9	4

4.1.5 Summary of seasonal variability

- All investigated glacio-chemical parameters derived from UTS samples exhibited a clear seasonal cyclicity (the seasonal signal was calculated as mean over all snow pits during the course of individual years).
- $\delta^{18}O$ exhibited maximum values during the austral summer half-year and minimum values during austral winter. The smoothing of seasonal $\delta^{18}O$ amplitude with increasing depth was attributed to water vapour diffusion.
- The sea-salt aerosol (Na^+ and Cl^-) showed maximum concentrations during austral winter and minimum concentrations during the austral summer period. A multi-annual feature (~ 4 years cyclicity) of enhanced sea-salt concentrations during winter seasons could be imaged and was found in line with previous studies that attributed the cyclicity to the Antarctic Dipole.
- At least one maximum peak of sulphate concentration occurred during austral summer period (spring, summer, autumn), minimum sulphate concentrations were found during austral winter
- Maxima of nitrate concentrations were displayed during austral summer within the first two years after deposition, the adjacent amplitude decrease could be attributed to post-depositional nitrate loss, minimum concentrations occurred during austral winter periods

4.2 Interannual variability

The mean annual $\delta^{18}O$ ratio, the mean annual accumulation rate and the mean annual ion concentrations will be presented and discussed in this chapter as derived from the UTS dataset. Mean water weighted concentrations of ions were calculated after equation 16. The variability of annual means is indicated in relative values, calculated according to equation 23.

Correlation tests using the T-test method were performed to test the annual variability for correlation between individual parameters within the same snow pit, and also of the same parameter in between the different snow pits. This was to find out about systematic coherences and if the annual variability is a representative parameter from which climatic signals can be calculated that are representative for meteorological variability of the whole study area. The correlations were considered significant, when a significance level of ≥ 95 % was reached. According to a number of 12 years, the significance level of ≥ 95 % was given for correlation coefficients of $r \geq 0.58$ or $r \leq -0.58$.

In addition to the discussion of the annual variability from 1994-2005, the presentation of the SO_4^{2-} annual variability was expanded by selected snow pits reaching back in time to 1991 and 1990. These snow pits are of particular interest as they show high, simultaneous SO_4^{2-} emissions assigned to the SO_4^{2-} release from the volcanic eruptions of Mount Pinatubo (June, 15th of 1991) and Cerro Hudson (August 12th – 15th of 1991).

4.2.1 Interannual variability of $\delta^{18}O$

The essential $\delta^{18}O$ data derived from the DML snow pits are presented in Table 15 for each site. The $\delta^{18}O$ records reveal annual mean values in between -45 ± 2 ‰ DML 77 and -48 ± 2 ‰ at DML 90. As displayed in Table 15, the annual means of the $\delta^{18}O$ signal vary on average between 2 % and 7 % at DML 76 and 79, respectively.

Table 15: Annual means of $\delta^{18}O$ [‰] signal per pit and annual variability of $\delta^{18}O$ [%]

	statistics of annual means from $\delta^{18}O$ values									
DML	**76**	**77**	**79**	**81**	**83**	**85**	**87**	**88**	**89**	**90**
mean±std [‰]	-46±1	-45±2	-46±3	-46±1	-45±2	-47±3	-47±2	-48±3	-48±2	-48±2
min [‰]	-47	-48	-53	-48	-50	-52	-50	-52	-50	-52
max [‰]	-44	-43	-42	-43	-41	-43	-42	-43	-44	-44
mean [%]	2	4	7	3	5	5	5	5	4	5

The annual $\delta^{18}O$ records result from annual meteorological parameters (such as annual mean temperature) that were expected to similarly affect all DML snow pits records if systematic, e.g. altitude dependent, spatial variations were excluded. If single annual mean $\delta^{18}O$ data from individual snow pits displayed a pure climatic signal which was representative for the respective year, the annual $\delta^{18}O$ records of individual snow pits were expected to correlate. Unexpectedly, the annual $\delta^{18}O$ snow pit signals showed no correlation in between the snow pit sites with a significance level of ≥ 95 % at all. This finding is also described by KARLÖF et al. (2006), who found no correlation of $\delta^{18}O$ records between closely linked pairs of firn cores in DML.

There are two post-depositional processes that bias the $\delta^{18}O$ signal and inhibit the correlation in between the $\delta^{18}O$ records, the diffusion of water vapour in the snow matrix and the redistribution of snow by wind drift.

Post-depositional bias of the annual $\delta^{18}O$ signal due to diffusion of water vapour within the snow column

During firnification, snow grains form by combined processes of sintering and mass exchange of water vapour in dependence of the snow density and the mean vapour pressure within the firn (JOHNSEN, 1997; SCHLOSSER & OERTER, 2002). The diffusion of water vapour and the sintering of grains cause a vertical mixing of water vapour and transport the $\delta^{18}O$ signal within the snow, thus, smoothing the $\delta^{18}O$ signal. The vertical mixing due to sintering process is cut off, when the successive compaction of snow results in densities of > 550 kg/m^3 (Johnsen, 1997). Diffusion of water vapour stops, when complete gas bubble formation cuts further diffusion processes off. The mean snow density of the DML snow pits was calculated as 370 ± 4 kg/m^3 for the 200 - 210 cm interval of depth in snow, so diffusion of water vapour took place and affected the $\delta^{18}O$ signal.

The wave length of the $\delta^{18}O$ profile is a critical parameter of how strong the $\delta^{18}O$ signal is smoothed out. JOHNSON (1997) discussed a diffusion length of 200 mm snow or 70-80 mm in ice equivalent which obliterates $\delta^{18}O$ signals of shorter wave lengths. Since central DML is of particular low accumulation rate (39 ± 8 mm WE – 57 ± 22 mm WE) the accumulated snow consequently includes $\delta^{18}O$ profiles of even shorter wave lengths. Thus, the water vapour diffusion is expected to strongly affect the primary $\delta^{18}O$ signal of the precipitation in DML snow pits as can be observed in DML 88 according to Figure 19. In DML 88, the $\delta^{18}O$ signal of the upper years still exhibits a strong gradient, while the gradient of $\delta^{18}O$ successively smoothes out, which can particularly be observed in the depth interval of 300 – 500 mm WE.

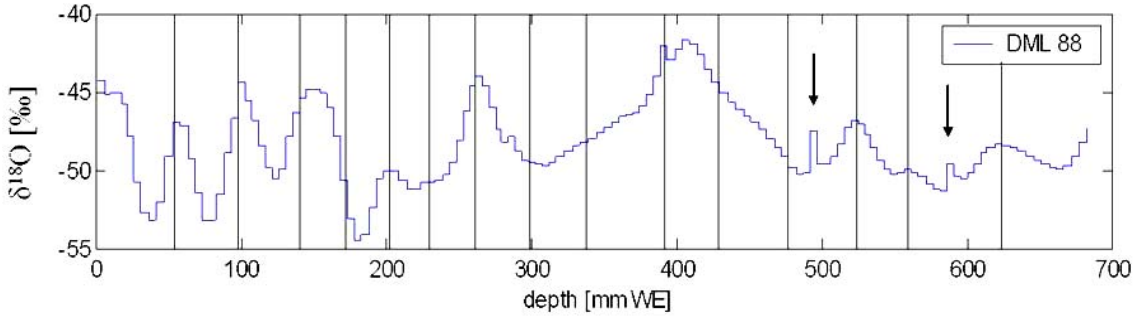

Figure 19: The $\delta^{18}O$ record of DML 88 shows the $\delta^{18}O$ signal in the depth between 0 and 690 mm WE, the gray lines mark the annual boundaries. Eye catching is the smoothing of the gradient with depth in the displayed $\delta^{18}O$ record. While the $\delta^{18}O$ gradient is steep down to a depth of approximately 180 mm WE, it continuously smoothes during the record as can be particularly observed at the depth interval between 300 and 500 mm WE. The 2 arrows within at approximately 500 and 600 mm WE indicate 2 maximum peaks of the $\delta^{18}O$ record, where the $\delta^{18}O$ increase slowly builds up during 2 measurements and then suddenly displays a maximum peak. These features are most likely caused by import of snow material from another site by wind drift, where the area of origin contained a higher $\delta^{18}O$ signal.

Post-depositional bias of the annual $\delta^{18}O$ signal due to snow redistribution by wind drift

Within the snow pit records, individual annual layers are randomly affected by either loss or gain of $\delta^{18}O$ carrying snow material that gets laterally removed or added to the snow pit site by wind drift. The two arrows in Figure 19 exemplary indicate two layers of the $\delta^{18}O$ profile, where the exceptional strong gradients of the $\delta^{18}O$ signal most likely result from the deposition of snow material by wind drift, that finally add to a higher annual $\delta^{18}O$ signal. Thus, the observed annual $\delta^{18}O$ record results from the $\delta^{18}O$ of the actual precipitation at the particular site only in a first step. Moreover, surplus or loss of snow superimpose the balance

of annual $\delta^{18}O$ signal and, thus, bias the annual mean $\delta^{18}O$ record in dependence of the $\delta^{18}O$ of the snow that was added or removed. Due to the redistribution of snow and the strong periodicity of precipitation, annual $\delta^{18}O$ records were found to lack complete seasonal sections of $\delta^{18}O$ (HELSEN et al., 2005) that inhibit the correlation between the annual records such as the $\delta^{18}O$ record.

Within the DML snow pit records, the annual $\delta^{18}O$ signal is therefore corrupted by strong, independent noise that completely masks the climatic variability of the annual $\delta^{18}O$ signal, resulting in lacking correlations of the $\delta^{18}O$ records that can be observed in Figure 20. The interannual variability of the $\delta^{18}O$ record is strongly heterogenic throughout the study area during 1994-2005 and does not exhibit comparable progressions of $\delta^{18}O$ signals during individual years. Therefore, the interannual variability of the $\delta^{18}O$ record can not be interpreted as representative climatic signal that allows for the reconstruction of temperatures and precipitation of DML on an annual timescale.

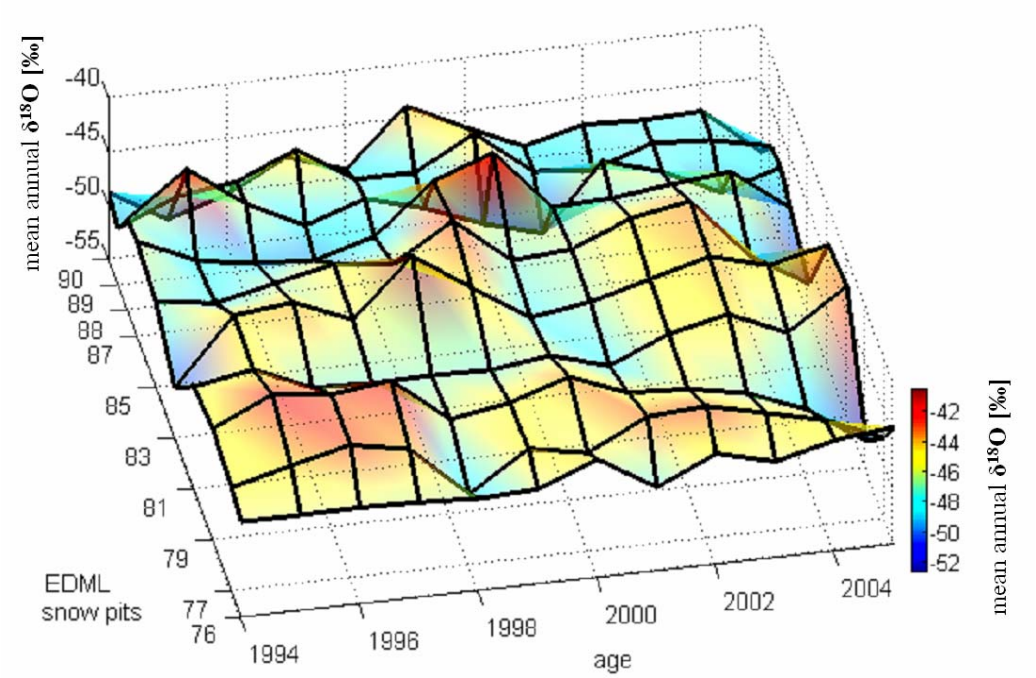

Figure 20: Comparison of annual $\delta^{18}O$ variability for all DML sites 76-90, the $\delta^{18}O$ records for the years 2005-1994 show no correlation in between the DML snow pit sites and disqualify the $\delta^{18}O$ signal from allowing temperature and precipitation reconstructions that are representative for the DML study area.

Correlation of $\delta^{18}O$ and Na^+ at DML 79, 85, 88

A systematic negative correlation coefficient was found for the correlation test of the annual variability of $\delta^{18}O$ and both sea-salt aerosol derived ions Na^+ and Cl^- as exemplary shown for Na^+ in Figure 21. In three snow pits, the correlation between the annual variability of $\delta^{18}O$ and Na^+ was found at r = -0.7, -0.65, and -0.83 (DML 79, 85 and 88).

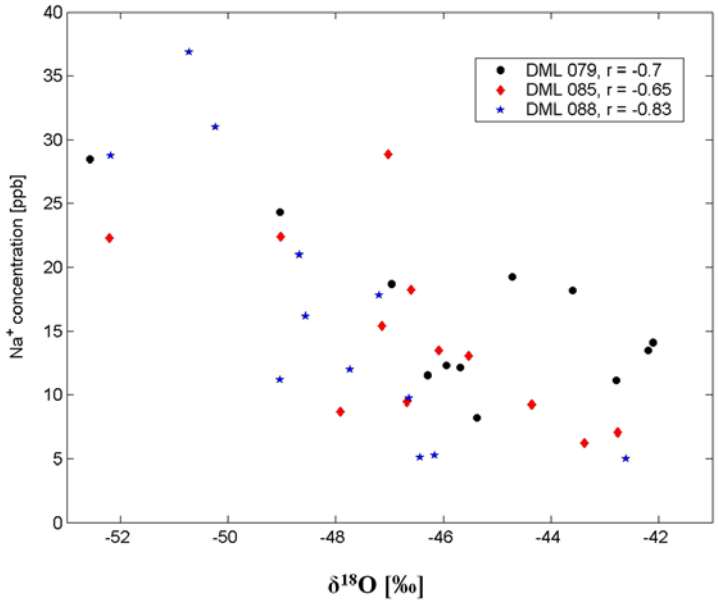

Figure 21: The annual mean values of $\delta^{18}O$ and Na^+ concentration from DML 79, 85 and 88 show a negative correlation on a significance level of > 95%.

The negative correlation between $\delta^{18}O$ and Na^+ can be explained by lacking precipitation for periods with increased $\delta^{18}O$ signal and lower sea-salt concentration. The concentrations of sea-salt aerosols in Antarctic snow reach maximum values during the winter half of the years (SOMMER et al. 2000b; GÖKTAS 2002b). The seasonality of sea-salt aerosol concentration is based on enhanced source strength (due to frost flower formation during sea ice expansion (RANKIN et al. 2002; KALESCHKE et al. 2004) and increased transport of sea-salt aerosols (due to higher cyclonic activity during austral winter periods (GÖKTAS, 2002b). REIJMER & VAN DEN BROEKE (2001) found up to 80% of the annual precipitation in DML to occur in four major precipitation events during 1998. Therefore it is likely, that whole seasons remain underrepresented in terms of their amount of precipitation (HELSEN et al., 2005). If the hydrological calendar lacks precipitation during spring, summer or autumn, the winter precipitation would be relatively overrepresented, including its content of sea-salt deposits.

4.2.2 Interannual variability of accumulation rate

The annual accumulation of snow for each snow pit is determined by the annual boundaries derived from the dating of the snow pits (see chapter dating). The mean accumulation rate with its standard deviation is displayed for each snow pit in Table 16. Also shown are the mean, the minimum and the maximum interannual changes of accumulation [%] observed within the records of the individual snow pits.

Table 16: Annual accumulation rates are displayed for all DML snow pits including the mean and standard deviation. Below, the relative interannual variability of accumulation is presented by its mean, minimum and maximum values according to each snow pit.

	DML 76	DML 77	DML 79	DML 81	DML 83	DML 85	DML 87	DML 88	DML 89	DML 90
mean [mm WE]	51±13	57±22	46±15	50±17	49±16	51±14	47±9	39±8	39±14	44±13
min [mm WE]	30	23	18	31	18	29	34	28	19	23
max [mm WE]	72	87	66	87	74	80	62	55	64	63
variab.[%]	33	54	64	46	49	30	23	18	28	37

The mean accumulation rate detected for the DML snow pit sites during 1994-2005 varied between 39 ± 8 mm WE * a^{-1} at DML 88 and 57 ± 22 mm WE * a^{-1} at DML 77. The year-to-year variation of annual accumulation at individual sites varied from 18 % at DML 88 to 64 % at DML 79. The mean annual accumulation rates found in this study are slightly lower than the accumulation rates reported by SOMMER et al., (2000a) (63, 61 and 44 mm WE * a^{-1}), who described 30 % as "typical year-to-year variation" of accumulation rate for DML. Table 16 provides an overview on the mean, minimum and maximum values of annual accumulation that were found within the records of each snow pit site.

The question to answer was, if the annual accumulation signal reflects the actual variability of annual precipitation in DML. If that was the case, the annual accumulation was expected to show positive correlations among the snow pit sites for the respective years. A correlation test revealed no correlation of accumulation between neighbouring snow pit sites on a 95 % significance level. Thus, the interannual accumulation was found to vary independently at each individual site and does not serve as an indicator of annual accumulation that is representative for the respective year. SOMMER et al. (2000a) support the finding of lacking intersite correlation of annual accumulation, as they only found a weak intersite correlation of accumulation in DML ice cores, when high frequencies with periods of less than 30 years were removed from the total signal.

In fact, annual accumulation in DML reveals a particular local pattern, because it results from the two synergetic processes: annual precipitation and the annual pattern of post-depositional redistribution of snow. Both occur in strong spatio-temporal variability themselves. The variability of accumulation is described by HELSEN et al. (2005) and references therein, who applied automatic weather stations in DML and measured the interannual variability of precipitation to be large. The post-depositional snow redistribution then determines how much of the precipitated snow eventually accumulates at the respective site, thus, it superimposes the precipitation signal as it either adds to the annual precipitation or reduces its amount. The determination of the annual accumulation values of the snow pit records do not distinguish between the two depositional processes. The annual accumulation rather presents the sum of snow that actually precipitated at the particular site and the snow, which is added or removed by post-depositional redistribution as inextricable information of the respective site during the respective year. Since DML with its annual accumulation of $<57 \pm 22$ mm WE is an area of very low accumulation (HELSEN et al., 2005), the records of annual accumulation are particularly vulnerable to the biasing effects of snow redistribution. Hence, the variability of accumulation within the records (up to 64 %) represents a high potential of noise corruption that determines the accuracy of the accumulation signal. Figure 22 displays the distribution of annual accumulation of all snow pit sites during 1994-2005 and shows the heterogenic variability of accumulation throughout the years.

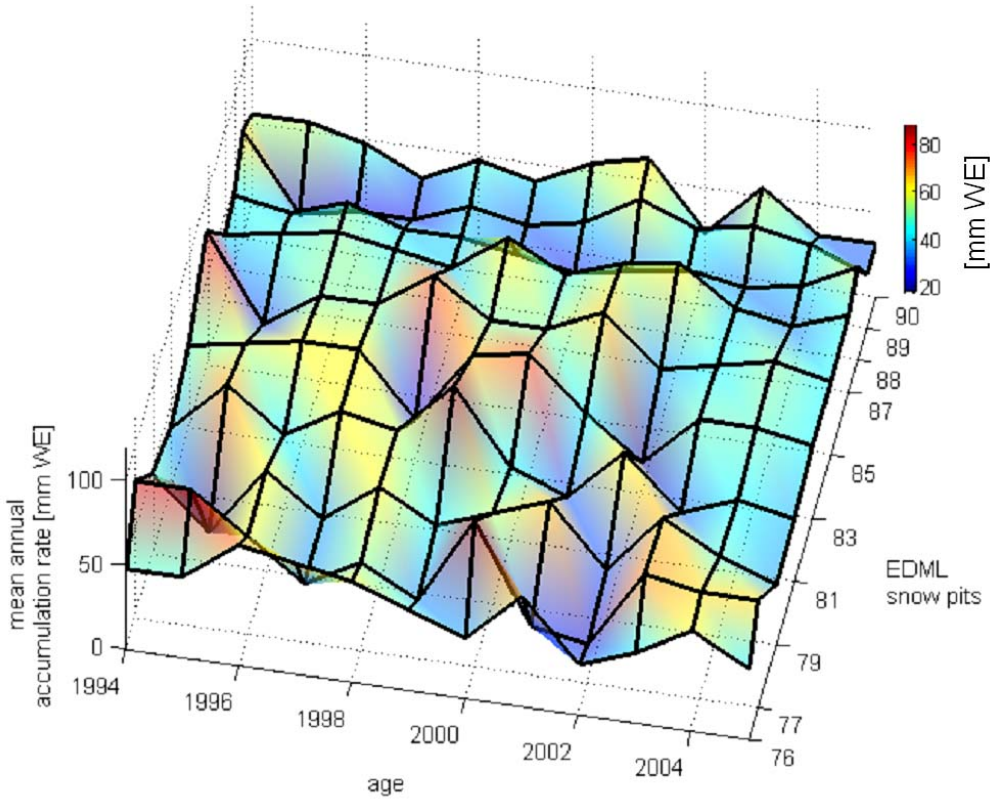

Figure 22: Interannual variability of accumulation, the comparison between all DML sites 76-90 during 1994-2005 shows no systematic pattern of annual accumulation

4.2.3 Interannual variability of sodium concentrations

Because most Na^+ and Cl^- ultimately derive from the ocean, the variability of annual Na^+ and Cl^- concentrations almost reveals the same pattern. Therefore, the discussion of the interannual variability from sea-salt derived aerosols will focus on Na^+ only.

Regarding the annual concentration range of Na, mean values between 14 ± 8 ppb and 23 ± 15 ppb were found at DML 89 and DML 76, respectively. The interannual variability of Na^+ ranges between 26 % at DML 87 towards 66 % at DML 76 (Table 17). Thus, the interannual variability of sea-salt aerosols is considered high.

Even though the validation between UTS and UTD measurements exhibited the Na^+ values from DML 83 and 85 to suffer slightly from contamination, the range of annual Na^+ concentrations and the interannual variability of Na^+ at these particular sites are comparable to the snow pits considered free of any contamination. Therefore, the Na^+ records of DML 83 and 85 were further on considered in the discussion.

Table 17: Means of annual Na^+ concentration per snow pit and variability of Na^+ on relative scale

Statistics of annual means from Na^+ concentration [ppb]										
DML	**76**	**77**	**79**	**81**	**83**	**85**	**87**	**88**	**89**	**90**
mean [ppb]	23±15	15±7	16±6	17±8	21±9	15±7	17±4	17±11	14±8	16±9
min [ppb]	9	8	8	9	13	6	11	5	4	5
max [ppb]	57	33	28	38	44	29	22	37	29	39
ann. variab [%]	66	48	37	48	43	49	26	65	58	54
mean accu. rate [mm WE]	51±13	57±22	46±15	50±17	49±16	51±14	47±9	39±8	39±14	44±13

Figure 23 displays the mean annual concentrations of Na^+ for all snow pits between 1994 and 2005. Few of the presented annual Na^+ records exhibit a weak pattern of increased annual Na^+ concentration during 1996, 2000 and 2004, which might result from considerably increased seasonal concentration of sea-salt aerosol (see chapter 4.1). The pattern is considered weak because only a fraction of the snow pits shows increased Na^+ concentrations; furthermore deviations on timing occur, where the latter could be a result of the dating error, which is determined at ±1 year.

Apart from the weak indication of the four year cyclicity of increased annual Na^+ concentrations, each snow pit has its individual signal of Na^+ concentration with an interannual variability of 50 %. Due to the high interannual variability, climatically induced variations of annual Na^+ concentration are obliterated as shown in Figure 23.

All annual Na^+ records of all DML sites were tested for intersite correlation. The results are shown in Table 18 and indicate that only 5 out of 45 calculations show the annual Na^+ records to correlate on a significance level ≥ 95 % according to $r < -0.58$ and $r > 0.58$. Hence, the majority of annual variations within individual Na^+ records are determined by a local pattern of Na^+ deposition rather than by climatic variations that accounted for all Na^+ records of the DML snow pits.

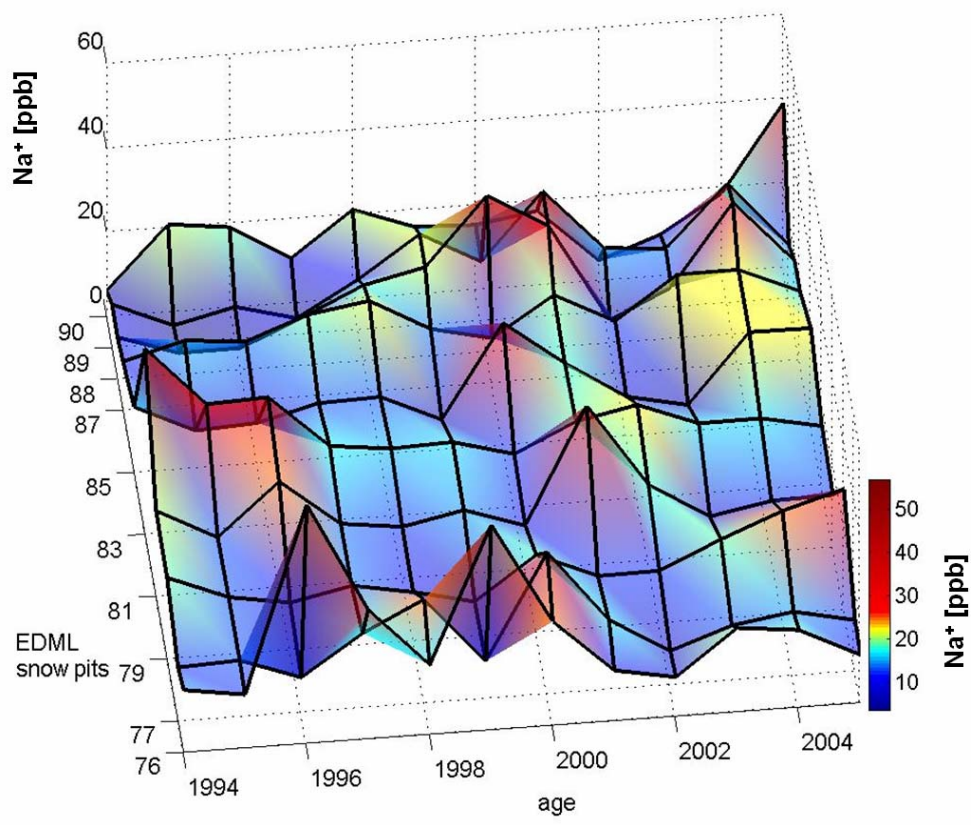

Figure 23: Comparison of annual Na^+ variability for all DML sites during 1994-2005

Table 18: The table displays the coefficients of correlation that were calculated for the correlation between all Na^+ snow pit records. The coefficient of $r < -0.58$ or $r > 0.58$ indicate a correlation above a significance level of ≥ 95 %. The r values that indicate correlations ≥ 95 % are printed in bold characters.

	DML 76	DML 77	DML 79	DML 81	DML 83	DML 85	DML 87	DML 88	DML 89	DML 90
DML 76	1	-0.20	-0.45	0.07	0.02	-0.30	-0.20	-0.08	-0.14	-0.04
DML 77	-0.20	1	0.11	-0.26	-0.41	**0.66**	0.04	**0.65**	0.00	0.06
DML 79	-0.45	0.11	1	-0.37	-0.13	**0.61**	0.16	0.25	0.09	0.43
DML 81	0.07	-0.26	-0.37	1	0.33	-0.04	-0.08	0.00	0.36	-0.10
DML 83	0.02	-0.41	-0.13	0.33	1	-0.31	-0.42	-0.57	-0.36	-0.36
DML 85	-0.30	0.66	0.61	-0.04	-0.31	1	-0.08	**0.75**	0.31	0.36
DML 87	-0.20	0.04	0.16	-0.08	-0.42	-0.08	1	0.15	0.29	0.18
DML 88	-0.08	0.65	0.25	0.00	-0.57	0.75	0.15	1	**0.69**	0.19
DML 89	-0.14	0.00	0.09	0.36	-0.36	0.31	0.29	0.69	1	0.03
DML 90	-0.04	0.06	0.43	-0.10	-0.36	0.36	0.18	0.19	0.03	1

4.2.4 Interannual variability of sulphate concentrations

From 1994-2005, the annual means of SO_4^{2-} concentration pits ranged between 64 ± 13 ppb at DML 76 and 112 ± 41 ppb at DML 89. The mean annual variations within individual snow pits ranged around 20 % at all DML snow pit site according to Table 19.

Table 19: Shown are annual means of SO_4^{2-} concentration per pit and annual variability of SO_4^{2-} on absolute and relative scale.

statistics of annual means from SO_4^{2-} concentration [ppb]										
DML	**76**	**77**	**79**	**81**	**83**	**85**	**87**	**88**	**89**	**90**
mean [ppb]	64±13	81±13	71±11	87±18	82±17	94±24	92±19	83±16	112±41	87±19
min [ppb]	44	59	57	63	54	64	63	54	72	63
max [ppb]	91	106	90	123	110	144	137	120	227	121
ann. variab. [%]	21	16	15	21	21	26	21	20	37	22
mean accu. rate [mm WE]	51±13	57±22	46±15	50±17	49±16	51±14	47±9	39±8	39±14	44±13

The calculated intersite correlations of the SO_4^{2-} records are displayed in Table 20 and show that a fraction of ~15 % of the SO_4^{2-} records reveals an intersite correlation on a significance level of ≥ 95 % (7 out of 45 records). This indicates that the majority of annual SO_4^{2-} concentrations show no significant correspondence among the DML records.

Table 20: Displayed are the coefficients of correlation that were calculated for the correlation between all SO_4^{2-} snow pit records. The coefficient of r < - 0.58 or r > 0.58 indicate a correlation above a significance level of ≥ 95 %. The r values that indicate correlations ≥ 95 % are printed in bold characters.

	DML 76	DML 77	DML 79	DML 81	DML 83	DML 85	DML 87	DML 88	DML 89	DML 90
DML 76	1	0.14	0.02	-0.04	-0.22	-0.29	0.02	-0.54	0.42	0.03
DML 77	0.14	1	-0.19	0.39	0.43	0.03	-0.14	0.01	0.22	0.45
DML 79	0.02	-0.19	1	-0.08	0.34	0.07	**0.68**	0.00	-0.09	0.23
DML 81	-0.04	0.39	-0.08	1	0.48	0.46	0.13	0.02	0.52	**0.61**
DML 83	-0.22	0.43	0.34	0.48	1	**0.67**	0.33	0.32	0.37	**0.88**
DML 85	-0.29	0.03	0.07	0.46	0.67	1	0.17	**0.61**	0.28	**0.70**
DML 87	0.02	-0.14	0.68	0.13	0.33	0.17	1	0.31	0.34	0.48
DML 88	-0.54	0.01	0.00	0.02	0.32	0.61	0.31	1	0.07	0.33
DML 89	0.42	0.22	-0.09	0.52	0.37	0.28	0.34	0.07	1	**0.62**
DML 90	0.03	0.45	0.23	0.61	0.88	0.70	0.48	0.33	0.62	1

In Figure 24, the interannual variability of SO_4^{2-} concentrations is displayed for all DML snow pits during the period of 1994-2005. It is visualized that the annual variations of the SO_4^{2-} concentration signal do not exhibit a consistent pattern that accounts for all SO_4^{2-} records but shows the individual SO_4^{2-} records to vary independently. Thus, the annual variability of SO_4^{2-} determined for the DML snow pits does not reflect an unambiguous parameter of climatic variability.

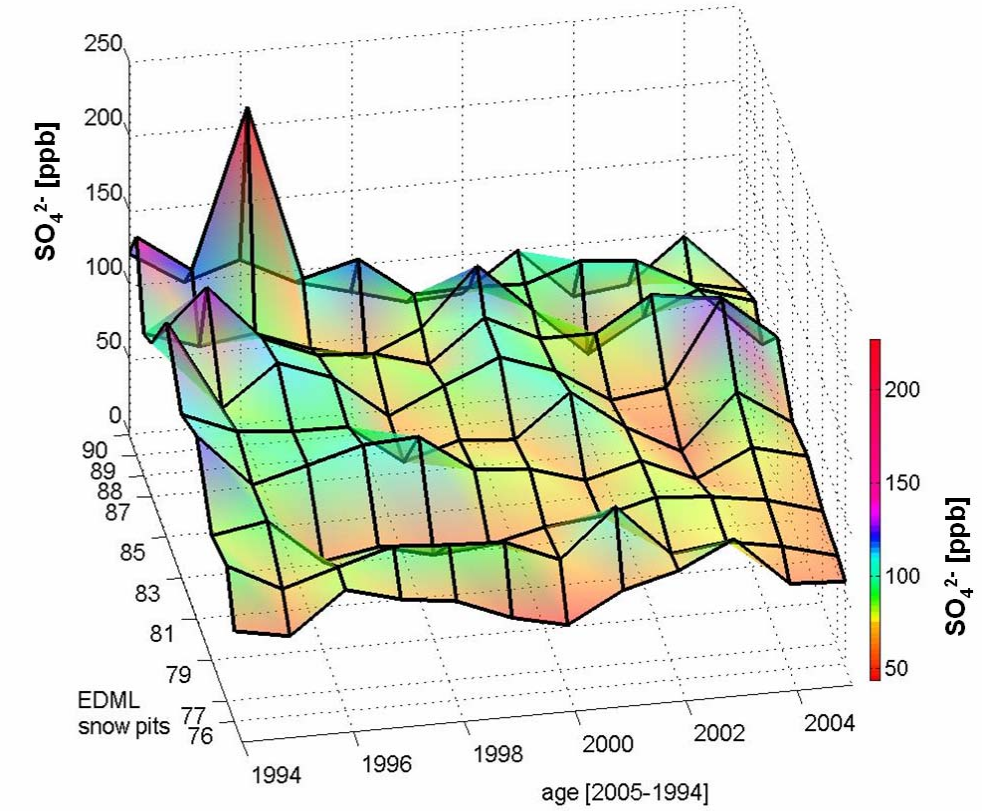

Figure 24: Comparison of annual SO_4^{2-} variability for all DML sites during 1994-2005

The records of annual SO_4^{2-} concentration exhibit a multi-annual variability (Figure 24). Following the line of annual SO_4^{2-} concentrations from 1994 to 2005 across all records, the mean annual SO_4^{2-} concentration decreased throughout the period. This is explained by a sudden increase of atmospheric SO_4^{2-} concentrations due to the volcanic eruptions of Mount Pinatubo (June 1991) and Mount Cerro Hudson (August 1991). The SO_4^{2-} concentrations decreased during the following years until they reach background level in 1996/1997. Cole-Dai & Mosley-Thompson (1999) found the volcanic signal of the Pinatubo and Cerro Hudson eruptions in South Pole snow pits until 1994.

4.2.5 Interannual variability of nitrate concentrations

The mean annual concentrations of NO_3^- range from 36 ± 15 ppb at DML 90 to 62 ± 14 ppb at DML 77 (Table 21). The mean interannual variability ranges around 30 % and reaches up to 53 % at DML 89.

Table 21: Displayed are annual means of NO_3^- concentration per pit [ppb] and annual variability of NO_3^- concentration [%]. In addition, the mean annual accumulation rate of each snow pit is shown.

statistics of annual means from NO_3^- concentration [ppb]										
DML	**76**	**77**	**79**	**81**	**83**	**85**	**87**	**88**	**89**	**90**
mean [ppb]	51±13	62±14	55±12	54±8	52±6	53±21	47±15	41±12	45±23	36±15
min [ppb]	29	46	34	42	43	24	29	23	25	25
max [ppb]	70	101	79	72	65	107	85	63	110	79
ann. variab. [%]	26	23	22	15	12	39	32	30	53	41
mean accu. rate [mm WE]	51±13	57±22	46±15	50±17	49±16	51±14	47±9	39±8	39±14	44±13

The most striking feature of the NO_3^- records from DML snow pits is the consistent pattern of decreasing NO_3^- concentration during the period of 2003-2005. During these years, the NO_3^- profiles exhibit a particular steep concentration gradient (Figure 25 A and B). Once NO_3^- is deposited, it can outgas into the atmosphere as gaseous HNO_3 or gets destroyed by photolysis (RÖTHLISBERGER et al., 2002a). Because the photo oxidative mechanism requires sunlight, it exclusively takes place during the summer and is furthermore restricted by the penetration depth of sunlight into the snow layers. WELLER et al. (2004) describe the post-depositional loss of NO_3^- in snow from DML to be restricted to the first 5.4 to 6.5 years after deposition. This can also be observed within the DML snow pit records of NO_3^-, where the deposits older than 2001 reach a stable NO_3^- concentration (Figure 25 B).

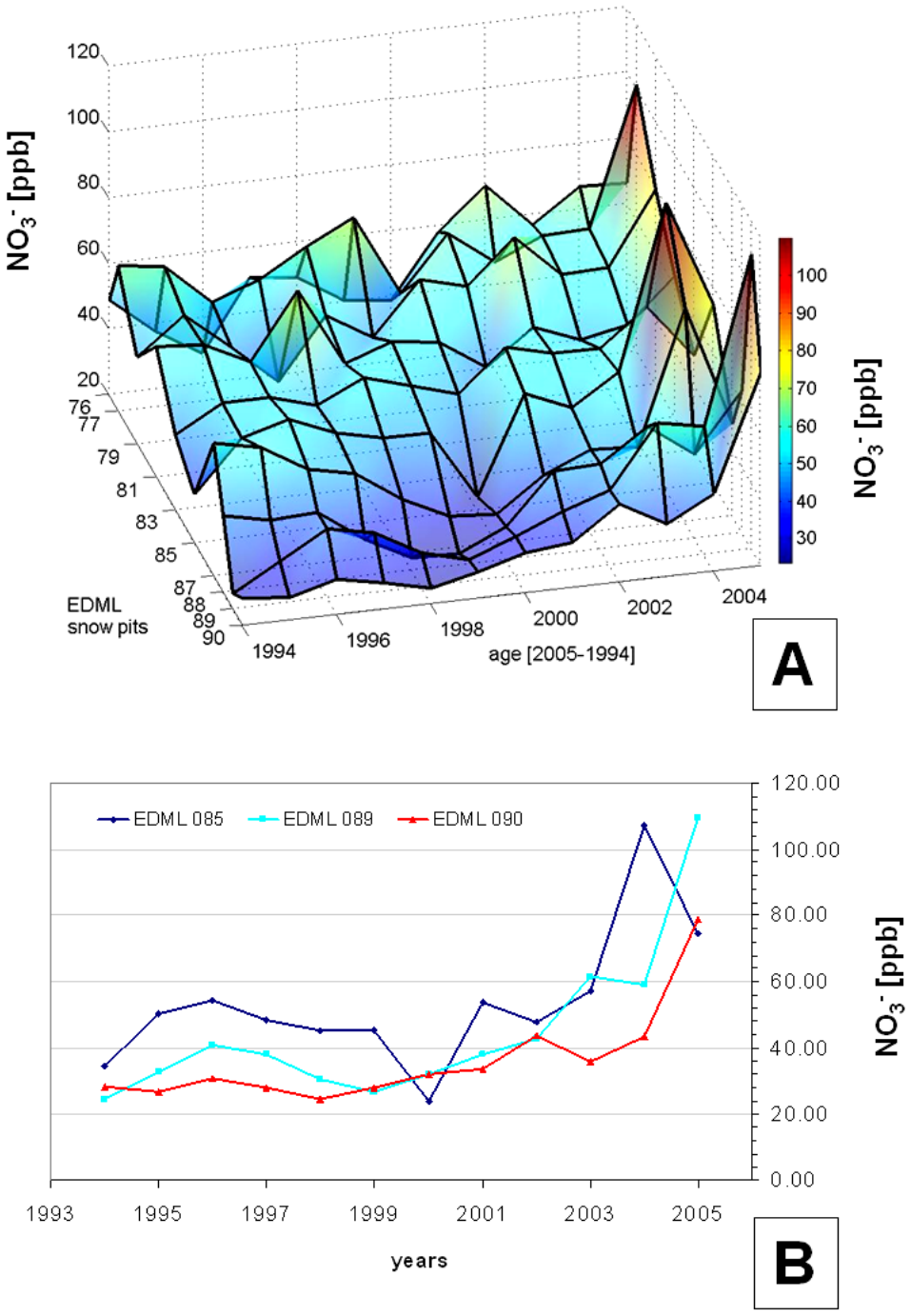

Figure 25: The figures show the interannual variation of NO_3^- concentration in all snow pits (A) and from 3 particular snow pit records DML 77, 89, and 90 (B). In all records of A and B, the annual variability of NO_3^- concentrations is of the greatest amounts within the first year and significantly decreases by a factor of ~2 within 5 years after deposition.

Owing to the steep concentration gradient within the upper layers, the NO_3^- records from the DML snow pits exhibit intersite correlations in 11 out of 45 comparisons that made 25 % of all calculations (Table 22). Apart from the decreasing NO_3^- concentration after the first years of deposition, the NO_3^- records of the 10 DML snow pits show no consistent pattern of annual NO_3^- concentration (Figure 25 A). In fact, the variability of annual NO_3^- concentration is a local characteristic of individual annual NO_3^- snow pit records that do not allow for climatic interpretation on an annual base.

Table 22: The table displays the coefficients of correlation that were calculated for the correlation between all NO_3^- snow pit records. The coefficient of $r < -0.58$ or $r > 0.58$ indicate a correlation above a significance level of ≥ 95 %. The r values that indicate correlations ≥ 95 % are printed in bold characters.

	DML 76	DML 77	DML 79	DML 81	DML 83	DML 85	DML 87	DML 88	DML 89	DML 90
DML 76	1	0.35	0.56	-0.05	0.49	0.54	0.33	0.57	0.56	**0.62**
DML 77	0.35	1	0.46	0.27	-0.09	0.33	0.04	0.45	0.69	**0.72**
DML 79	0.56	0.46	1	-0.21	0.23	0.28	0.05	**0.64**	**0.68**	**0.78**
DML 81	-0.05	0.27	-0.21	1	-0.58	-0.07	0.15	0.01	0.17	0.18
DML 83	0.49	-0.09	0.23	-0.58	1	**0.76**	0.46	0.22	0.20	0.12
DML 85	0.54	0.33	0.28	-0.07	0.76	1	**0.73**	0.49	**0.61**	0.52
DML 87	0.33	0.04	0.05	0.15	0.46	0.73	1	0.41	0.23	0.18
DML 88	0.57	0.45	0.64	0.01	0.22	0.49	0.41	1	**0.79**	**0.75**
DML 89	0.56	0.69	0.68	0.17	0.20	0.61	0.23	0.79	1	**0.94**
DML 90	0.62	0.72	0.78	0.18	0.12	0.52	0.18	0.75	0.94	1

According to Figure 26, the variability of annual means from NO_3^- and Clx correlates in 3 snow pits on a significance level of ≥ 95 % with values of $r = 0.82$ at DML 76, $r = 0.63$ at DML 79 and $r = 0.59$ at DML 90. A possible explanation for the correlation would be that both NO_3^- and Cl^- can be deposited in the gas phase as either HNO_3 or HCl. Both HNO_3 and HCl can be dry deposited as well as transported to the ground by scavenging processes (Piel 2004). The correlation of NO_3^- and Clx can therefore result from the identical pathway of NO_3^- and Cl^-, the latter being an essential factor to represent the Clx. On top of the described correlations in the snow pits DML 76, 79 and 90, further positive correlations between NO_3^- and Clx were found, but they do only appear with a significance level of ≤ 95 %.

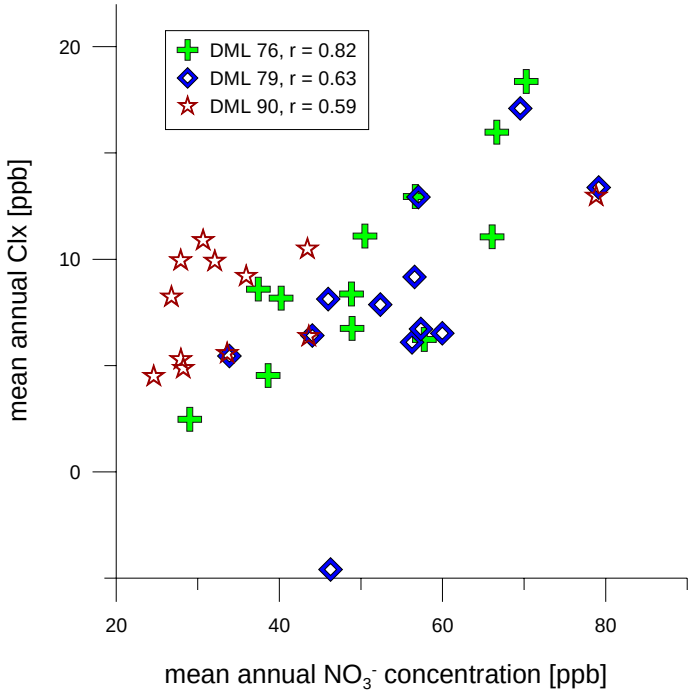

Figure 26: Correlation of mean annual NO_3^- and Clx concentration from DML 76, 77, 90

4.2.6 Interannual variability of chloride excess

The mean annual Clx concentration ranged between 3±4 ppb at DML 83 and 14±17 ppb at DML 89. According to the low mean of Clx, the interannual variability within individual snow pit records exhibits high variations between 32 % at DML 88 and 123 % at DML 89 (Table 23).

Table 23: Displayed are annual means of Clx concentration per pit [ppb] and annual variability of Clx concentration [%]. In addition, the mean annual accumulation rate of each snow pit is shown.

statistics of annual means from Clx concentration [ppb]										
DML	**76**	**77**	**79**	**81**	**83**	**85**	**87**	**88**	**89**	**90**
mean [ppb]	10±5	7±3	8±4	12±4	3±4	9±4	12±4	13±4	14±17	8±3
min [ppb]	2	2	-5	6	-4	1	8	7	-20	4
max [ppb]	18	11	17	19	11	16	20	19	34	13
ann. variab. [%]	48	41	67	34	109	44	36	32	123	34
mean accu. rate [mm WE]	51±13	57±22	46±15	50±17	49±16	51±14	47±9	39±8	39±14	44±13

In all DML snow pit records, no intersite correlation between the Clx records was found at all that revealed a significance level of ≥ 95 %. The high interannual variability of Clx was found to be specific to each individual site and represented no annual climatic signal that could be considered representative for DML. This finding is indicated in Figure 27, where the annual variability of the Clx profiles does not correspond throughout individual years.

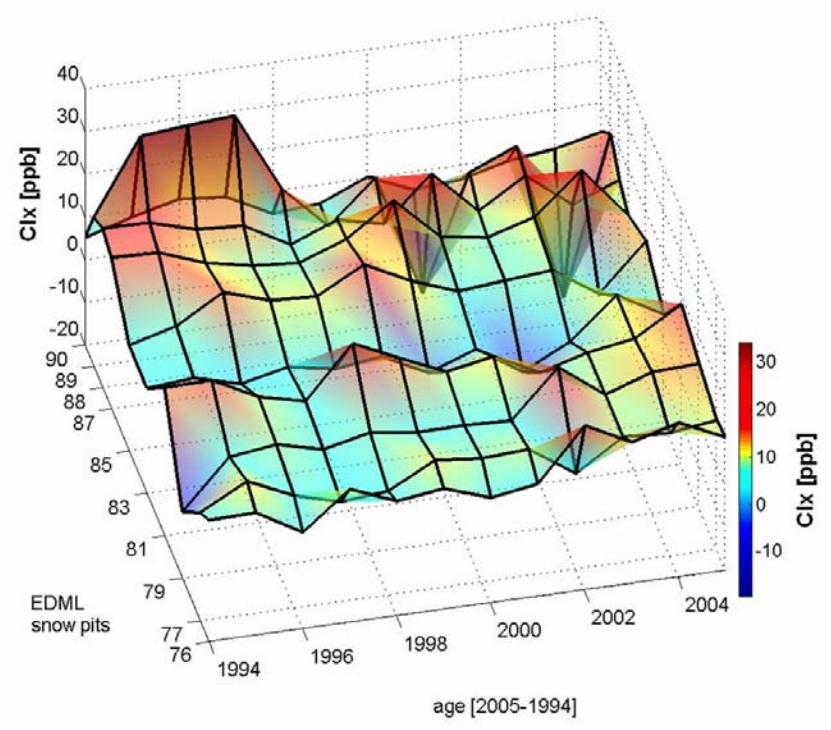

Figure 27: Comparison of annual Clx variability for all DML sites during 1994-2005

4.2.7 Summary of interannual variability

- Post-depositional redistribution of snow biased the annual signals of all glacio-chemical parameters ($\delta^{18}O$, annual accumulation, Na^+ representative for sea-salt aerosol, SO_4^{2-}, NO_3^-, Clx) and masked climatic pattern of the records that were expected on annual time scale

- additional post-depositional process of water vapour diffusion altered the $\delta^{18}O$ signal, no significant intersite correlation could be demonstrated for $\delta^{18}O$

- variability of annual accumulation pattern was not synchronized between individual snow pits

- Five significant intersite correlations between 45 comparisons could be demonstrated between the sodium records of all individual snow pits

- Seven significant intersite correlations (out of 45 comparisons) were demonstrated between all sulphate records. Continuously decrease of elevated sulphate concentrations towards biogenic background concentration from 1994 to 1996 was attributed to residual sulphate input resulting from volcanic emissions (eruptions of Mount Pinatubo and Cerro Hudson in 1991)

- eleven significant intersite correlations between all 45 comparisons were found, relatively high intersite correlation attributed to post-depositional nitrate loss (outgassing) that occurred in all snow pits

- no intersite correlation could be demonstrated for chloride excess

5. Spatial variability of glacio-chemical parameters in snow

5.1 Spatial variability of $\delta^{18}O$

The oxygen isotope records of the DML snow pits exhibited a linear relation of decreasing $\delta^{18}O$ values with increasing distance to the EDML drill site of r = 0.88, (Figure 28). The depletion of $\delta^{18}O$ results from the cooling of air masses (DANSGAARD, 1964) during progressively inclining altitudes with increasing distance to EDML, Figure 29 B.

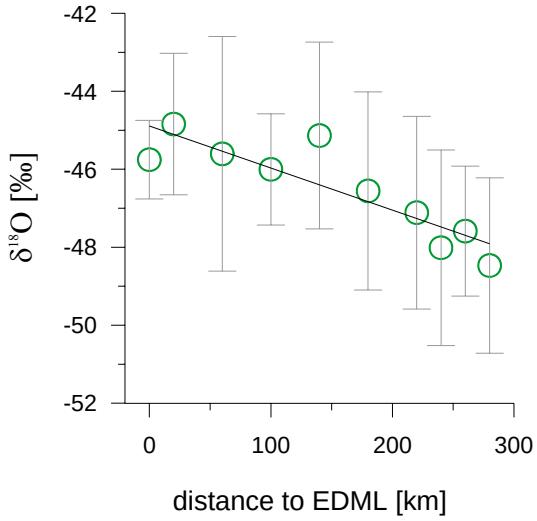

Figure 28: Displayed is the decrease of mean $\delta^{18}O$ in linear relation with increasing distance to EDML asl (r = 0.88).

HUYBRECHTS et al., (2007) found the inclining altitude upstream EDML to cause a temperature decrease of 2.5 °C per 100 km. Transferred on the total distance of 280 km covered by the DML snow pits, a total decrease of 7 °C caused the systematic depletion of $\delta^{18}O$ as observed in the snow pit records. Thus, the $\delta^{18}O$ records exhibit a systematic spatial signal that also affects the $\delta^{18}O$ record of EDML. Hence, the EDML $\delta^{18}O$ record is suggested for correction according to the following regression:

$$(UTS): \quad Y = -0.011 * X - 44.9; \quad (r^2 = 0.78) \tag{25}$$

5.2 Spatial variability of accumulation rate

Figure 29 A shows the spatial decline of mean accumulation rates [mm WE * a^{-1}] to be in linear relation with increasing distance to the EDML deep drilling site [km] (r = 0.75) (Figure 29 B). Since the EDML drill site is located at a saddle position on the ice divide, further distances upstream EDML go along with increasing altitude asl (r = 1), (Figure B).

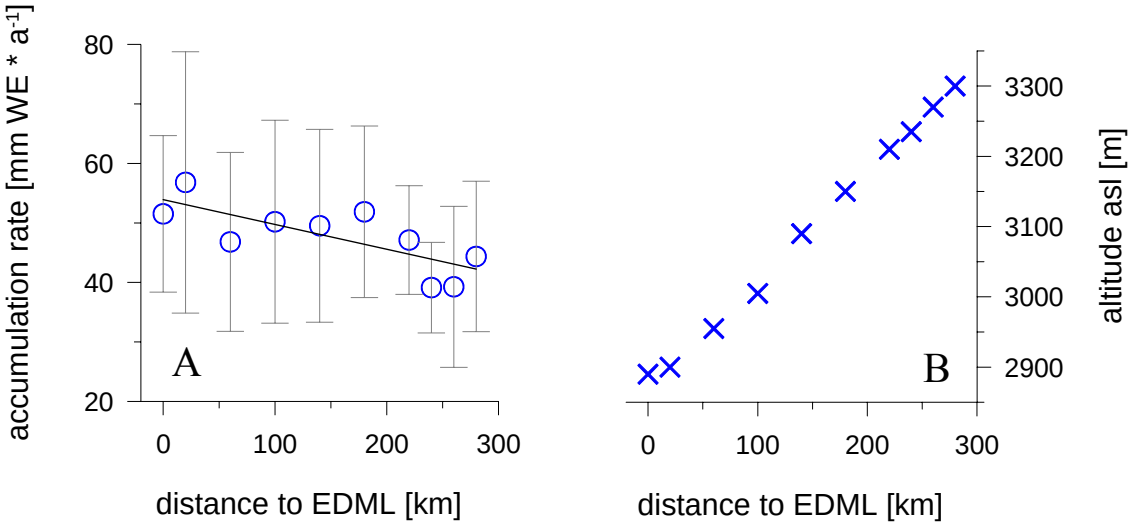

Figure 29: A shows the decrease of mean accumulation in linear relation to increasing distance to EDML (r = 0.75). B: The spatial increase of altitude with increasing distance to the EDML deep drilling site correlates with r = 1.

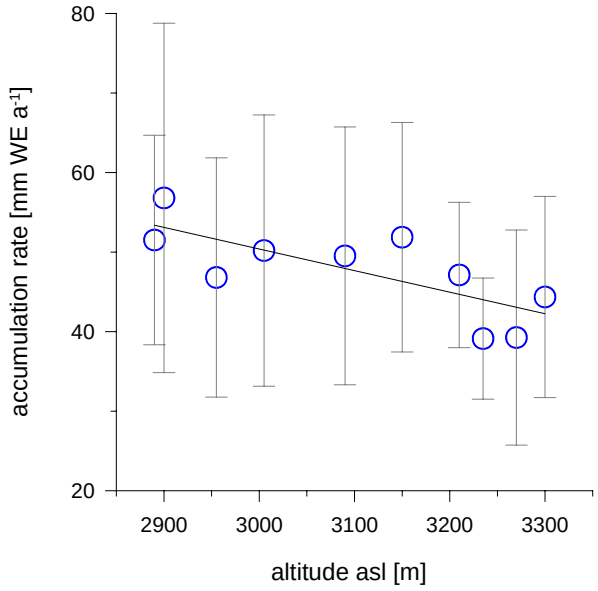

Figure 30: Displayed is the decrease of mean accumulation in linear relation with increasing altitude asl (r = 0.75).

Thus, the spatial variation of accumulation is of linear relation to the spatial variation in altitude with r = 0.75 (Figure 30).

The accumulation in DML was discussed to be of high interannual variability with a mean value of ~40 % where the high variability is caused by local redistribution of snow (see chapter 4.2). RICHARDSON & HOLMLUND (1999) found the accumulation on the Antarctic plateau in DML to exhibit a systematic spatial pattern which can be grouped in three zones: From 2400 m to 2840 m asl, the accumulation successively decreases. The following intermediate altitude (2840 m to 3140 m asl) is characterized by net erosion where RICHARDSON-NÄSLUND (2004) found the highest spatial variations in accumulation of 50 %. The third zone between 3140 m and 3450 m exhibited a slow and successive decrease in accumulation (RICHARDSON & HOLMLUND, 1999).

The investigated DML snow pits are located within the upper two zones according to the classification of RICHARDSON & HOLMLUND (1999) Figure 29 A). In the lower zone from 2890 m to 3100 m (DML 76 - DML 83), the accumulation rate slightly decreases by 14 % from 57 mm WE * a^{-1} to 49 mm WE * a^{-1}. Chapter 4.2 presents a high interannual variability of accumulation at DML 76 - DML 83 that ranges between 33 % and 64 % as indicated by large error bars (Figure 29 A). This zonal pattern of accumulation is in good agreement to the description of the respective area by RICHARDSON & HOLMLUND (1999).

In altitudes higher than 3100 m asl, the spatial decrease of annual accumulation reaches 24 % from 51 mm WE * a^{-1} to 39 mm WE * a^{-1} (DML 85 - DML 90) and coincides with decreased interannual variations of annual accumulation (18 % - 37 %). Thus, the accumulation pattern in DML snow pits from altitudes > 3100 m asl also meet the suggested classification of RICHARDSON & HOLMLUND (1999). Furthermore, the finding of decreasing accumulation above 3100 m asl is in accordance with the stratigraphy derived from air radar measurements of DML (STEINHAGE, unpublished data) as well as the accumulation rates calculated by GÖKTAS et al. (2002). GÖKTAS et al. (2002) found accumulation rates of ~70 mm WE * a^{-1} at two comparable snow pit sites (DML 15 and DML 16) at altitudes of 2970 m and 3100 m above sea level, respectively. Here, the intermediate firn core DML 17 (19.57 m in length) taken at 3160 m above sea-level also exhibited a significant decrease in average accumulation rate to 47 mm WE * a^{-1}.

The finding of a spatially non linear decreasing rate of annual accumulation further upstream the EDML ice core could be valuable information to the dating of the EDML ice core and to the interpretation of ion concentrations that depend on the accumulation rate. To find robust conclusions on the spatial change of the accumulation rate on the Antarctic plateau further investigations are suggested.

5.3 Spatial variability of sodium

Due to the constant mixing ratio of sodium and chloride in sea water, the spatial variability of sodium concentrations is considered representative for the spatial variability of sea salt aerosol in DML snow pits. According to Figure 31 A, the Na^+ concentrations stay on a constant level of 16 ppb (UTS) to 15 ppb (UTD) and show minor variations. The apparent exception is the sodium concentration of ~23 ppb at DML 76 which occurs in both the UTS and the UTD data. Since DML 76 is located in the vicinity of Kohnen Station, the higher concentrations can possibly result from contamination due to the operation of Kohnen (start of operation in 2001). At DML 83, an outstanding sodium concentration of ~21 ppb is exclusively apparent within the UTS record. Higher sodium concentrations in the UTS records of DML 83 are previously described to possibly result from contamination of the UTS sampling gear or strong local variability of ion deposition on a scale of meters (chapter 3.3.4 and 3.3.5).

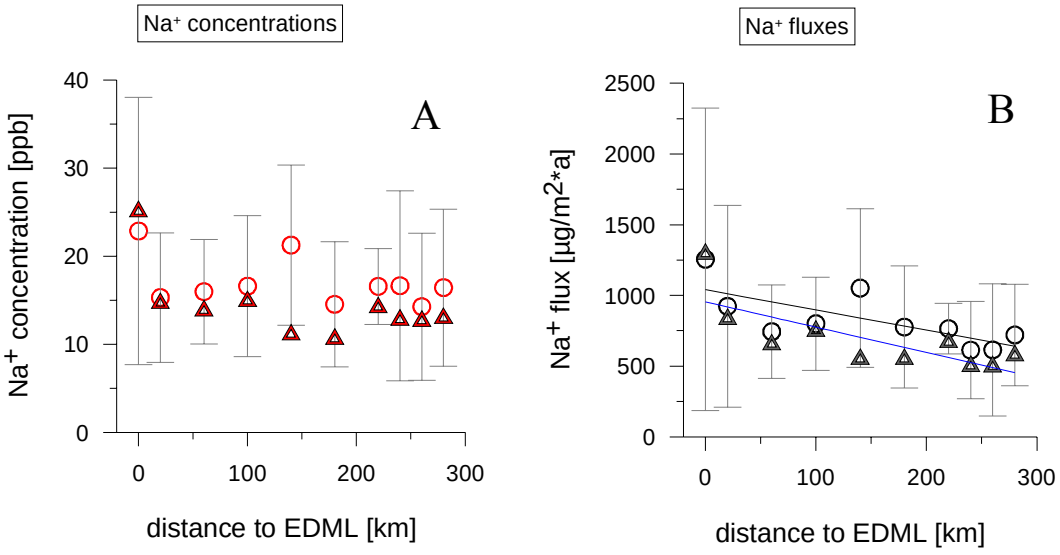

Figure 31: Shown are sodium concentrations (A) and fluxes (B) determined in UTS (circles) and UTD (triangles) samples over distance to the EDML deep drilling site. The UTD concentrations and fluxes were determined as averages from sampled snow pit wall down to a depth level equivalent to the bottom depth of the 12th year from the respective UTS sampling. Due to the averaging, no measure of variability can be given. In Figure B, the linear fit of the UTS data is presented as black line, the respective linear fit of the UTD data is shown in blue.

GÖKTAS et al. (2002a) describe the concentration of sea salt derived ions to decrease exponentially with increasing altitude. At altitudes > 2750 m asl (taken from plot in GÖKTAS et al. 2002a), the spatial decrease of sea salt aerosol concentrations levelled out. Spatial variations of the threshold of 2750 m asl could possibly explain the higher sodium concentrations within the UTS and the UTD samples of the lower most snow pit DML 76 while the sodium concentrations of all other snow pits show the constant range described by GÖKTAS et al. (2002). Thus, the spatial pattern of sea-salt derived ion concentrations of this study is in good agreement to the pattern described by GÖKTAS et al. (2002a).

Besides DML 76, the sodium concentrations within the DML snow pit samples exhibit a constant level with the spatial decline of accumulation rates. Referring to equation (7), a predominance of wet deposition mechanisms can be inferred for the deposition of sea salt derived aerosol in DML snow. This is because the concentration of sea salt ions remains stable despite the reduced dilution of the fraction of the dry deposited sea salt ions by the declining mean of accumulation. Thus, the concentration of sea-salt ions is also mathematically independent from the spatial variability of accumulation. As a consequence of the spatial decline in annual accumulation, the net deposition of sea salt decreases, which can

be inferred from equation (6). The spatial decline of sea salt fluxes with decreasing accumulation is verified by a linear regression of $r = 0.72$ (UTS) and $r = 0.76$ (UTD) according to Figure 31. Alternatively, a spatial decrease in atmospheric sea salt aerosol concentrations with altitude could be compensated by the decline in accumulation rate, if a considerable fraction of sea salt aerosol was dry deposited. However, in view of the maritime character of air masses bringing sea salt aerosol and moisture, wet deposition of sea salt aerosol seems to be most likely.

A correction of the EDML deep ice core record for systematic spatial variability of sea salt derived ion concentration seems therefore not necessary.

5.4 Spatial variability of chloride excess

The UTD dataset exhibits a distinct spatial variability of increasing chloride excess concentrations ($r = 0.88$) and fluxes ($r = 0.67$) with higher distance to the EDML deep drilling site, (Figure 32). (Clx reflects the Cl^- fraction not directly linked to sea salt aerosol particles.) In the UTS dataset (which is subject to occasional contamination of samples), the linear relation between rising Clx concentrations and increasing distance to EDML is insignificant ($r = 0.39$; Figure 32 A), while the Clx flux derived from UTS samples doesn't even show a spatial gradient at all ($r = 0.02$; Figure 32 B). One possible explanation for the lacking spatial variability of Clx concentration in the UTS dataset would be a slight contamination that might have possibly biased the UTS dataset, as mentioned in chapter (see chapter 3.3.4 and 3.3.5). This potential contamination might have affected DML 83, which shows the lowest and most deviating mean Clx values. Note, the deviation is within a Clx range of ~5 ppb, which only represents a fraction of the annual mean from total chloride concentration (40 ppb).

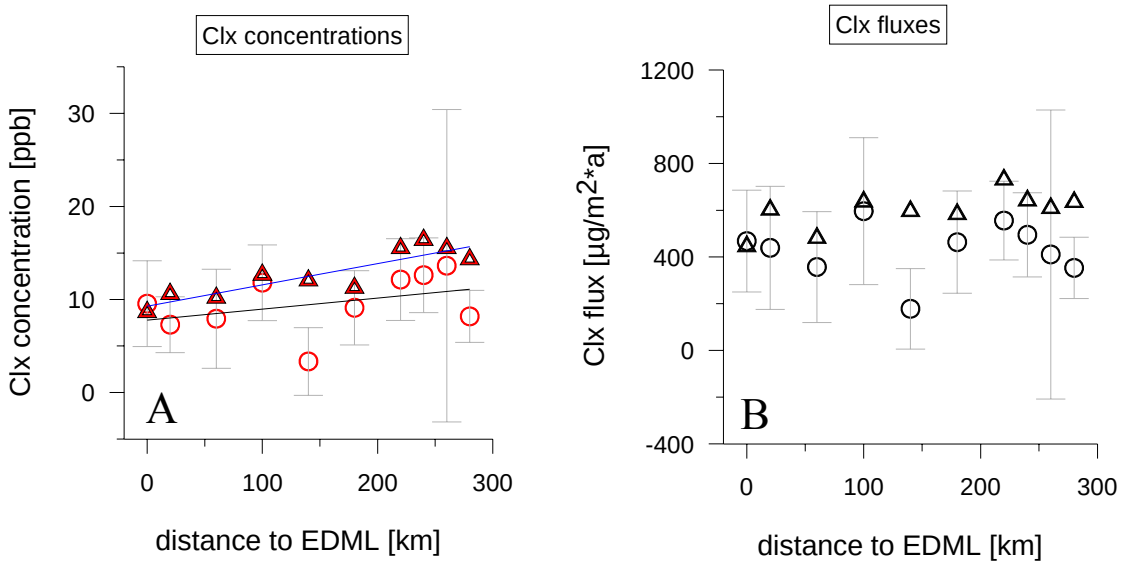

Figure 32: Chloride excess concentrations (A) and fluxes (B) determined in UTS (circles) and UTD (triangles) samples over distance to the EDML deep drilling site. The UTD concentrations and fluxes were determined as averages from sampled snow pit wall down to a depth level equivalent to the bottom depth of the 12th year from the respective UTS sampling. Due to the averaging, no error can be numbered. In plot A, the linear fit of the UTS data is presented as black line, the respective linear fit of the UTD data is shown in blue.

A possible explanation for Clx concentration to successively increase upstream EDML would be the progressive proximity to a further Cl^- source that is not the ocean. While WELLER et al. (2004) found no evidence for post-depositional chloride loss in DML, RÖTHLISBERGER et al. (2003) observed distinct chloride losses from EPICA Dome C ice core, which was drilled at an ultra-low accumulation site (25 mm WE a^{-1}) on the Antarctic plateau. If the ultra-low accumulation Antarctic plateau serves as HCl source area, downhill transported HCl would add to the local chloride budget and, thus, increase the Clx concentration at the place of its deposition. If the Antarctic plateau above the DML snow pits releases HCl that gets transported downhill towards EDML, this process could possibly explain the observed higher Clx concentrations in higher altitude, as these DML snow pits are nearest to the HCl source.

Additionally, a predominance of dry deposition could explain rising Clx concentrations with increasing altitude (including the deposition of discussed HCl from Antarctic source). According to equation (7), the spatially inclining Clx concentration could result from the coupling of largely dry deposited Clx and the decline of accumulation. The driving mechanism is explained within chapter 5.8 in detail. The mean Clx concentrations are plotted in relation to the inverse accumulation rate (Figure 33), where the slope of the regression

expresses the total amount of dry deposited Clx (FISCHER, 1997). The calculated regression for Clx concentration in UTD samples over the inverse accumulation rate is found to be:

$$(UTD): \quad Y = 784 * X - 4.0; \quad (r^2 = 0.61) \tag{26}$$

According to the regression, 784 µg/m^2 * a of Clx would be dry deposited on average over DML. Since this amount exceeds the total amount of annual Clx flux (Figure 32 B), the calculated flux most likely contains a high error range and is, thus, inappropriate to explain the spatial pattern of Clx deposition without correction.

The positive and increasing Clx concentration with altitude, hence declining snow accumulation, rules out a post-depositional loss of HCl from the snow pack and is, thus, in line with results of WELLER et al. (2004). Otherwise, lower accumulation sites, where single snow strata are exposed to the surface over a longer time, should show lower Clx concentrations.

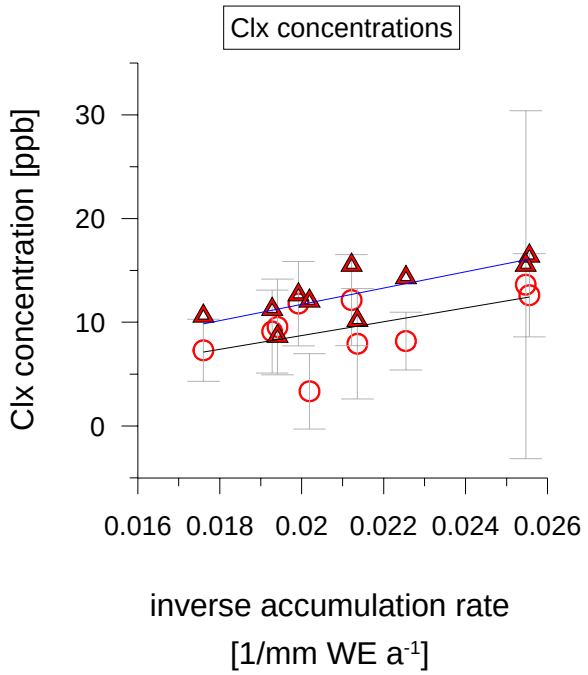

Figure 33: Chloride excess concentrations over inverse accumulation rate show the linear relation between Clx concentration and inverse accumulation rate of r = 0.88 of the UTD samples and only r = 0.39 for the UTS samples.

Both the UTS and the UTD dataset of Clx records do reflect systematic spatial variations in Clx concentrations with spatial incline of the study area, where a significant linear relation was assigned to the UTD dataset. The UTD data were deliberated more robust than the UTS data due to the weakness of the UTS dataset resulting from potential contamination. The indication of significant spatial relation between Clx concentration and distance to the EDML deep drilling site by the UTD dataset is, thus, accepted as stronger argument than is the lack of significant relation as derived from the UTS dataset. According to the presented interpretation of the Clx record from the UTD dataset, a correction of the Clx concentration record of the EDML deep ice core is suggested with regards to the following regression:

$$(UTD): \quad Y = 0.023 * X + 9.3; \quad (r^2 = 0.78) \tag{27}$$

Note, the suggestion for correction is also supported by the UTS dataset; however, the UTS data lack a significance level of ≥ 95 %.

5.5 Spatial variability of non sea-salt calcium

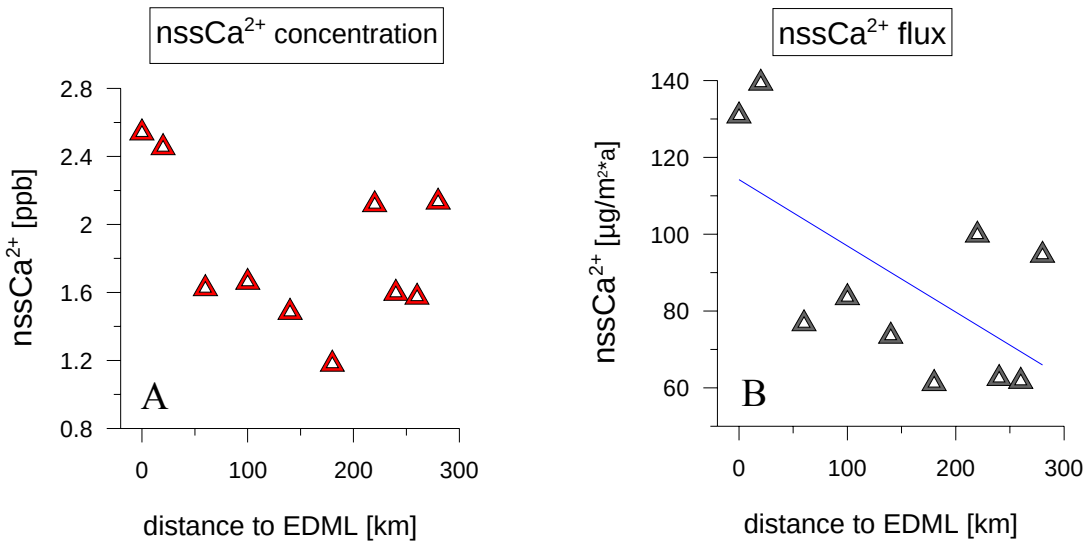

Figure 34: Shown are non sea salt calcium concentrations (A) and fluxes (B) determined in UTD samples over distance to the EDML deep drilling site. The UTD concentrations and fluxes were determined as averages from sampled snow pit wall down to a depth level equivalent to the bottom depth of the 12th year from the respective UTS sampling. Due to the averaging, no error can be numbered. The linear fit of the UTD data is presented as blue line in Figure B.

Most of the UTS samples were found to be contaminated in calcium. Therefore, the discussion of $nssCa^{2+}$ refers to the UTD dataset, only. The very low concentration range of non sea salt calcium of ≤ 2.5 ppb is just above the detection limit of the applied ion chromatography. Interpreting the variability of $nssCa^{2+}$ records is, therefore, limited. Similar to the pattern of sodium concentrations and fluxes, $nssCa^{2+}$ concentrations do not show a significant spatial effect within the concentration records as result from decreasing accumulation (Figure 34). The independence of accumulation would imply the dominance of wet deposition mechanisms for $nssCa^{2+}$, which is also indicated by a spatial decline of $nssCa^{2+}$ flux with decreasing accumulation according to equation (6). However, due to the detection problem any inferences on deposition mechanisms for calcium bearing particles has to be regarded as preliminary until better measurements are available e.g. from continues flow analysis (SOMMER, et al., 2000).

The applied interpretative method to investigate the spatial variability of non sea salt calcium concentrations gives evidence that there is no need to correct for the $nssCa^{2+}$ record of the EDML deep ice core. However, this suggestion is not based on robust data due to the very low concentrations of $nssCa^{2+}$ and the potential source of errors due to the proximity of $nssCa^{2+}$ concentrations to the technical detection limit of the IC.

5.6 Spatial variability of nitrate

The mean annual nitrate concentrations in the DML snow pits clearly decreases with increasing distance to the EDML deep drilling site in both datasets of UTS and UTD samples (Figure 35). The coefficient of correlation is calculated as $r = 0.82$ for the UTS and as $r = 0.78$ for the UTD samples. The mean annual NO_3^- fluxes exhibit a similar pattern and decrease with increasing distance to the EDML deep drilling site (Figure 35). The linear relation of mean annual NO_3^- flux and distance to the EDML site is marked by $r = 0.83$ for both the UTS and UTD data.

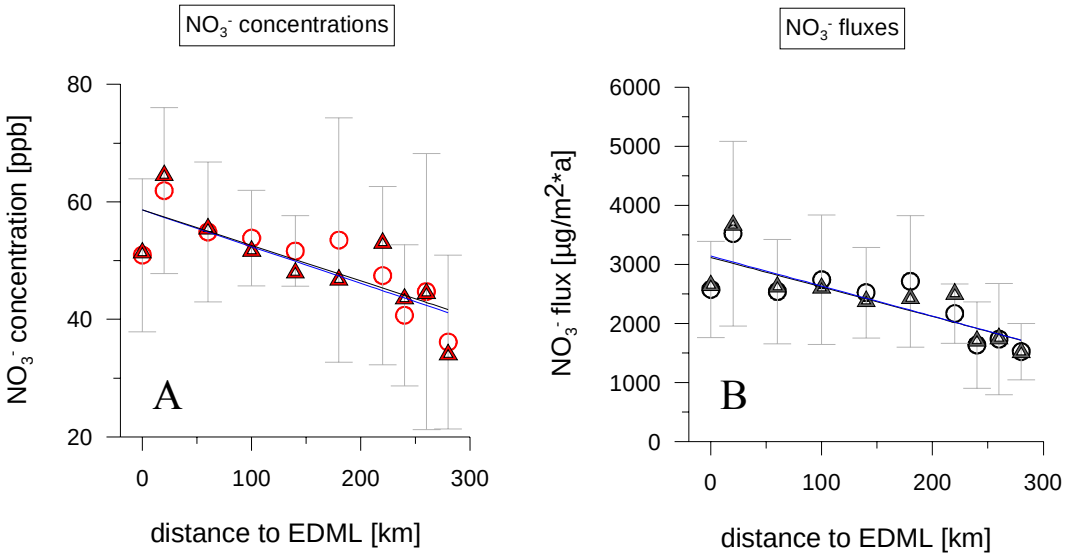

Figure 35: Presented are nitrate concentrations (A) and fluxes (B) determined in UTS (circles) and UTD (triangles) samples over distance to the EDML deep drilling site. The UTD concentrations and fluxes were determined as averages from sampled snow pit wall down to a depth level equivalent to the bottom depth of the 12th year from the respective UTS sampling. Due to the averaging, no error can be numbered. In plot A and B, the linear fit of the UTS data is presented as black line, the respective linear fit of the UTD data is shown in blue.

Fractions of deposited Nitrate are described to be transferred into gaseous HNO_3 within the upper snow layers. Gaseous HNO_3 can be emitted into the atmosphere, where the nitrate loss of snow layers depends on the time of its exposition to the atmosphere (FISCHER, 1997; RÖTHLISBERGER et al., 2002a). The previously discussed decreasing accumulation with increasing distance to the EDML site results in a thinning of the annual snow coverage. Less coverage of snow allows sunlight to penetrate in stratigraphically older snow layers and, thus, amplifies the effectiveness of NO_3^- photolysis that eventually amplifies the post-depositional loss of nitrate.

According to WELLER et al. (2004), an overburden of 1.2 m - 1.4 m of snow prevents from HNO_3^- outgassing. Thus, the observed losses of NO_3^- coincide with the spatial variability in annual accumulation. This finding is supported by the DML snow pit dataset, where the annual means of accumulation rate and NO_3^- concentration from individual snow pits show a correlation of r = 0.81 for UTS and r = 0.67 for UTD (Figure 36).

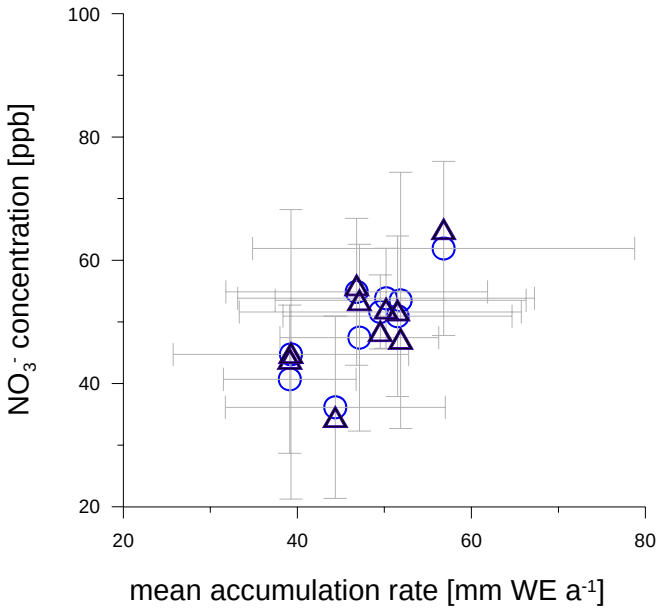

Figure 36: Scatter plot of mean annual accumulation rate and mean NO_3^- concentration in UTS data (circle) and UTD data (triangle).

Due to the systematic spatial variability of decreasing annual nitrate concentrations and fluxes with increasing distance to the EDML deep drilling site, a correction of the NO_3^- record is suggested for the long EDML ice core record according to the linear regression:

$$(UTD): \quad Y = -0.062 * X + 58.6; \quad (r^2 = 0.61) \tag{28}$$

5.7 Spatial variability of methane sulfonate

A distinct spatial decline of both MSA^- concentrations and fluxes with increasing distance to the EDML deep drilling site is observed in the UTD dataset of DML snow pits (Figure 37). The linear relationships between the spatial variations of distance to EDML and both MSA^- concentrations and fluxes are determined with r = 0.69 and r = 0.85, respectively.

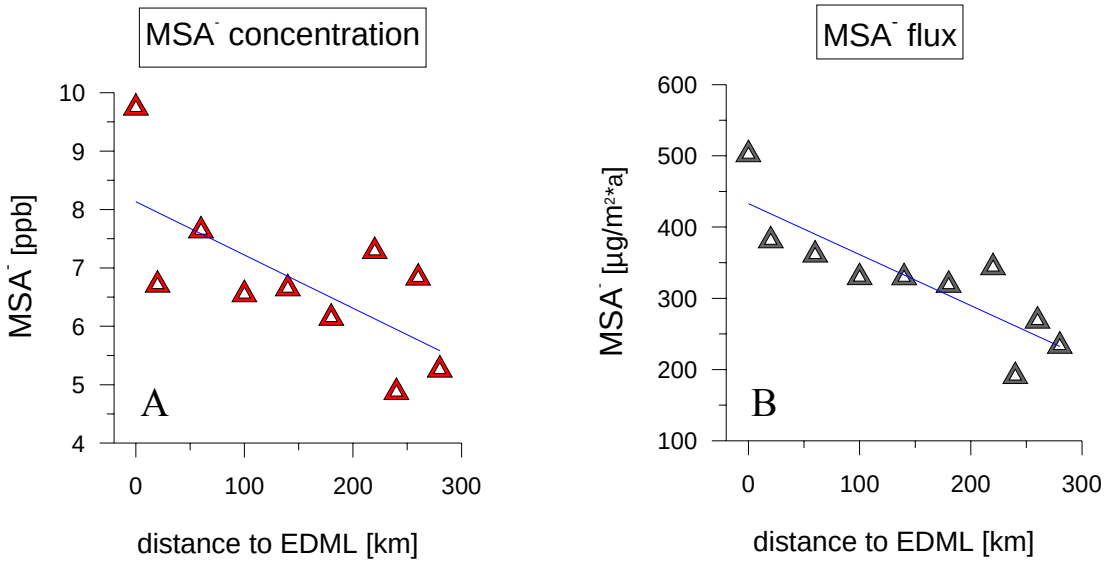

Figure 37: Shown are MSA^- concentrations (A) and fluxes (B) determined in UTD samples as function of distance to the EDML deep drilling site. The MSA^- concentrations and fluxes were determined from the UTD dataset as averages from sampled snow pit wall down to a depth level equivalent to the bottom depth of the 12th year from the respective UTS sampling. Due to the averaging, no error can be numbered. The linear fit of the UTD data is presented as blue line in Figure B.

Similar to the observations for nitrate, significant post-depositional losses determine the budget of methane sulfonate, (chapter 5.6). The spatial decrease of MSA^- concentration in Antarctic snow deposits is, thus, coupled to the spatial variability of annual accumulation (WELLER et al., 2004) (Figure 38). The variability of annual snow cover arbitrates between the deposited and re-emitted amounts of MSA^-. Hence, increasing fractions of the once archived MSA^- are re-emitted into the snow-atmosphere boundary layer with the observed spatial decrease of annual accumulation. Though, the linear relation between spatial variability of MSA^- concentrations and annual accumulation could be determined with $r = 0.40$ only. WELLER et al. (2004) found strong variations in the intensity of post-depositional methane sulfonate losses between the investigated sites and considered a loss of 51 ± 20 % of the initially deposited MSA^- as typical. The high intersite variability could possibly explain the low coefficient of correlation ($r = 0.40$) observed for annual accumulation and MSA^- concentration.

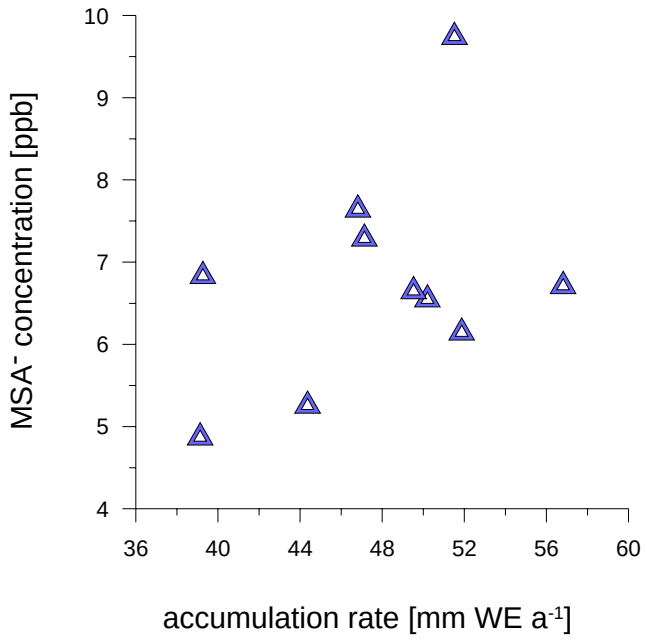

Figure 38: Indicated is the spatial variability of MSA^- concentrations as function of varying annual accumulation).

A correction of the MSA^- record from the EDML deep ice core was recommended by WELLER et al. (2004). The presented interpretation of the DML snow pit data taken upstream the EDML ice core also concludes to correct for the MSA^- record from EDML by the following regression:

$$(UTD): \quad Y = -0.009 * X + 8.1; \quad (r^2 = 0.48) \tag{29}$$

5.8 Spatial variability of sulphate

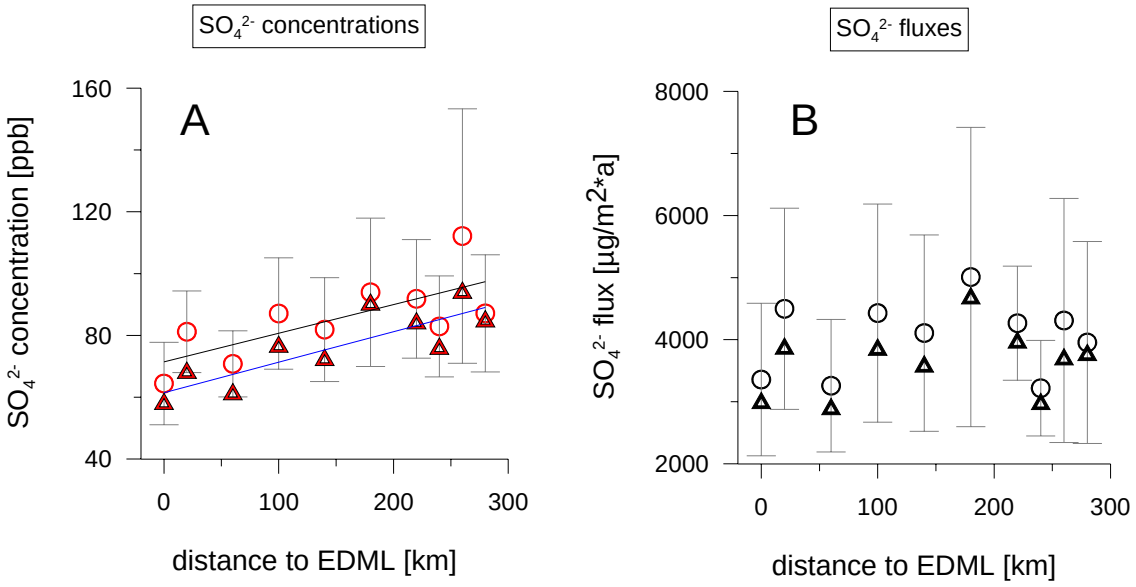

Figure 39: Sulphate concentrations (A) and fluxes (B) determined in UTS (circles) and UTD (triangles) samples over distance to the EDML deep drilling site. The UTD concentrations and fluxes were determined as averages from sampled snow pit wall down to a depth level equivalent to the bottom depth of the 12th year from the respective UTS sampling. Due to the averaging, no error can be numbered. In Figure A, the linear fit of the UTS data is presented as black line, the respective linear fit of the UTD data is shown in blue.

Sulphate shows a distinct spatial variability within both datasets of UTS and UTD samples (Figure 39 A). The sulphate concentrations were found to rise linearly with increasing distance to the EDML deep drilling site with r = 0.72 (UTS) and r = 0.76 (UTD). Regardless of the concentration variability, the sulphate fluxes remain rather constant (Figure 39 B). Thus, systematic spatial variations relating to increased distance to EDML and declining accumulation rates are exclusively observed for the sulphate concentrations and not for the sulphate fluxes.

According to equation (6), the total amount of annually deposited sulphate is composed of the wet and the dry deposited fractions. The spatial increase of sulphate concentrations can be explained by predominance of dry depositional processes. Hence, dry deposited sulphate gets diluted by spatially varying snow accumulation according to equation (7). On the other hand, the dominance of dry deposition is expressed by the stable spatial distribution of sulphate fluxes by equation (6). Hence, the wet deposited sulphate is multiplied by the spatially

variable accumulation. This does not lead to significant spatial dependence of sulphate fluxes because the magnitude of sulphate fluxes is controlled by dry deposition.

When the sulphate concentration is plotted over the inverse accumulation rate, the amount of dry deposited sulphate can be directly inferred from the slope of the linear regression (FISCHER, 1997) as shown in Figure 40.

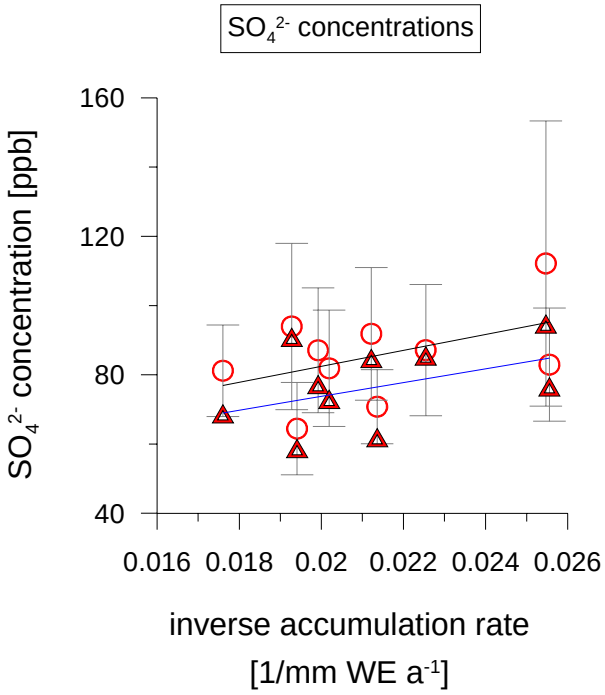

Figure 40: The sulphate concentrations over inverse accumulation rate show the linear relation between sulphate concentration and inverse accumulation rate of r = 0.46 (UTS) and r = 0.43 (UTD). This method of demonstration should allow for the determination of the amount of dry deposited sulphate as indicated by the slope of the linear regression [µg/m² * a] ($Y = 2297 * X + 36.5$ for UTS; $Y = 1988 * X + 34.0$ for UTD unexpectedly, the linear relation does not occur with a significance level of ≥ 95 %, thus the derived conclusions have to be considered statistically weak.

The regressions show the following relation of accumulation and sulphate concentration:

$$(UTS): \quad Y = 2297 * X + 36.5; \quad (r^2 = 0.21) \tag{30}$$

$$(UTD): \quad Y = 1988 * X + 34.0; \quad (r^2 = 0.19) \tag{31}$$

Unexpectedly, the regression analysis of sulphate concentration and inverse accumulation rate shows a correlation of r = 0.46 (UTS) and r = 0.43 (UTD) only. Therefore, the quantification of dry sulphate deposition is of limited reliability. Nevertheless, dry deposition fluxes derived by regressions of both UTS and UTD are comparable of 2297 µg/m^2 * a and 1988 µg/m^2 * a and can explain up to 2/3 of the total sulphate deposition (FISCHER, 1997). GÖKTAS et al. (2002) found an even larger sulphate fraction of 75 % to be dry deposited.

The lack of significant correlation is assumed to result from influencing processes that could not unambiguously be identified so far. One possible explanation for the spatial increase of sulphate concentration would be a spatial increase of sulphate concentrations in the air. In addition to the dominance of dry depositional processes, this could account for the spatial increase of sulphate concentrations in DML snow that are only insignificantly dependent on the accumulation rate, see equation (7).

If the regressions and therefore the amounts of dry deposited sulphate were considered true, the amount of dry deposited sulphate could be calculated from the dry deposited and the total amount of sulphate in order to quantify the amount of wet deposited sulphate according to equation (4).
The total flux is calculated as mean sulphate flux over all snow pits. Given the total sulphate fluxes of 4040 µg/m^2 * a for the UTS and 3612 µg/m^2 * a for the UTD samples, the wet deposited sulphate is numbered as:

$$(UTS): \quad J_{wet} = 4040 \frac{\mu g}{m^2 a} - 2297 \frac{\mu g}{m^2 a} = 1743 \frac{\mu g}{m^2 a} \tag{32}$$

$$(UTD): \quad J_{wet} = 3612 \frac{\mu g}{m^2 a} - 1988 \frac{\mu g}{m^2 a} = 1624 \frac{\mu g}{m^2 a} \tag{33}$$

In case of UTS, dry and wet depositional processes contribute to the total amount of sulphate deposition with 2297 µg/m^2 * a and 1743 µg/m^2 * a, respectively. Within the UTD records, dry and wet depositional processes account for 1988 µg/m^2 * a and 1624 µg/m^2 * a, respectively. The quantification of dry and wet depositional processes would allow for the calculation of the relative contribution from each depositional process. Therefore, 57 %

(UTS) and 55 % (UTD) of the sulphate in DML snow pits would be dry deposited, whereas 43 % (UTS) and 45 % (UTD) would be wet deposited.

FISCHER (1997) described the general predominance of dry deposition for sulphate in Greenland snow but also a critical accumulation rate of equilibrium between wet and dry deposition in areas of annual accumulation below 60 mm WE * a^{-1} during pre-industrial times. The critical accumulation rate derived from the regressions of this study suggest balance of wet and dry deposition for mean annual accumulation of 58 mm WE * a^{-1} (UTD) and 63 mm WE * a^{-1} (UTS) in line with the results by FISCHER (1997). Accordingly, the partitioning of sulphate deposition processes seems to be only dependent on the physicochemical characteristic of sulphate aerosol particles and seems independent of the local sulphate air concentration, which (e.g.) is significantly different in Greenland and Antarctica.

The quantification of UTS and UTD sulphate fluxes result from mean values over all DML snow pits. Interestingly, UTS and UTD samples exhibit the fluxes derived from UTS samples to be increased by 10 %. This difference could be either due to spatial variations of annual sulphate fluxes as environmental noise or reflect slightly contaminated UTS sampling gear. However, this remains unresolved for now but suggests referring on the well established UTD dataset for the discussion of spatial concentration effects on the deep EDML ice core, as the UTD data are considered more robust.

The mean sulphate concentrations of the DML snow pits were discussed to exhibit a significant spatial variation of increasing concentration with increasing distance to the EDML deep drilling site. Therefore, a correction for the sulphate concentration within the EDML deep ice core record is suggested according to the linear regression between sulphate concentrations of the UTD dataset [ppb] and distance to the EDML deep drilling site [km]. The suggested regression is given as:

$$(UTD): \quad Y = 0.099 * X + 61.5; \quad (r^2 = 0.70) \tag{34}$$

5.9 Spatial variability of volcanic sulphate

Due to the decreasing accumulation rate upstream the ice divide, the records from snow pits of higher altitudes reach further back in time as compared to the snow pits of lower altitude.

In DML 87, 88, 89 and 90 records reach back to 1991 and 1990. All four snow pits contained elevated SO_4^{2-} fluxes in a time layer dated to 1992 and 1993 (Figure 41). These increased signals are explained by the emission of volcanic SO_4^{2-} by the eruptions of Mount Pinatubo (June 1991) and Mount Cerro Hudson (August 1991), (GÖKTAS et al., 2002; LEGRAND & WAGENBACH, 1999; COLE-DAI & MOSLEY-THOMPSON, 1999).

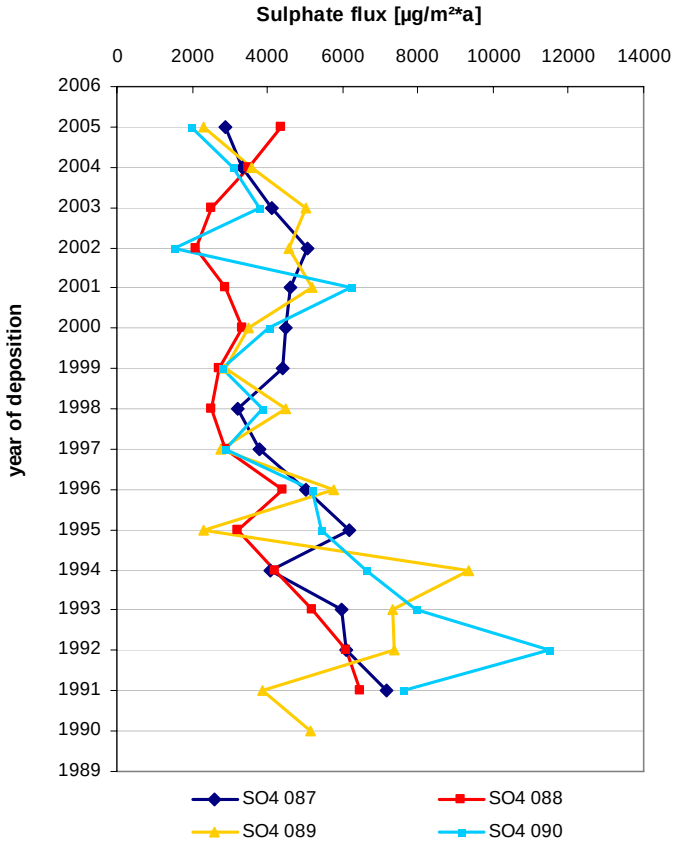

Figure 41: The figure illustrates the effect of Pinatubo emissions on annual SO_4^{2-} fluxes. The uneven scheduling probably results from the early increase of SO_4^{2-} deposition late 1991 at site DML 87, 88 and 90. During the dating process, the annual boundary 1991/1992 was placed right at the peak of the Pinatubo signal, thus the flank of the rising SO_4^{2-} peak already accounts for the elevated SO_4^{2-} flux in 1991. Apart from that, a potential error of dating [+1; –1] could have shifted the onset of the Pinatubo signal, but can not be controlled since no earlier year is completely enclosed in the snow pit records. The spatial increase of sulphate concentrations with increasing distance to EDML drill site (DML 87-90) can be observed in this figure.

The magnitude of volcanic induced SO_4^{2-} fluxes is calculated by subtracting the mean annual SO_4^{2-} fluxes of years without volcanic compound (1996-2005):

$$J_{annual} = C_{annual} * A_{annual} \quad [\mu g / m^2 * a] \tag{35}$$

$$volcanic\ J_{1992} = J_{1992} - mean\ (J_{1996-2005}) \tag{36}$$

$$volcanic\ J_{1993} = J_{1993} - mean\ (J_{1996-2005}) \tag{37}$$

With J as ion flux [µg/m^2*a], C as annual concentration [ppb] and A as annual accumulation [mm WE].

Table 24: Volcanic SO_4^{2-} fluxes for the years 1992 and 1993 as calculated from the records of DML 87, 88, 89 and 90 [µg/m^2*a] including the mean SO_4^{2-} fluxes and the standard deviation of the interval 1996-2005 [µg/m^2*a]. The values in brackets indicate the fraction of the flux which is of volcanic origin from the total SO_4^{2-} flux of the respective year. In addition to the volcanic SO_4^{2-} fluxes, the accumulation of the respective years are presented for each snow pit)

year	Parameter	DML 87	DML 88	DML 89	DML 90
1992	volcanic SO_4^{2-} flux [µg/m^2*a]	2020 (33%)	2971 (49%)	3373 (46%)	7958 (69%)
1993	volcanic SO_4^{2-} flux [µg/m^2*a]	1865 (31%)	2092 (40)	3311 (45%)	4418 (56%)
	mean flux 1996-2005 [µg/m^2*a]	4094	3117	4006	3539
	standard deviation [µg/m^2*a]	±763	±778	±1171	±1413
1992	accumulation [mm WE]	28	33	38	54
1993	accumulation [mm WE]	40	50	38	39

The volcanic compound of the annual SO_4^{2-} fluxes of the DML snow pits 87 - 90 is presented in Table 24. For the year 1992, the volcanic contribution of SO_4^{2-} increased the total SO_4^{2-} fluxes by 33 % to 69 %, which caused the total SO_4^{2-} flux to increase by 2020 ± 763 µg/m^2 * a to 7958 ± 1413 µg/m^2 * a.

In the records of 1992, the volcanic SO_4^{2-} fluxes successively increase by a factor of 4 upstream the ice divide (DML 87 to DML 90), (Table 24). In the same year, the annual accumulation of snow increased by a factor of 2 upstream the ice divide. According to equation (5), the increase of annual snow accumulation can only explain the SO_4^{2-} fluxes to increase by a factor of 2, while the further doubling of SO_4^{2-} fluxes during 1992 remains unexplained.

After 1992, the amount of volcanic SO_4^{2-} fluxes decrease in all four SO_4^{2-} records in 1993, but still accounted for 30 - 50 % of the total SO_4^{2-} deposits in 1993. During 1993, the volcanic SO_4^{2-} fluxes exhibit the same spatial pattern as in 1992 and increase upstream from DML 87 to DML 90 by a factor of 2. At the same time, the accumulation upstream the ice divide remains almost constant (40 mm WE at DML 87, 39 mm WE at DML 90), (Table 24).

In contrast, the annual background fluxes of SO_4^{2-} without volcanic compound (1996 - 2005) do not reveal a spatial gradient upstream the ice divide above the range of the standard deviation (Table 24). Hence, a systematic increase of SO_4^{2-} fluxes along the ice divide by a factor of 2 is exclusively observed for the volcanic compound of SO_4^{2-} fluxes during both years (1992 and 1993).

TRAUFETTER et al. (2004) calculated the total volcanic SO_4^{2-} deposition derived from Pinatubo (for all following years of increased sulphate concentrations) to vary between 11900 ± 2500 µg/m^2 at DML 07, 17300 ± 7900 µg/m^2 at DML 05 and 19100 ± 5900 µg/m^2 at DML 17, where all of the sampling sites are located near the snow pits of this study. The data of Traufetter et al. (2004) also include a spatial gradient of volcanic SO_4^{2-} deposition, where the SO_4^{2-} flux also increases by a factor of 2 with an altitude increase of ~ 500 m. COLE-DAI & MOSLEY-THOMPSON (1999) reported of spatial variations in sulphate flux of up to 20 % at South Pole, attributed to post-depositional redistribution of snow that is significantly lower than the spatial variability at DML.

However, the strong increase found in this study on a very short spatial scale (about 60 km) and a limited change in altitude (about 100 m) is unexpected and not in line with those previous studies.

The finding of decoupled SO_4^{2-} fluxes suggests that both the volcanic and biogenic SO_4^{2-} are separately transported into DML. While the non volcanic SO_4^{2-} is mostly of oceanic origin and is transported by air masses that travel from coastal Antarctica inland. The volcanic SO_4^{2-} of the Pinatubo and Cerro Hudson eruptions was transported through the lower stratosphere towards high latitudes, from where it advected into central Antarctica (LEGRAND & WAGENBACH, 1999). To further explain the doubling of the volcanic SO_4^{2-} fluxes along the ice divide, further investigations are suggested.

5.10 Summary of spatial variability

- The oxygen isotope records exhibited a systematic spatial variability of decreasing $\delta^{18}O$ with increasing distance to EDML/increasing altitude due to decrease of temperatures, a correction of the EDML $\delta^{18}O$ record for the spatial signal is suggested according to: $Y = -0.011 * X - 44.9$; $(r^2 = 0.78)$

- A spatial decrease of accumulation was demonstrated with increasing distance to EDML/increasing altitude.

- The sea-salt derived ion concentrations were demonstrated to remain constant with increasing distance to EDML/increasing altitude, thus, to correction for the sea-salt records of EDML is not suggested.

- Clx exhibited a systematic increase of concentration with increasing distance to EDML/increasing altitude, thus the EDML record is suggested to be corrected for Clx according to: $Y = 0.023 * X + 9.3$; $(r^2 = 0.78)$

- The variability of non sea-salt calcium concentrations exhibited no spatial dependence to increasing distance to EDML/increasing altitude, thus, no evidence to correct for the EDML records was found.

- Nitrate concentrations upstream EDML exhibited a systematic spatial decrease with increasing distance to EDML/ decreasing accumulation rates, thus to correct the EDML record for the spatial nitrate variability is suggested according to:
  $Y = -0.062 * X + 58.6$; $(r^2 = 0.61)$

- A systematic spatial decrease was demonstrated for MSA^- concentrations with increasing distance to EDML/decreasing accumulation rates, thus, to correct the EDML record for the spatial MSA^- signal is suggested according to:
  $Y = -0.009 * X + 8.1$; $(r^2 = 0.48)$

- Increasing SO_4^{2-} concentrations were demonstrated for increasing distance to EDML/decreasing accumulation rates. The EDML record is suggested to be corrected for the spatial SO_4^{2-} signal according to: $Y = 0.099 * X + 61.5$; $(r^2 = 0.70)$

- Increased SO_4^{2-} concentrations in snow pits that reached back to at least 1991 were demonstrated to result from emissions due to volcanic eruptions of Mount Pinatubo and Cerro Hudson (1991). A strong spatial increase of volcanic SO_4^{2-} fluxes with increasing distance to EDML/decreasing accumulation rate was reported but requires further explanations to be explained.

6. Conclusion

The key goal of this study was to investigate the high and coarse resolution snow pit samples from Dronning Maud Land, Antarctica for spatio-temporal variability of ion concentrations. A systematic seasonal variability was detected for all snow-chemical parameters within the high resolution records. Maximum concentration values of both sea-salt derived ions Na^+ and Cl^- were found during the austral winter period as consequence of enhanced storminess and source strength due to frost flower formation. In contrast, the maximum values of $\delta^{18}O$, Clx, SO_4^{2-} and NO_3^- occurred during the austral summer half-year. The seasonality of $\delta^{18}O$ exclusively results from temperature difference between the site of evaporation and condensation and is therefore consequently coupled to the seasonal cycle of temperature. In contrast, both Clx and SO_4^{2-} aerosols result from biogenic sources, their concentrations are therefore coupled to the intensity of biological activity which is most pronounced during the summer half-year. Distinct maximum peaks of SO_4^{2-} were detected in snow those pits that reached back in time to 1991 and 1990, which was attributed to emissions of the volcanic eruptions of Mount Pinatubo and Mount Cerro Hudson during 1991. The maximum of stratospheric NO_3^- input during austral summer coincides with its high summer concentrations in Antarctic snow, where the NO_3^- signal significantly decreased with snow depth due to post-depositional loss.

Pronounced local differences of annual snow accumulation and ion deposition caused patterns of annual deposition free of coherency between the snow pits. The high interannual variability could be attributed to erosion and redistribution of snow. Thus, evidence for systematic annual variations of snow characteristics is sparse.

The spatial variability of glacio-chemical parameters was investigated upstream the ice divide, where the altitude increased in dependence of distance to the EDML drill site. As consequence of increasing altitude, mean temperature decreased and coincided with $\delta^{18}O$ depletion. A correction for the EDML $\delta^{18}O$ record is therefore suggested. The annual accumulation of snow decreased by 30 % from 57 mm WE a^{-1} to 39 mm WE a^{-1} with inclining altitude. The concentration of the sea-salt derived aerosols Na^+ and Cl^- in snow remained almost constant, while the net deposition of sea salt ions decreased with declining

annual snow accumulation as consequence. Thus, Na^+ and Cl^- were addressed to be mostly wet deposited.

A decline of $nssCa^{2+}$ was determined for both concentrations and fluxes. Very low $nssCa^{2+}$ concentrations close to the detection limit of the IC system do not allow for robust interpretation of the data. However, a decline of $nssCa^{2+}$ air concentrations with increasing altitude seem to be the most reasonable argument to reduce $nssCa^{2+}$ concentrations and fluxes in snow upstream EDML.

Both MSA^- and NO_3^- exhibit decreasing concentrations with less annual accumulation. A gradual thinning of annual snow coverage with inclining altitude allows for increasing rates of post-depositional losses of both ions. Due to this systematic MSA^- and NO_3^- concentration pattern of spatial variability, a correction of the respective EDML records is suggested for both ions.

Another effect of spatial variability is found for SO_4^{2-} and Clx, both of them exhibit increasing concentrations with inclining altitude. An average of 55 % of the net deposited SO_4^{2-} is shown to be dry deposited. Therefore, the concentration of dry deposited SO_4^{2-} is systematically less diluted by decreasing annual accumulation of snow with inclining altitude. A systematic increase of HCl deposits with inclining altitude is discussed to increase the net concentration of deposited chloride. Hence, the spatial variability of SO_4^{2-} and Clx concentration records of the EDML core are concluded to be corrected for the spatial increase of SO_4^{2-} and Clx concentrations that were found in the snow pits upstream EDML.

Outlook

The investigation of annual variability of glacio-chemical parameters was particularly limited by the localized effects of post-depositional processes such as re-distribution of snow by wind drift and NO_3^- outgassing. So far, there is no solution to disentangle the merged information of primary depositional variability and post-depositional bias of the ion and accumulation signal apart from averaging records for several annual cycles. Year-round sampling of freshly fallen snow could overcome the uncertainty and prevent from unidentified information gaps

within the records due to post-depositional processes. Ideally, such a sampling campaign would cover a time span of several years.

Likewise on a year-round base, a continuous sampling method (e.g. using symmetric airfoils) that particularly allows for quantification of wet and dry deposited aerosol would greatly contribute to explain depositional pattern upstream EDML (methods described by BERGIN et al., 1995). The investigation of temporal and spatial variability within processes of deposition could possibly allow verifying the dependence of ion concentrations on accumulation rate and thus contribute to further understanding of how deep ice core records drilled on ice divide locations contain a spatial signal.

This study discussed the increasing amounts of volcanic sulphate deposition with increasing altitudes. The elevated sulphate deposit can possibly be explained by a localized descend of sulphate rich stratospheric air masses due to advection. An extension of the Pinatubo and Cerro Hudson deposits upstream the ice divide that crosses the area of highest stratospheric deposition would help localizing and quantifying the driving processes. It could be of further interest to quantify the general contribution of sulphate that is deposited by stratospheric air masses, as it represents the counterpart to both, source and transport of biogenic sulphate that originates from proximate coastal areas.

7. References

ANSCHÜTZ, H., 2006. Variability of the recent accumulation rate in coastal Dronning Maud Land, Antarctica, University of Bremen, Dissertation, p. 100

BARNOLA et al., 1987. Vostok ice core provides 160.000 year record of atmospheric CO_2, Nature, 329, p. 408-414

BERGIN et al., 1995. The contributions of snow, for, and dry deposition to the summer flux of anions and cations at Summit, Greenland, Journal of Geophysical Research, Vol. 100, No. D8, p. 16.275-16.288

BERTLER, N. et al., 2005. Snow chemistry across Antarctica, Annals of Glaciology 41, p. 167-179

BIGLER et al., 2006. Aerosol deposited in East Antarctica over the last glacial cycle: Detailed apportionment of continental and sea-salt contributions, Journal of Geophysical Research, Vol. 111, D08205, p. 1-14

BLIESNER, D. M., 2006. Validating Chromatographic Methods, John Wiley & Sons, Inc., Hoboken, New Jersey, p. 291

BOWEN, R., 1991. Isotopes and Climate, Elsevier science publisher ltd. Essex, England, p. 483

COLE-DAI, J. and E. MOSLEY-THOMPSON, 1999. The Pinatubo eruption in South Pole snow and its potential value to ice-core paleovolcanic records, annals of Glaciology, Vol. 29, p. 99-105

DANSGAARD, W., 1964. Stable isotopes in precipitation. *Tellus* **16**(4): 436-468.

EPICA COMMUNITY MEMBERS, 2004. Eight glacial cycles from an Antarctic ice core, Nature, 429, p- 623-628

EPICA COMMUNITY MEMBERS, 2006. One-to-one coupling of glacial climate variability in Greenland and Antarctica, Nature 44, p. 195-198

EUROPEAN SCIENCE FOUNDATION (ESF), 2008. http://www.esf.org/activities/research-networking-programmes/life-earth-and-environmental-sciences-lesc/completed-esf-research-networking-programmes-in-life-earth-and-environmental-sciences/european-project-for-ice-coring-in-antarctica-epica-page-1.html, 18.04.2008)

FAN et al., 2003. Impact of air pollution on deposition of mineral dust: Implication for ocean productivity, American Geophysical research Union, Fall meeting 2003, Abstract B21F-0770

FISCHER, H., 1997. Räumliche Variabilität in Eiskernzeitreihen Nordostgrönlands, Ruprecht-Karls-Universität Heidelberg, Dissertation, p. 188

FISCHER, H. pers. com. (lecture notes)

FISCHER et al., 2007a. Glacial/Interglacial changes in mineral dust and sea salt records in polar ice cores: sources, transport, deposition, Reviews of Geophysics, Vol. 45, RG 1002

FISCHER et al., 2007b. Reconstruction of millennial changes in dust emission, transport and regional sea ice coverage using the deep EPICA ice cores from the Atlantic and Indian Ocean sector of Antarctica, earth and Planetary Science Letters 260, p. 340-354

FLÜCKIGER et al., 2002. High-resolution Holocene N_2O ice core record and its relationship with CH_4 and CO_2, Global Biogeochemical Cycles, Vol. 16, No. 1, p. 1-8

FLÜCKIGER et al., 2004. N_2O and CH_4 variations during the last glacial epoch: Insight into global processes, Global Biogeochemical Cycles, Vol. 18, p. 1-14

FORTMANN, M., 2004. Influence of tropospheric aerosol on the Arctic climate, University of Potsdam, Dissertation, Berichte zur Polarforschung 486, Alfred Wegener Institut, Bremerhaven, p. 142

FUNDEL, F., 2005. Long-term variability in biogenic sulphur aerosol from the Southern Ocean, University of Bremen, Dissertation, p. 111

GÖKTAS, F. et al., 2002a. A glacio-chemical characterization of the new EPICA deep-drilling site on Amundsenisen, Dronning Maud Land, Antarctica Annals of Glaciology, Vol. 35, p. 347-354

GÖKTAS, F., 2002b. Characterisation of glacio-chemical and glacio-meteorological parameters of Amundsenisen, Dronning Maud Land, Antarctica, University of Bremen, Dissertation, Berichte zur Polarforschung 425, Alfred Wegener Institut, Bremerhaven, p. 170

GRAF, W. et al., 2002. Stable-isotope records from Dronning Maud Land, Antarctica, Annals of Glaciology 35, p. 195.201

HARRISON, S. P. et al., 2000. The role of dust in climate changes, today, at the last glacial maximum and in future, Earth-Science Reviews, Vol. 54, p. 43-80

HARTMANN, D. L., 1994. Global Physical Climatology, Academic Press, Inc. San Diego, California

HELSEN et al., 2005. Oxygen isotope variability in snow from western Dronning Maud Land, Antarctica and its relation to temperature, Tellus, 57B, p. 423-435

HEWITT, C. N., W. T. STURGES, 1993. Global atmospheric chemical change, Elsevier Science Publisher Ltd., Great Britain, p. 470

HOFFMAN, J., 2000. Seasonal and short-periodic variability of sea-salt aerosol and near-surface ozone in Antarctica (Neumayer Station) in consideration of sea-ice coverage, University of Bremen, Dissertation, Berichte zur Polarforschung 376, Alfred Wegener Institut, Bremerhaven, p. 192

HUYBRECHTS et al., 2007. Ice thinning, upstream advection, and non-climate biases for the upper 89% of the EDML ice core from a nested model of the Antarctic ice sheet, Climate of the Past, 3, p 577-589

INTERGOVERNMENTAL PANEL ON CLIMATE CHANGE (IPCC), 2007a. http://www.ipcc.ch/pdf/assessment-report/ar4/wg1/ar4-wg1-spm.pdf, (18.04.2008)

INTERGOVERNMENTAL PANEL ON CLIMATE CHANGE (IPCC), 2007b. http://www.ipcc.ch/pdf/assessment-report/ar4/wg2/ar4-wg2-spm.pdf, (18.04.2008)

JOHNSEN, S. J., 1977. Stable isotope homogenization of polar firn and ice, International Association of Hydrological Sciences Publication 118 (Symposium at Grenoble 1975 – Isotopes and Impurities in Snow and Ice): p. 210-219

JOUZEL et al., 1997. Validity of the temperature reconstruction from water isotopes in ice cores, Journal of Geophysical Research, Vol. 102, C12, p. 26.471-26.487

KALESCHKE et al., 2004. Frost flowers on sea ice as a source of sea salt and their influence on tropospheric halogen chemistry, Geophysical Research Letters, Vol. 31, p. 1-4

KARLÖF et al., 2006. How representative is a time series derived from a firn core? A study at a low accumulation site on the Antarctic plateau, Journal of Geophysical Research 111

KOJIMA, K., 1964. Densification of snow in Antarctica. In Mellor, M. (editor): Antarctic Snow and Ice Studies. Antarctic Research Series 2: 157-218.

LEGRAND, M. & P. MAYEWSKI, 1997. Glaciochemistry of polar ice cores: A review, Review of Geophysics, 35, 3, p. 219-243

LEGRAND, M. and D. WAGENBACH, 1999. Impact of the Cerro Hudson and Pinatubo volcanic eruptions on the Antarctic air and snow chemistry, Journal of Geophysical Research, Vol. 104, D 1, p. 1581-1596

LILJEQUIST, G. H. & K. CEHAK, 1994. Allgemeine Meteorologie, Springer Verlag, 3rd Edition, p. 396

LISIECKI, L. E., M. E. RAYMO, 2005. A Pliocene-Pleistocene stack of 57 globally distributed benthic ^{18}O records, Paleoceanography, 2005, 20

MEYER, V.R., 2004. Praxis der Hochleistungs-Flüssigchromatographie, 9th Edition,

MIEDING, B., 2004. Rekonstruktion tausendjähriger aerosolchemischer Eiskernrekords aus Nordostgrönland: Quantifizierung zeitlicher Veränderungen in Atmosphärenzirkulation, Emission und Deposition, Universität Bremen, Dissertation, p. 118

MINIKIN, A., 1994. Spurenstoff-glaziologische Untersuchung von Eisbohrkernen des Filchner-Ronne-Schelfeises, Antarktis: Bestimmung der Tiefenverteilung und der Kontinentaleffekte ionischer Aerosolkomponenten, Shaker Verlag, Ruprecht-Karls-Universität Heidelberg, Dissertation, p. 218

NORTH GREENLAND ICE-CORE PROJECT MEMBERS, 2004. High-resolution record of the Northern Hemisphere climate extending into the last interglacial period, Nature, 431, p. 147-151

OERTER et al., 2000. Accumulation rates in Dronning Maud Land, Antarctica, as revealed by dielectric-profiling measurements of shallow firn cores, Annals of Glaciology, 30p. 27-34

PIEL, C., 2004. Variability of chemical and physical parameters of aerosol in the Antarctic troposphere, University of Bremen, Dissertation, Berichte zur Polarforschung 476, Alfred Wegener Institut, Bremerhaven, p. 157

RANKIN, A. M., E. W. WOLFF, S. MARTIN, 2002. Frost flowers: Implications for tropospheric chemistry and ice core interpretation, Journal of Geophysical Research, Vol. 107, NO D23

REIJMER, C. H. & M. R. VAN DEN BROEKE, 2001. Moisture source of precipitation in western Dronning Maud Land, Antarctica, Antarctic Science 13 (2): p 210-220

REIJMER, C. H. and J. ORLEMANS, 2002a. Temporal and spatial variability of the surface energy balance in Dronning Maud Land, East Antarctica, Journal of Geophysical Research, Vol. 107, D24, p. 1-12

REIJMER, C. H. and M. R. VAN DEN BROEKE, M. P. SCHEELE, 2002b. Air Parcel Trajectories and Snowfall Related to Five Deep Drilling Locations in Antarctica Based on the ERA-15 Dataset, American Meteorological Society, p. 1957-1968

RICHARDSON, C., P. HOLMLUND, 1999. Spatial variability in shallow snow layer depths in central Dronning Maud Land, East Antarctica, Annals of Glaciology 29, p. 10-16

RICHARDSON-NÄSLUND, C., 2004. Spatial characteristics of snow accumulation in Dronning Maud Land, Antarctica, Global and Planetary Change 42, p. 31-43

RÖTHLISBERGER, R. et al., 2002a. Nitrate in Greenland and Antarctic ice cores: a detailed description of post-depositional processes, Annals of Glaciology 35, p. 209-216

RÖTHLISBERGER, R. et al., 2002b. Dust and sea salt variability in central East Antarctica (Dome C) over the last 45 kyrs and its implications for southern high-latitude climate, Geophysical research Letters, Vol. 29, No. 20, p. 1-4

RÖTHLISBERGER, R. et al., 2003. Limited dechlorination of sea-salt aerosols during the last glacial period – Evidence from the EPICA Dome C ice core, Journal of Geophysical Research, Vol. 108 (D16): 4526,

ROTSCHKY, G., et al., 2007a. A new surface accumulation map for western Dronning Maud Land, Antarctica, from interpolation of point measurements, Journal of Glaciology, 53 (182): p. 385-398

ROTSCHKY, G., 2007b. Spatial distribution of snow accumulation and snowpack properties in Dronning Maud Land, Antarctica: Observational techniques and methods for surface mass-balance assessments of polar ice sheets, Alfred Wegener Institut für Polar- und Meeresforschung, Berichte zur Polarforschung 552, p. 90

SCHLOSSER, E. & H. OERTER, 2002. Seasonal variations of accumulation and the isotope record in ice cores: a study with surface snow samples and firn cores from Neumayer station, Antarctica, Annals of Glaciology, 35, p. 97-101

SHORT, N.M., 2008. http://rst.gsfc.nasa.gov/Sect14/Sect14_1c.html, (20.04.2008)

SOMMER, S. et al., 2000a. Glacio-chemical study spanning the past 2 kyr on three ice cores from Dronning Maud Land, Antarctica; 1. Annually resolved accumulation rates, Journal of Geophysical Research, Vol. 105, NO D24, p. 29.411-29.421

SOMMER et al., 2000b. Glacio-chemical study spanning the past 2 kyr on three ice cores from Dronning Maud Land, Antarctica, 2. Seasonally resolved chemical records, Journal of Geophysical Research, Vol. 105, NO D24, p. 29.423.29.433

STAFFAN, N. O., 2007. Hygroscopic Properties of organic and inorganic aerosols, University of Zürich (ETH): Dissertation

STEINHAGE, D., 2001. Contributions of geophysical measurements in Dronning Maud Land, Antarctica, locating an optimal drill site for a deep ice core drilling, University of Bremen, Dissertation, Berichte zur Polarforschung 384, Alfred Wegener Institut, Bremerhaven, p. 91

STORCH, V. H. & A. NAVARRA, 1999. Analysis of climate variability, Springer Verlag Berlin Heidelberg, 2nd edition, p. 342

THOMPSON L. G. et al., 2002. Kilimanjaro ice core records: Evidence of Holocene climate change in tropical Africa , Science, 298, p. 589-593

TIJM-REIJMER, C. H., M. R. VAN DEN BROEKE, 2000. Moisture sources of precipitation in Western Dronning Maud Land, Antarctica, Antarctic Science 13, p. 210-220

TRAUFETTER et al., 2004. spatio-temporal variability in volcanic sulphate deposition over the past 2 kyr in snow pits and firn cores from Amundsenisen, Antarctica, Journal of Glaciology, Vol. 50, No. 168, p. 137-146

WAGENBACH, D. et al., 1998. Atmospheric near-surface nitrate at coastal Antarctic sites, Journal of Geophysical Research, Vol. 103, D 9, p. 11007-11020

WELLER et al., 2002. Seasonality of reactive nitrogen oxides (NO_y) at Neumayer Station, Antarctica, Journal of Geophysical Research, Vol. 107, D23, p. 11

WELLER et al., 2004. Postdepositional losses of methane sulfonate, nitrate, and chloride at the European Project for Ice Coring in Antarctica deep-drilling site in Dronning Maud Land, Antarctica, Journal of Geophysical Research, Vol. 109, p. 1-9

WELLER, R. and D., WAGENBACH (2007. Year-round chemical aerosol records in continental Antarctica obtained by automatic samplings, Tellus, B 59, p. 755-765

WESCHE, C., et al., 2007. Surface topography and ice flow in the vicinity of the EDML deep-drilling site, Antarctica., JOURNAL OF GLACIOLOGY, 53(182): 442 - 448

WESTON, A. & P.R. BROWN, 1997. HPLC and CE, Principles and Practise, Academic Press, San Diego, p. 280

8. Appendix

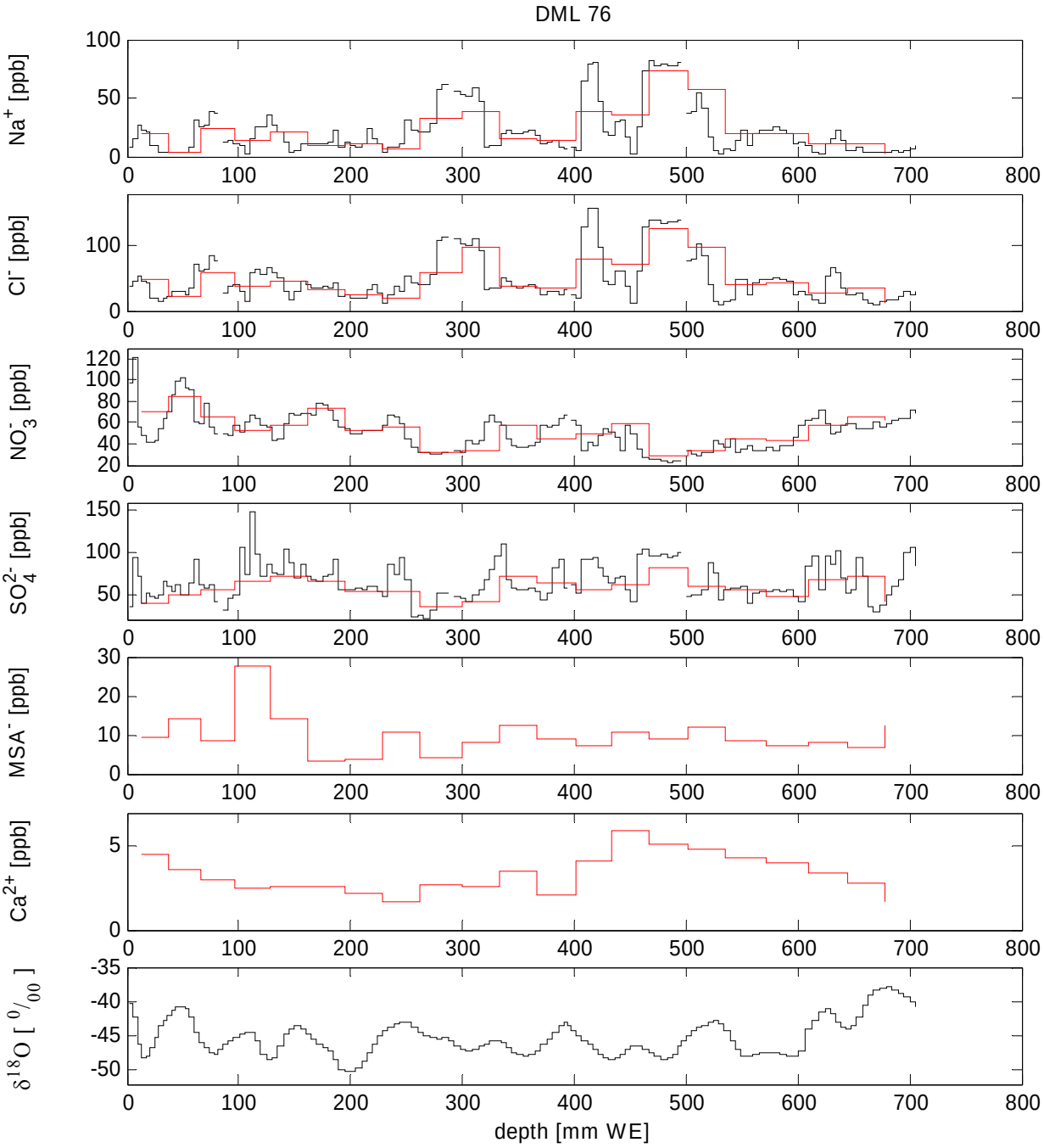

Figure 42: Raw data records from DML 76 of sodium, chloride, nitrate, sulphate, methane sulfonate, calcium and $\delta^{18}O$. The high resolution records of the UTS samples are displayed as black line, the coarse resolution records of the UTD samples are presented as red line. Note, MSA^- was measurable in UTD records only. Data of $\delta^{18}O$ were available from UTS samples, only.

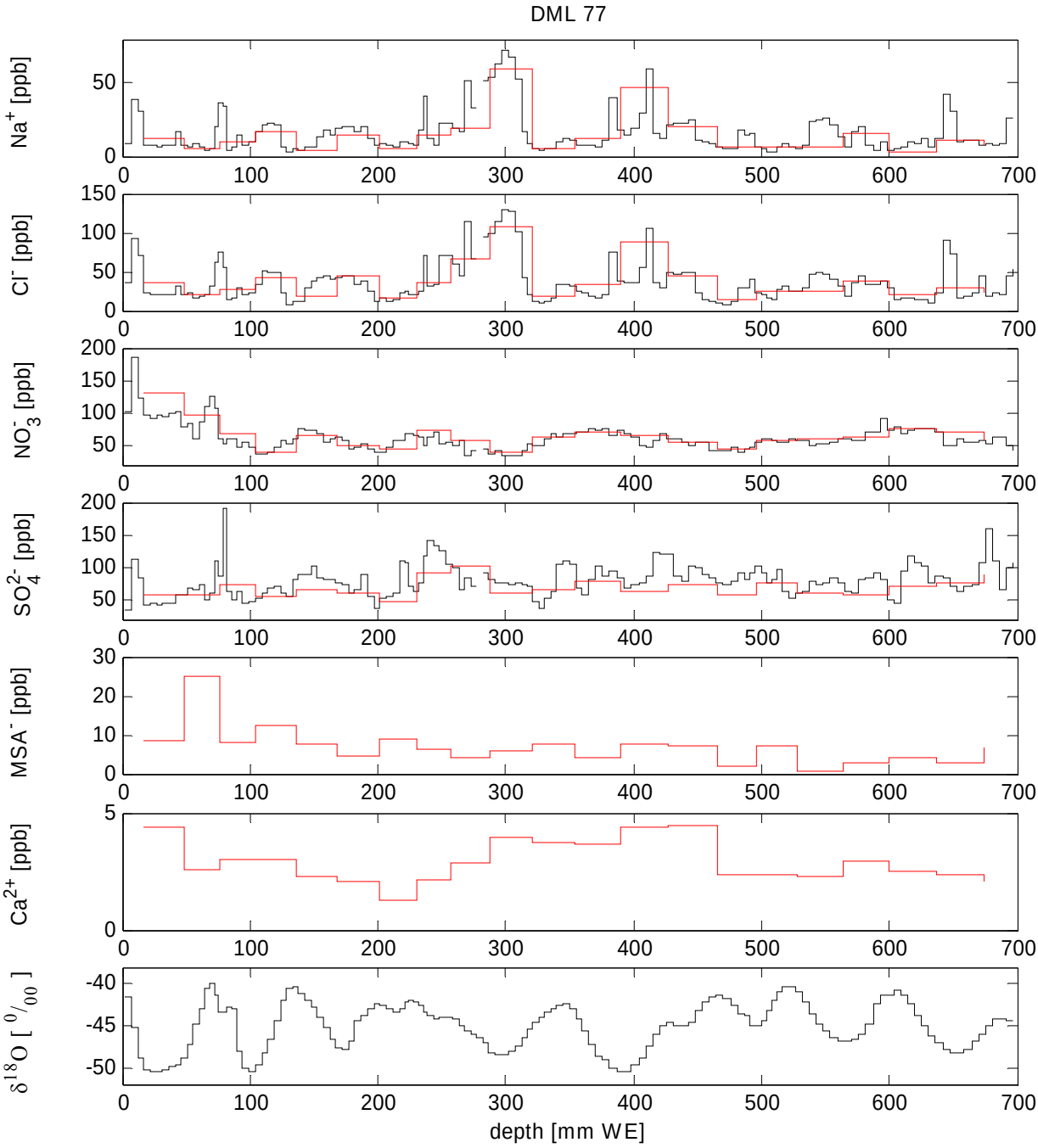

Figure 43: Raw data records from DML 77 of sodium, chloride, nitrate, sulphate, methane sulfonate, calcium and $\delta^{18}O$. The high resolution records of the UTS samples are displayed as black line, the coarse resolution records of the UTD samples are presented as red line. Note, MSA^- was measurable in UTD records only. Data of $\delta^{18}O$ were available from UTS samples, only.

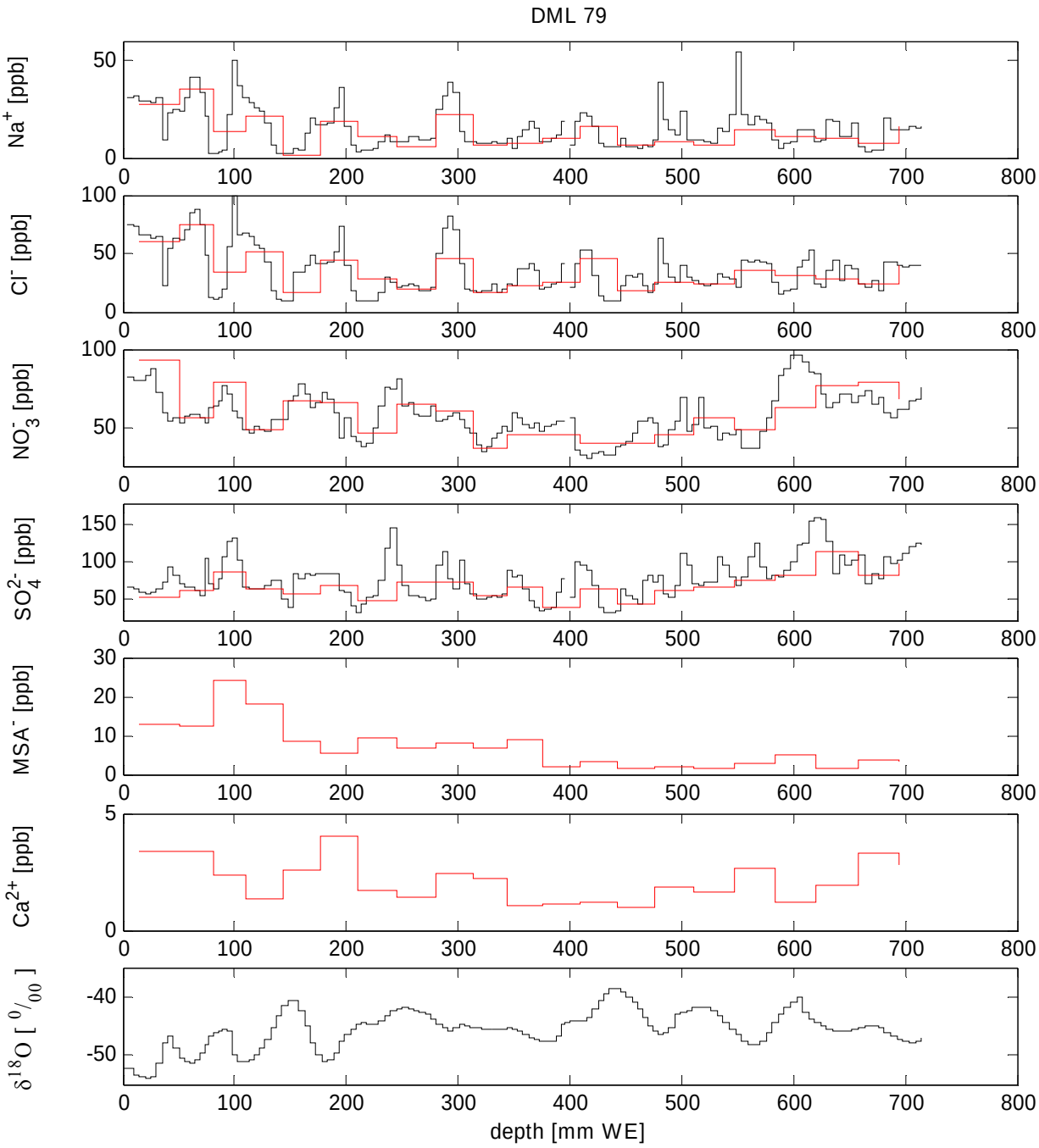

Figure 44: Raw data records from DML 79 of sodium, chloride, nitrate, sulphate, methane sulfonate, calcium and $\delta^{18}O$. The high resolution records of the UTS samples are displayed as black line, the coarse resolution records of the UTD samples are presented as red line. Note, MSA^- was measurable in UTD records only. Data of $\delta^{18}O$ were available from UTS samples, only.

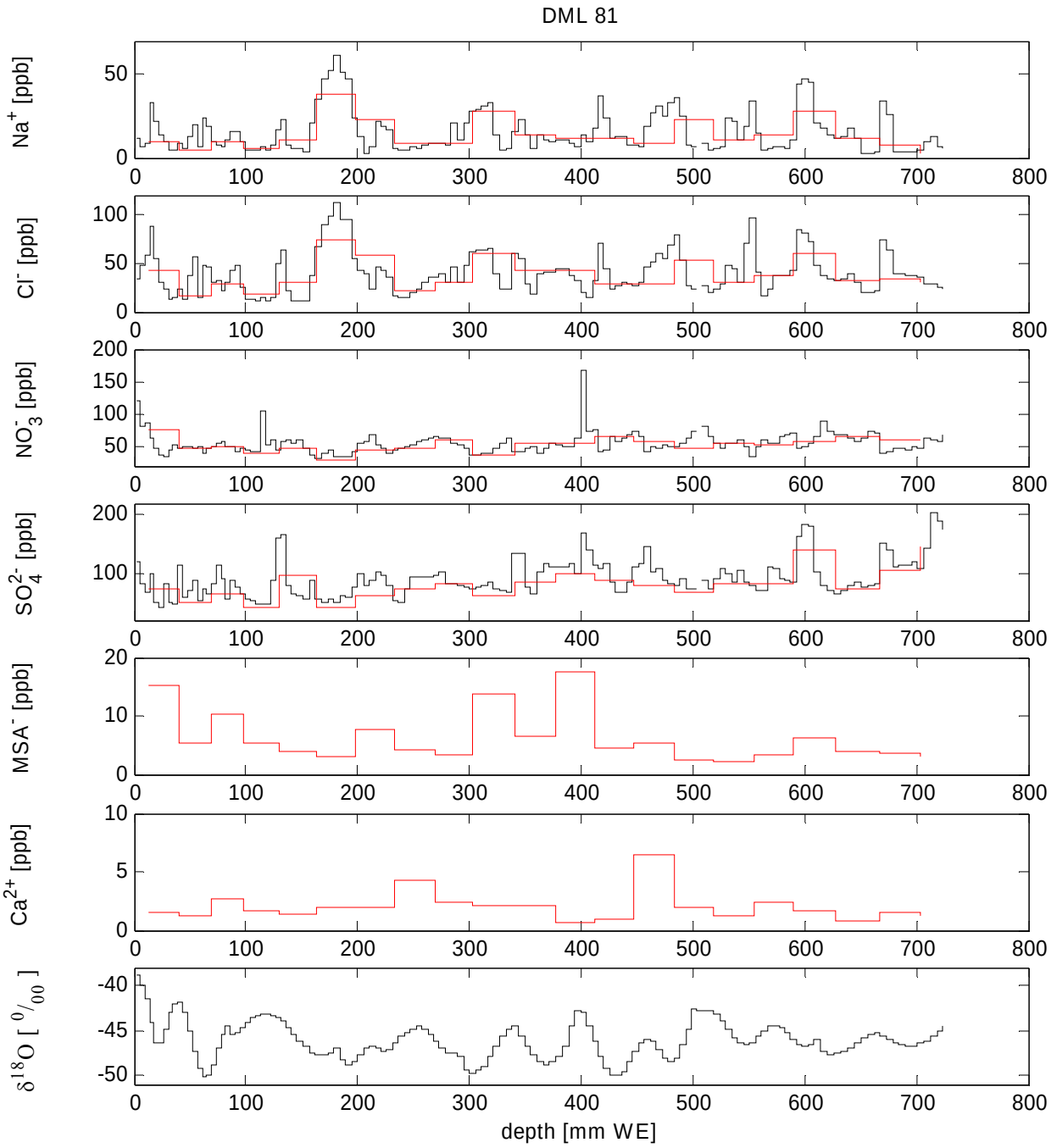

Figure 45: Raw data records from DML 81 of sodium, chloride, nitrate, sulphate, methane sulfonate, calcium and $\delta^{18}O$. The high resolution records of the UTS samples are displayed as black line, the coarse resolution records of the UTD samples are presented as red line. Note, MSA^- was measurable in UTD records only. Data of $\delta^{18}O$ were available from UTS samples, only.

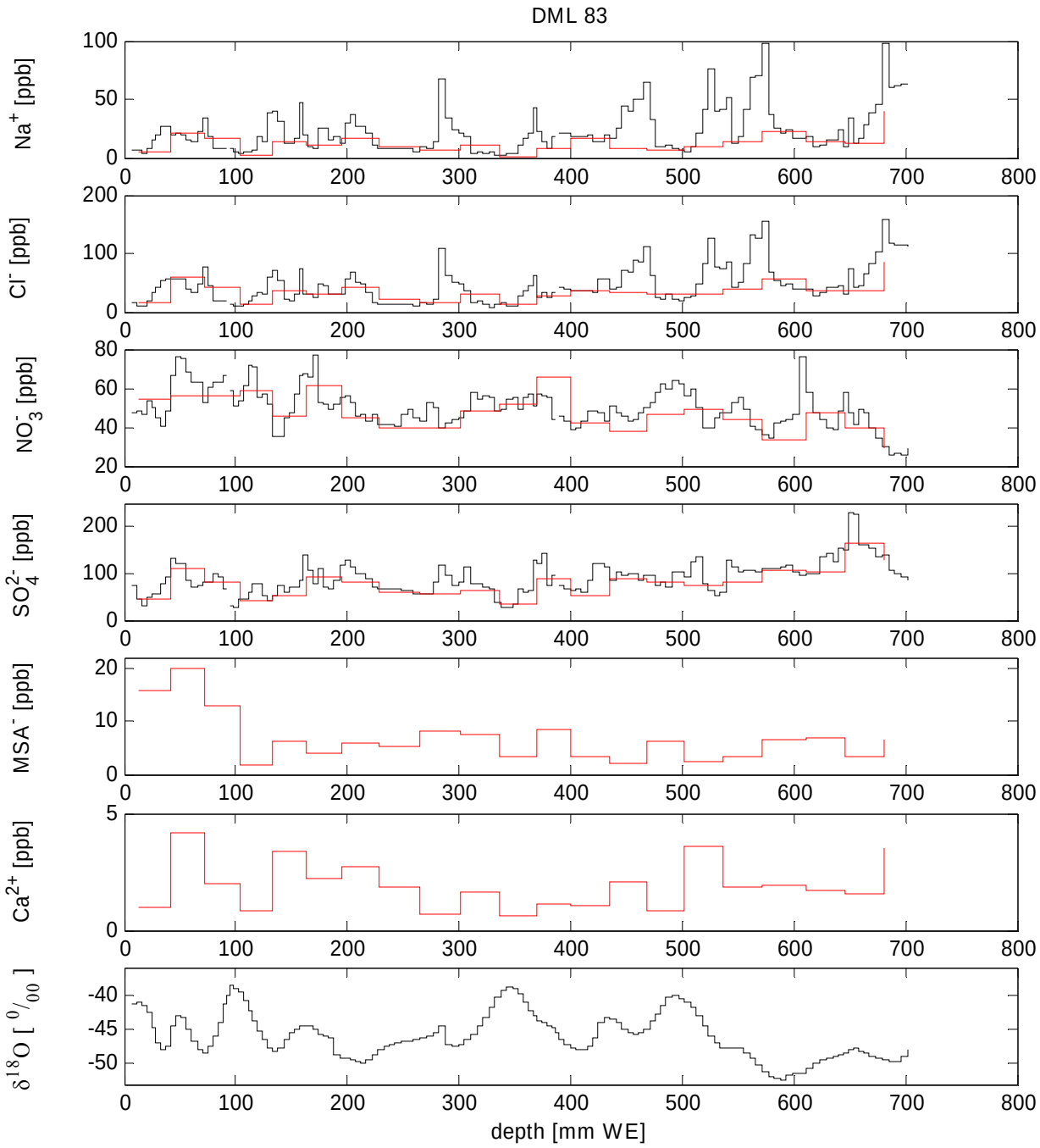

Figure 46: Raw data records from DML 83 of sodium, chloride, nitrate, sulphate, methane sulfonate, calcium and $\delta^{18}O$. The high resolution records of the UTS samples are displayed as black line, the coarse resolution records of the UTD samples are presented as red line. Note, MSA^- was measurable in UTD records only. Data of $\delta^{18}O$ were available from UTS samples, only.

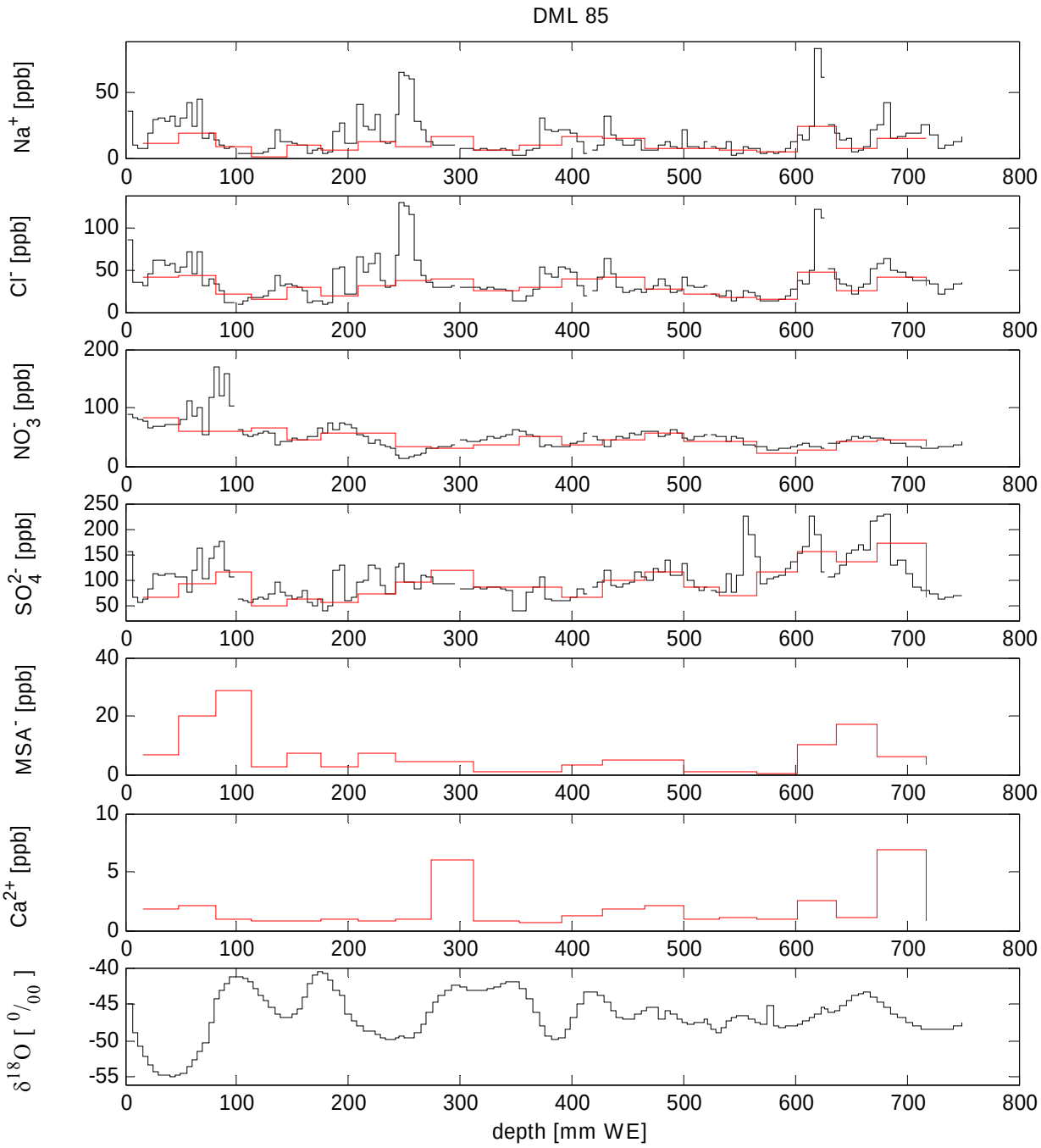

Figure 47: Raw data records from DML 85 of sodium, chloride, nitrate, sulphate, methane sulfonate, calcium and $\delta^{18}O$. The high resolution records of the UTS samples are displayed as black line, the coarse resolution records of the UTD samples are presented as red line. Note MSA^- was measurable in UTD records only. Data of $\delta^{18}O$ were available from UTS samples, only.

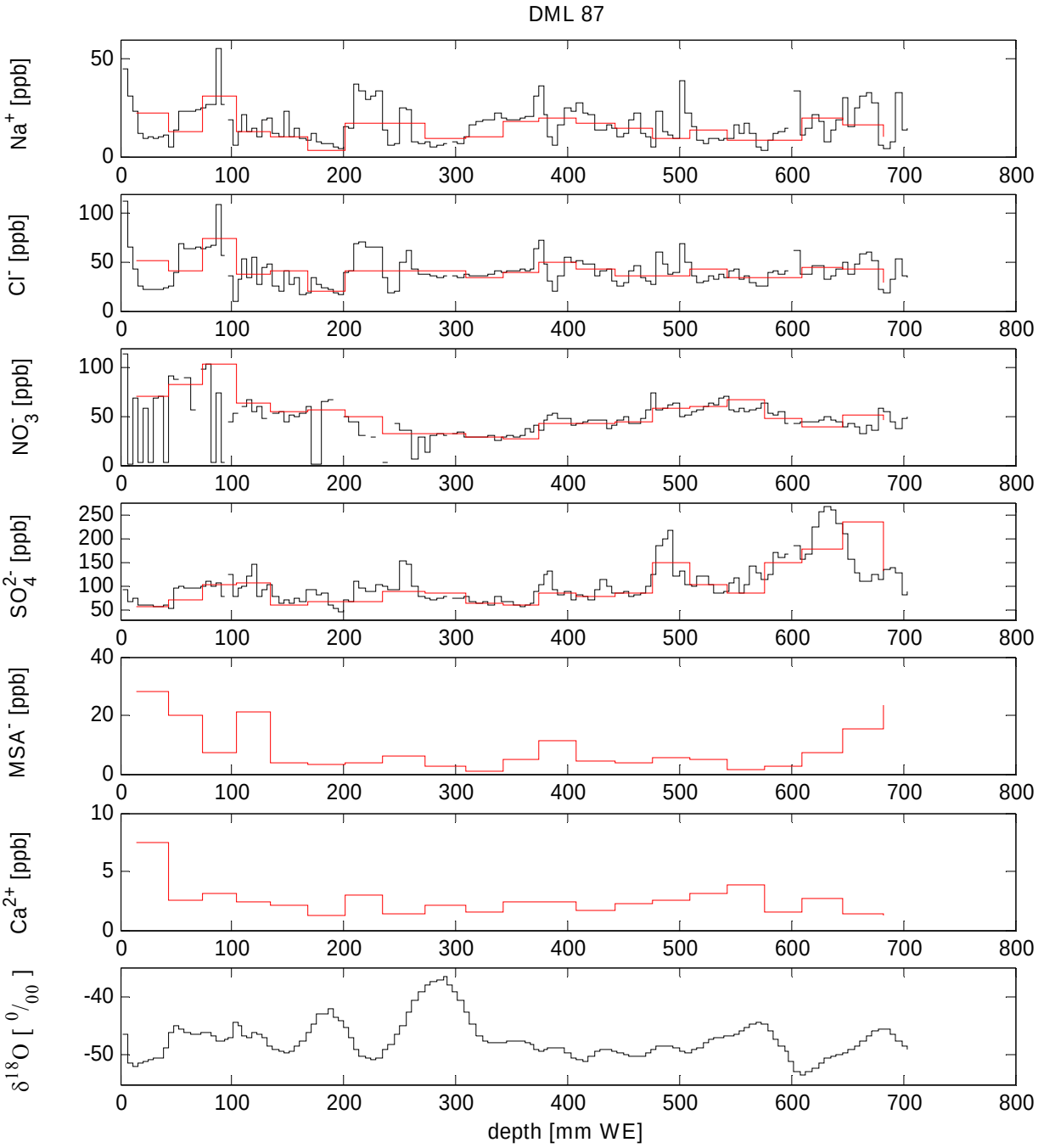

Figure 48: Raw data records from DML 87 of sodium, chloride, nitrate, sulphate, methane sulfonate, calcium and $\delta^{18}O$. The high resolution records of the UTS samples are displayed as black line, the coarse resolution records of the UTD samples are presented as red line. Note, MSA^- was measurable in UTD records only. Data of $\delta^{18}O$ were available from UTS samples, only.

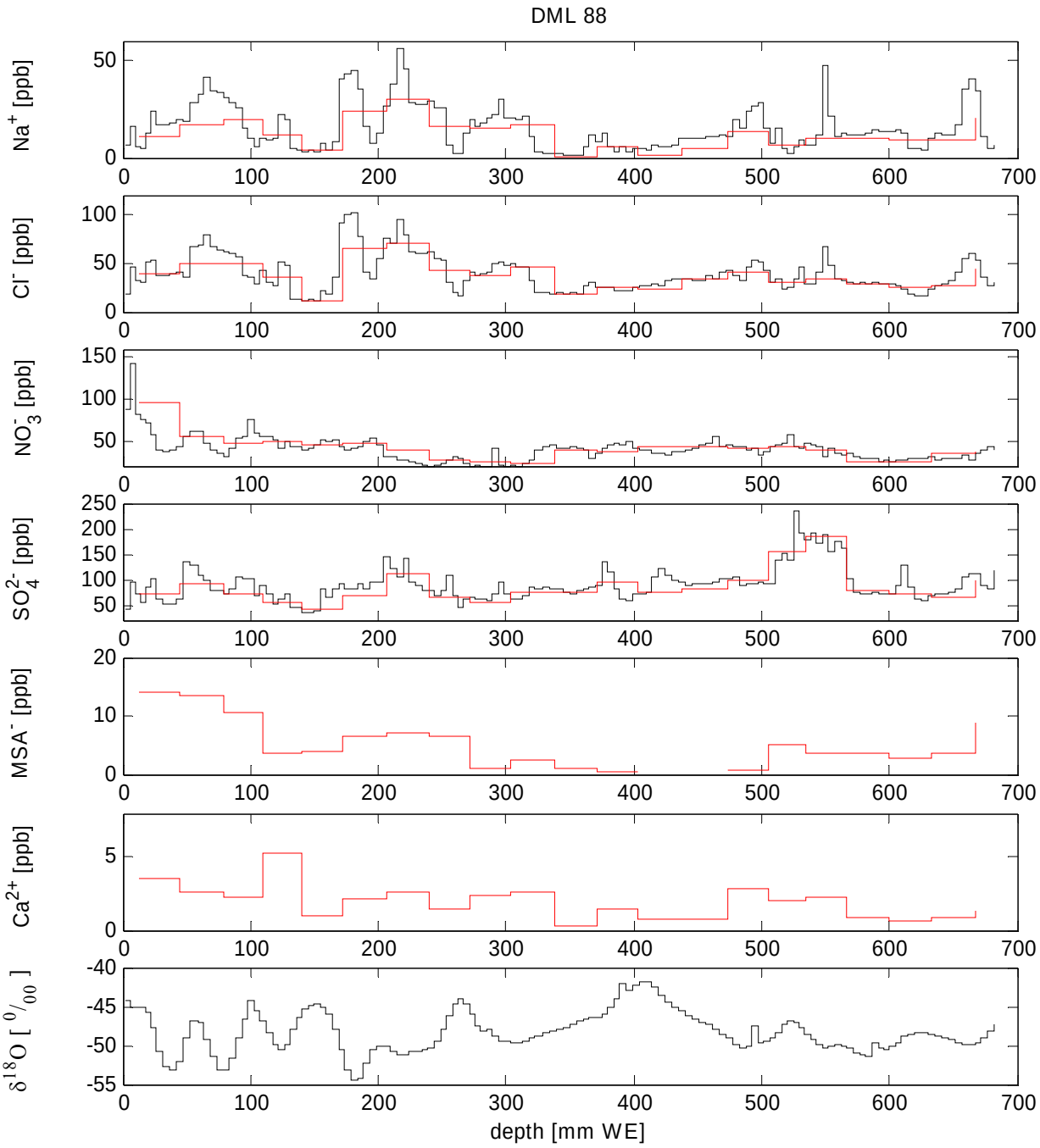

Figure 49: Raw data records from DML 88 of sodium, chloride, nitrate, sulphate, methane sulfonate, calcium and $\delta^{18}O$. The high resolution records of the UTS samples are displayed as black line, the coarse resolution records of the UTD samples are presented as red line. Note, MSA^- was measurable in UTD records only. Data of $\delta^{18}O$ were available from UTS samples, only.

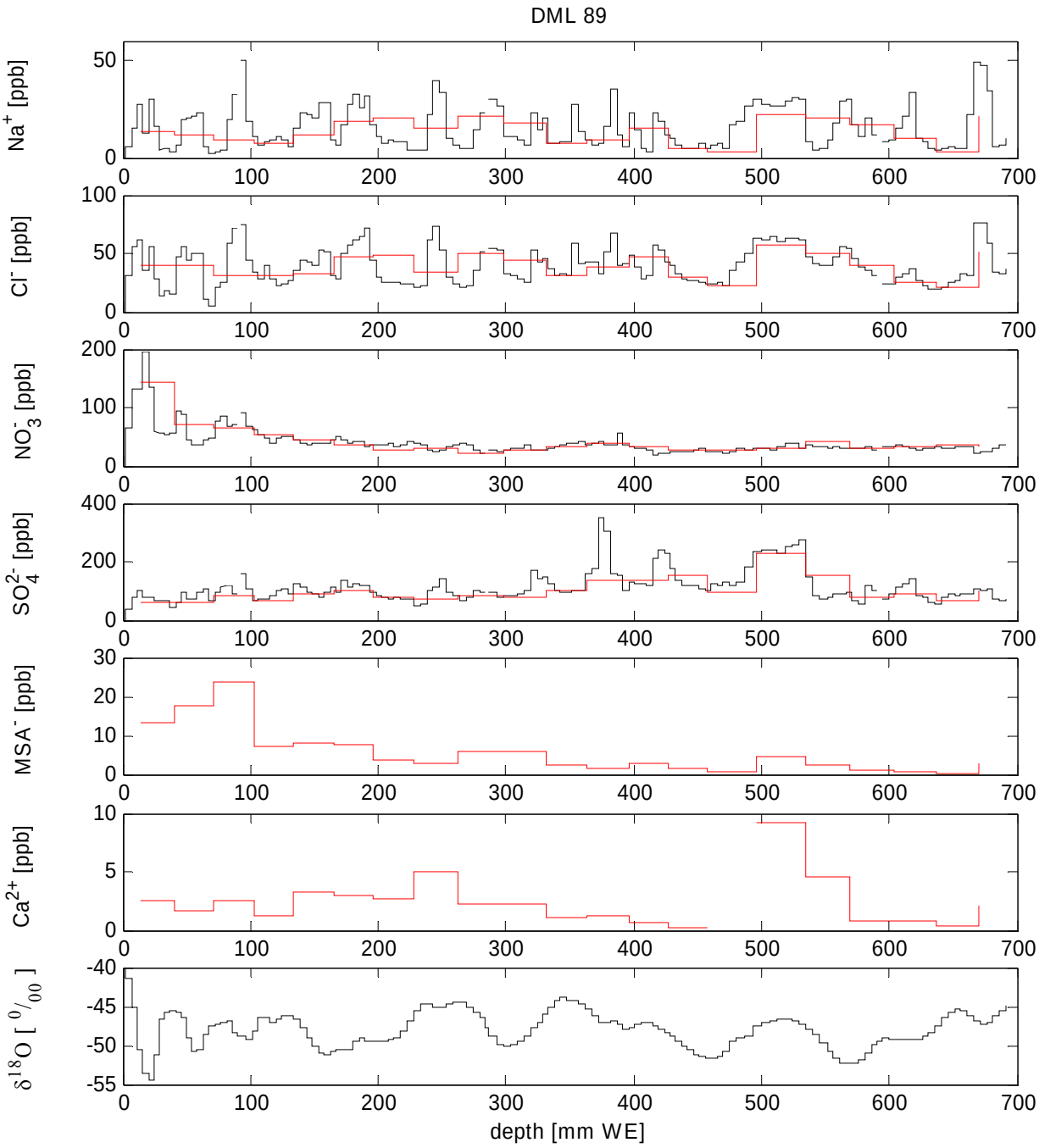

Figure 50: Raw data records from DML 89 of sodium, chloride, nitrate, sulphate, methane sulfonate, calcium and $\delta^{18}O$. The high resolution records of the UTS samples are displayed as black line, the coarse resolution records of the UTD samples are presented as red line. Note, MSA^- was measurable in UTD records only. Data of $\delta^{18}O$ were available from UTS samples, only.

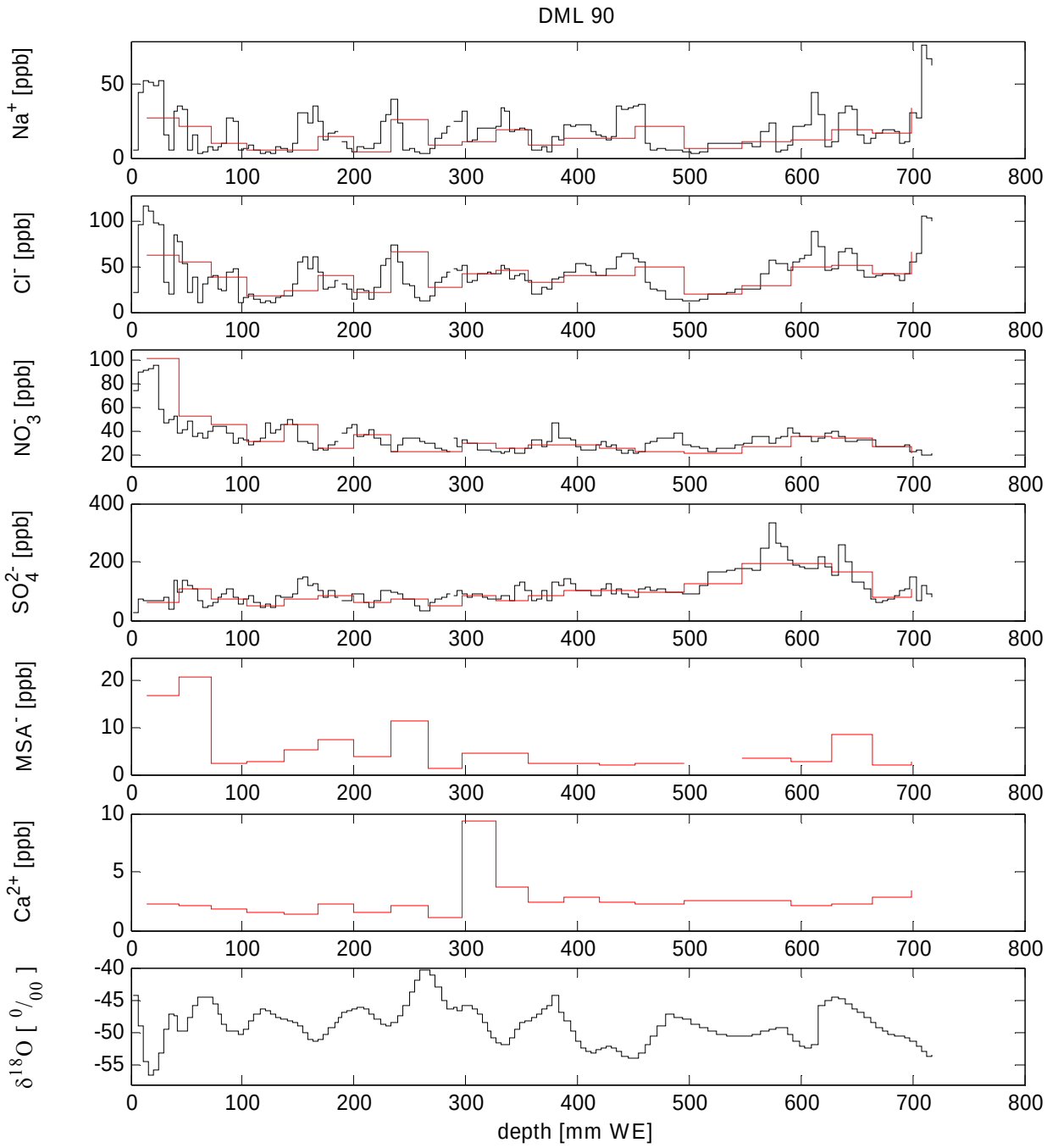

Figure 51: Raw data records from DML 90 of sodium, chloride, nitrate, sulphate, methane sulfonate, calcium and $\delta^{18}O$. The high resolution records of the UTS samples are displayed as black line, the coarse resolution records of the UTD samples are presented as red line. Note, MSA^- was measurable in UTD records only. Data of $\delta^{18}O$ were available from UTS samples, only.

9. Danksagung

Für seine wohlwollende Unterstützung und Bereitschaft, auch noch am Telefon bereitwillig Fragen zu beantworten danke ich meinem Betreuer Dr. Hubertus Fischer. Ebenso für die Überlassung des Themas und der Proben, die in unseren Breiten doch einen speziellen Seltenheitsgrad aufweisen.

Professor Tilo von Dobeneck danke ich für die Übernahme der Rolle des zweiten Begutachters.

Darüber hinaus möchte ich gegenüber meiner Familie, meinen Freunden und den Glaziologen am AWI die Freude bekunden, die mir die vergangene Zeit in Bremen, im AWI, in Raum 3400 und natürlich in Dome D bereitet hat!

Für die wertvolle Unterstützung während der Arbeit im Labor sei vor allem Birthe Twarloh gedankt. Neben Hubertus Fischer haben mich auch meine „Nachbarin“ Maria Hörhold, Anna Wegner und Jochen Schmitt in der entscheidenden Schlussphase unterstützt indem sie die ungeliebte Arbeit des Korrekturlesens bereitwillig übernahmen. Danke schön!

Dieser letzte Abschnitt meiner Studienzeit neigt sich in einigen Minuten seinem Ende entgegen; es bleibt spannend. Das Leben ist schön!